TAL TECH

DOCTORAL THESIS

Inflation in F(R) Palatini Gravity and Beyond

Christian Dioguardi

TALLINNA TEHNIKAÜLIKOOL
TALLINN UNIVERSITY OF TECHNOLOGY
TALLINN 2026

TALLINN UNIVERSITY OF TECHNOLOGY
DOCTORAL THESIS
22/2026

Inflation in F(R) Palatini Gravity and Beyond

CHRISTIAN DIOGUARDI

TAL TECH PRESS

TALLINN UNIVERSITY OF TECHNOLOGY
School of Science
Department of Cybernetics

National Institute of Chemical Physics and Biophysics
Laboratory of High Energy Physics

The dissertation was accepted for the defence of the degree of Doctor of Philosophy (Applied Physics) on 27th March 2026

Supervisor: Dr. Antonio Racioppi,
National Institute of Chemical Physics and Biophysics
Tallinn, Estonia

Co-supervisor: Dr. Gert Hütsi,
National Institute of Chemical Physics and Biophysics
Tallinn, Estonia

Opponents: Professor Salvatore Capozziello,
Scuola Superiore Meridionale
Naples, Italy

Dr. Syksy Räsänen,
University of Helsinki,
Helsinki, Finland

Defence of the thesis: 6th May 2026, Tallinn

Declaration:
Hereby I declare that this doctoral thesis, my original investigation and achievement, submitted for the doctoral degree at Tallinn University of Technology, has not been submitted for any academic degree elsewhere.

Christian Dioguardi

signature

ISSN 2585-6898 (publication)
ISBN 978-9916-80-493-3 (publication)
ISSN 2585-6901 (PDF)
ISBN 978-9916-80-494-0 (PDF)
DOI https://doi.org/10.23658/taltech.22/2026

Dioguardi, C. (2026). Inflation in F(R) Palatini Gravity and Beyond [TalTech Press]. https://doi.org/10.23658/taltech.22/2026

TALLINNA TEHNIKAÜLIKOOL
DOKTORITÖÖ
22/2026

Inflatsioon F(R) Palatini gravitatsioonis ja laiemalt

CHRISTIAN DIOGUARDI

TAL TECH
KIRJASTUS

Contents

List of Publications

The present Ph.D. thesis is based on the following publications that are referred to in the text by Roman numbers.

I Christian Dioguardi, Antonio Racioppi, and Eemeli Tomberg. Slow-roll inflation in Palatini F(R) gravity. *JHEP*, 06:106, 2022

II Christian Dioguardi and Antonio Racioppi. Palatini F(R,X): A new framework for inflationary attractors. *Phys. Dark Univ.*, 45:101509, 2024

III Konstantinos Dimopoulos, Christian Dioguardi, Gert Hütsi, and Antonio Racioppi. Quintessential inflation in palatini F(R,X) gravity. *The European Physical Journal Plus*, 140(11), November 2025

Author's Contributions to the Publications

In I, II, III, I was the main co-author, wrote the code, contributed to carry out the the analysis of the results, prepared the figures, and contributed to write the manuscript.

Abbreviations

SM	Standard Model
EM	Electromagnetic
GR	General Relativity
GW	Gravitational Wave
CMB	Cosmic Microwave Background
BBN	Big Bang Nucleosynthesis
FLRW	Friedmann-Lemaître-Robertson-Walker
KG	Klein-Gordon
ACT	Atacama Cosmology Telescope
DESI	Dark Energy Spectroscopic Instrument

Notation and Terms

In this thesis the mostly plus convention for the metric $(-+++)$ is used.

Greek indices take values $0,1,2,3$, where the index 0 denotes the timelike component, while 1,2,3 denote the spacelike components of vectors and tensors. The spacelike components of vectors and tensors are generally indicated by the letters i, j. For polar coordinates the Greek indices run over the time coordinate t, the radial coordinate r, and the two angular coordinates θ, ϕ.

The Einstein convention for the summation over repeated indices is used.

Calculations are carried in geometrized units by defining the reduced Planck Mass $M_P^2 \equiv \frac{1}{8\pi G} = 1$. However, physical observables can be sometimes expressed in GeV, when it is convenient for comparison with energy scales in Particle Physics. It is therefore recalled that $M_P = 2.43 \cdot 10^{18}$ GeV.

Planck dataset - denotes the dataset from the Planck CMB full-mission [4],[5].

Planck+Bicep/Keck Array dataset - denotes the dataset from the combination of Planck dataset and the results from Bicep and Keck Array observations [6].

Planck+ACT dataset - denotes the dataset from the combination of Planck+Bicep/Keck Array, DESI [7], and the Atacama Cosmology Telescope observations[8].

1 Introduction

The ΛCDM model represents today the Standard Cosmological Model. Together with the Standard Model of particle physics (SM) it constitutes the pinnacle of theoretical physics. The entire evolution of the Universe from the first fractions of seconds to the present days can be reconstructed by using our detailed knowledge of high-energy physics (SM) and by parametrizing the energy-density content of the Universe (ΛCDM).
The current picture is based on the description of four types of fundamental interactions. The Standard Model of particle physics describes three of them, the electromagnetic, strong, and weak interactions in terms of quantum relativistic fields. However, for what concerns the fourth interaction, gravity, there has not been any observation that might hint to a quantum behavior, at least in the range in which the theory was tested. All we know about gravity is classical. Quantizing gravity has been an obsession for theoretical physicists especially in the second half of last century. Yet, a self-consistent and predictive quantum formulation of the gravitational interaction has not been found. Only a formally consistent theory of quantum perturbations of the metric around a classical background has been achieved, as explicitly discussed in chapter 3. For this reason in this thesis only quantum perturbations of the metric are considered to introduce the inflationary paradigm. For all other purposes gravity will be considered as a purely classical interaction.
Currently, gravity is best described by Einstein theory of General Relativity (GR). The fundamental object is the metric tensor $g_{\mu\nu}(x)$, a classical field that allows to define distances and angles in the space-time. GR is based on the equivalence principle which is basically a statement of invariance of the equations describing gravitational interaction under general coordinate transformation. The source of gravitational interaction is energy density. Since the Universe is neutral under electromagnetic charge and weak, strong interaction are short range, gravity is the only interaction that determines the structure of the Universe from scales that go from solar system size to the cosmological Universe. All bound systems such as galaxies, clusters and large scale structures (LSS) are determined by gravitational interaction. The evolution of the Universe itself, its decelerating/accelerating expansion and its fate all depend by the energy-matter content of the Universe and by how gravity determines its evolution. This is the purpose of the Standard Cosmological Model known as ΛCDM. As far as ΛCDM concerns, the fundamental quantum nature of fields is almost irrelevant. What matters to ΛCDM is the nature of the energy-density as a fluid, in fact, depending on the fluid equation of state, the model predicts a different evolution of the Universe. In order to match the observations, the model needs four different types of energy content: Λ i.e. a cosmological constant describing an otherwise unknown type of energy-density which goes under the name of dark-energy. This makes up $\approx 70\%$ of the total observed energy budget of the Universe and is currently driving its accelerated expansion. Cold (i.e. non-relativistic) Matter which is further divided in baryonic matter making up $\approx 5\%$ of the total energy-density and Cold Dark-Matter corresponding to $\approx 25\%$ of total energy-density of the Universe [4]. The former is the standard non-relativistic matter whose interactions are described by the Standard Model. The latter is an unknown form of non-relativistic matter which has been present since the early Universe and that is necessary to allow the formation of LSS as we observe them. Its presence is also been proven at several scales from galaxy rotation curves [9], colliding clusters [10] ecc. (see [11] and references therein) but only through gravitational interactions. There is currently no detection of dark matter interactions in particle physics although several experiments and astrophysical observations are trying to detect its presence (see for example [12, 13, 14]). The last component of the model is radiation, i.e. relativistic fields such

as radiation and neutrinos, which today is negligible. While ΛCDM successfully manages to parametrize the evolution of the Universe, it is plagued by fine-tuning conditions that make impossible to reconcile it with the observed state of the Universe unless we choose extremely ad-hoc values of the parameters to set up the Universe. For this reason the ΛCDM is usually complemented by the inflationary paradigm [15, 16, 17]: a period of early accelerated expansion that drives the initial conditions of the Universe to the one necessary to achieve the current observed state. Another issue of the ΛCDM is the so-called cosmological constant problem. Indeed, the cosmological constant effectively works as a source of vacuum energy which is directly coupled to gravity. This source might have a quantum nature. For example, the Higgs field in the SM has a vacuum energy density of about ≈ 246 GeV [18, 19] which however is several orders of magnitude higher than the observed cosmological constant $\Lambda^{1/4} \approx 10^{-12}$GeV. Even if we assume that the total vacuum energy of the Universe needs to be zero due to some unknown symmetry, the model does not contain any explanation to why the value of Λ is so fine-tuned to become observable only in the recent times (unless we adopt the anthropic principle). It is then only natural to challenge the ΛCDM by introducing alternative explanations for the current dark-energy driven era. One of the most popular alternatives to the cosmological constant is quintessence, for which the dark-energy phase is actually described by a slow-rolling scalar field in a similar way to the mechanism that drives inflation.

On the observational side, the Standard Cosmological Model is even more importantly being challenged by recent cosmological observations. The Planck [5] and Bicep/Keck Array [6] collaborations strongly favored the most popular inflationary models such as Higgs [20] (and references therein) and Starobinsky inflation [21]. However, when those models are are compared with the latest Planck+ACT data [8] a $\approx 2\sigma$ tension arises with observations. Although statically not conclusive this hints at the possibility to put in discussion those popular models. As the observations of the Cosmic Microwave Background (CMB) improve and new probes such as LiteBird[22] and CMBS4 [23] are promising more data, it is fundamental to propose new solutions and ideas for viable inflationary scenarios. At the same time, new data coming from DESI [7] seems to hint at a dynamical nature for dark-energy. Furthermore and most importantly measurements of the current Universe expansion rate H_0 coming from Super-Novae Type1a are now in strong tension at $> 5\sigma$ confidence level with H_0 measurements coming from the Cosmic Microwave Background [24]. Whether this discrepancy represents or not a crisis for modern Cosmology is still a matter of debate. It is however clear that our current understanding of Cosmology is incomplete and needs further investigation.

Within this thesis an attempt to address the issue of inflation and dark-energy in the context of Palatini gravity is made. Palatini gravity is an alternative formulation with respect to standard General Relativity that predicts different phenomenology. The focus is on extended models of gravity, in particular $F(R)$ theories. The phenomenology of inflation and quintessence is discussed in this framework. The thesis is organized as follows. In chapter 2 the basics of General Relativity are discussed, the cosmological principle is introduced and the Friedmann equations, which are the fundamental equations of Cosmology, are derived. In chapter 3 the inflationary paradigm is introduced to solve the issue of the initial conditions of the Universe. The slow-roll computations are introduced and cosmological perturbation theory is briefly discussed in order to relate the slow-roll parameters with the CMB observables. Finally, the predictions for the most popular models of inflation i.e. chaotic, Higgs and Starobinsky inflation are discussed. In chapter 4 quintessence is introduced as an alternative to the cosmological constant. The dynamics of the general scalar field is studied in order to understand when it can be used to explain the late cosmic accel-

eration. The case of exponential and inverse-power-law quintessence is treated explicitly. In chapter 5 quintessential inflation is introduced as a way of describing both early and late time acceleration in terms of a single scalar degree of freedom. The phenomenology of these models is discussed, encompassing the whole evolution of the Universe from inflation to present days. Moreover, The Peebles-Vilenkin and $\alpha-$attractors quintessential inflation models and their viable parameter space are briefly explicitly reviewed. Finally, in chapter 6 the Palatini formulation of gravity is introduced. The differences with the standard metric formulation are explicitly discussed with an emphasis on the different phenomenology predictions, $F(R)$ theories in Palatini gravity are introduced and the inflationary phenomenology present in the literature is briefly discussed.

2 General Relativity and Cosmology

In this chapter General Relativity is introduced and the Friedmann equations that describe the cosmological evolution of the universe are derived. The content of the universe according to the ΛCDM model is also briefly discussed.

2.1 General Relativity

General Relativity (GR) has been standing as the best description of the gravitational interaction for over one hundred years. It has accomplished to survive an astonishing amount of experimental tests over the years in a wide range of scales. Any theory that aims to go beyond, either classical or quantum, has to recover GR in the limit where the experimental tests have proven no deviation. GR is based on the equivalence principle, which is a statement about the invariance of the equations of motion describing gravity, under arbitrary coordinate change. This requirement makes GR a geometric theory. The equivalence principle can be stated in three inequivalent ways [25]:

- Weak Equivalence Principle (WEP): the geodesics [1] of any test particle are the same independently of the particle composition
- Einstein Equivalence Principle (EEP): the laws of physics are the same in any free-falling frame
- Strong Equivalence Principle (SEP): includes strong self-gravitating bodies and gravitational interactions on top of the EEP.

GR is not the only theory that can address the equivalence principle, however it is the only metric theory of gravity that respects the SEP. In its standard formulation General Relativity is described in terms of curvature on a 4-dimensional manifold. The natural objects on the manifold are tensors. The gravitational field in GR is described by the metric field $g_{\mu\nu}(x^\sigma)$ a rank-two tensor defined at each point on the manifold, which defines the notion of lengths and angles. In absence of gravitational interaction the metric $g_{\mu\nu}(x^\sigma)$ becomes the flat Minkowski metric $\eta_{\mu\nu} = \text{diag}(-1,1,1,1)$. The coordinates x^σ with $\sigma = 0,1,2,3$ are local coordinates in $\mathbb{R}^4$ associated to each point of the manifold through a map. The mathematical implementation of the equivalence principle in GR is given by diffeomorphism invariance i.e. the invariance under infinitesimal coordinate transformations of the tensor fields on the manifold. The covariant derivative acts on the tensors of the manifold and represents the natural derivative preserving diffeomorphism symmetry. If we consider a rank-2 covariant tensor T^μ_ν, taking its covariant derivative gives (in component notation):

$$\nabla_\sigma T^\mu_\nu = \partial_\sigma T^\mu_\nu + \Gamma^\mu_{\lambda\sigma} T^\lambda_\nu - \Gamma^\lambda_{\sigma\nu} T^\mu_\lambda, \tag{1}$$

where $\partial_\sigma \equiv \frac{\partial}{\partial x^\sigma}$ is the standard derivative in flat space-time in the x^σ coordinate and Γ is the so-called affine connection, which geometrically defines the parallel transport of vectors along geodesics. The covariant derivative can be straightforwardly generalized to higher-rank tensors.
The object describing the strength of the gravitational interaction is curvature. The mathematical definition of curvature is obtained by considering the field-strength given by the commutation relation of the covariant derivatives acting on a vector field V^σ. We obtain:

$$[\nabla_\mu, \nabla_\nu] V^\rho = R^\rho_{\sigma\mu\nu} V^\sigma - S^\lambda_{\mu\nu} \nabla_\lambda V^\rho, \tag{2}$$

[1] A geodesic is, in simple terms, the shortest path between two points on the manifold, the natural generalization of a straight line in curved space.

where $R^{\rho}_{\sigma\mu\nu}$ is the Riemann tensor explicitly given by:

$$R^{\rho}_{\sigma\mu\nu} = \partial_{\mu}\Gamma^{\rho}_{\sigma\nu} - \partial_{\nu}\Gamma^{\rho}_{\sigma\mu} + \Gamma^{\rho}_{\lambda\mu}\Gamma^{\lambda}_{\sigma\nu} - \Gamma^{\rho}_{\lambda\nu}\Gamma^{\lambda}_{\sigma\mu}, \tag{3}$$

and $S^{\lambda}_{\mu\nu}$ is the torsion tensor defined as:

$$S^{\lambda}_{\mu\nu} \equiv \Gamma^{\lambda}_{\mu\nu} - \Gamma^{\lambda}_{\nu\mu}. \tag{4}$$

In GR the affine connection is *assumed* to be symmetric in the lower indices and the torsion tensor vanishes. In particular in General Relativity, Γ corresponds to the Levi-Civita connection related to the metric through:

$$\Gamma^{\lambda}_{\mu\nu} = \frac{1}{2} g^{\lambda\rho}(g_{\rho\nu,\mu} + g_{\mu\rho,\nu} - g_{\mu\nu,\rho}). \tag{5}$$

In order to find the equations of motion of GR, we need to build a scalar out of the curvature tensor so to provide the Lagrangian density for the theory. By using the fact that the $\Gamma^{\rho}_{\mu\nu}$ is symmetric in the lower indices one can show that the only non vanishing rank-2 tensor that one can build from the contractions of the Riemann tensor is the Ricci tensor $R_{\mu\nu} \equiv R^{\rho}_{\mu\rho\nu}$. Hence, by contracting it with the metric we get the simplest possible scalar that encodes the gravitational interaction $R = g^{\mu\nu}R_{\mu\nu}$ i.e. the curvature scalar, often referred in literature as Ricci scalar. In order to get the equation of motion for GR we can exploit the variational principle. We start by writing the general action[2]:

$$S = \int d^4x\sqrt{-g}\left(\frac{M_{\rm P}^2}{2}R + \mathscr{L}(g_{\mu\nu}, \phi, \nabla_{\mu}\phi)\right) \tag{6}$$

where $M_{\rm P} = \sqrt{1/8\pi G}$ is the reduced Planck mass, fixed in such a way to recover the Newton law at small curvature and $\mathscr{L}(g_{\mu\nu}, \phi, \nabla_{\mu}\phi)$ collectively denotes the Lagrangian density of the matter fields ϕ and their covariant derivatives $\nabla_{\mu}\phi$. Note that the matter Lagrangian is minimally coupled with the metric, i.e. matter is coupled to gravity only through the metric tensor $g_{\mu\nu}$. By taking the variation with respect to the metric field we finally get the equation of motion of GR, i.e. the Einstein equations:

$$G_{\mu\nu} = \frac{1}{M_P^2}T_{\mu\nu}, \tag{7}$$

where

$$G_{\mu\nu} \equiv R_{\mu\nu} - \frac{1}{2}g_{\mu\nu}R, \tag{8}$$

is the Einstein tensor, and

$$T_{\mu\nu} \equiv -\frac{2}{\sqrt{-g}}\frac{\partial(\sqrt{-g}\mathscr{L})}{\partial g^{\mu\nu}}. \tag{9}$$

is the energy-momentum tensor which sources the gravitational field. The solutions of the equations and the predicted phenomenology is impressively rich. Spherically and axisymmetric solutions in vacuum give rise to static and stationary black holes solutions: the so called Schwarzschild and Kerr black holes. Linearized solutions around the Minkowski background predict gravitational waves. Assuming homogeneity and isotropy of space allows us to study Cosmology. In this thesis we will focus on the latter.

[2]When necessary for clarity, we explicitly write $M_{\rm P}$ in the equations. Otherwise, we set $M_{\rm P} = 1$. For details on the notation, we refer to the Notation and Terms section.

2.2 The cosmological principle and the Friedmann equations

The aim of Cosmology is to study the Universe at large scales and to understand its evolution from its beginning to present days. The core assumption in Cosmology is the so-called cosmological principle: the Universe is assumed to be spatially homogeneous and isotropic at all times. The cosmological principle is confirmed by observation over scales $s > 150$ Mpc at the present day. An immediate consequence of the isotropic and homogeneous Universe is the Hubble law. When observing the sky the most useful measured quantity is the redshift

$$z \equiv \frac{\lambda_{\text{ob}} - \lambda_{\text{em}}}{\lambda_{\text{em}}}, \tag{10}$$

of the light coming from astrophysical object, i.e. the fractional difference between the light wavelength λ_{em} at emission and the light wavelength at λ_{ob} at observation. Experimentally one observes (see [26] and references therein) that the redshift $z = H_0 s$ is proportional to the proper distance s, with H_0 the proportionality factor known in literature as Hubble constant. This redshift can be interpreted as analogous to a Doppler shift which allows us to write $v = H_0 s$, where v is called peculiar velocity. This implies that galaxies that are farther from us recede faster than closer galaxies. This is indeed what it is expected in a Universe obeying the cosmological principle. By defining

$$s = a(t) r, \tag{11}$$

with $a(t)$ the time dependent scale factor and r the time independent comoving distance, one can show that the Hubble law

$$v = H(t) s, \tag{12}$$

is the only possible law in an homogenous and isotropic expanding Universe, where we defined

$$H(t) \equiv \frac{\dot{a}}{a}, \tag{13}$$

the Hubble function. The Hubble function at the present time t_0 corresponds to the observed value of the Hubble constant, $H(t_0) \equiv H_0$.

We can now write the Einstein equations for an isotropic and homogeneous universe. With this assumption the most general metric can be proven to be the Friedmann-Lemaître-Robertson-Walker (FLRW) metric [3]:

$$ds^2 = -dt^2 + a(t)^2 \left(\frac{1}{1-kr^2} dr^2 + r^2 d\theta^2 + r^2 \sin^2\theta d\phi^2 \right), \tag{14}$$

where $a(t)$ represents the relative size of the spacelike hypersurfaces Σ at coordinate time t and k is a constant that determines their geometry which can be hyperbolic $k = -1$, flat $k = 0$, or spherical $k = 1$. The spatial part of the metric is expressed in polar coordinates which is the most convenient choice given the isotropy of space. By assuming this metric, the non-zero Christoffel symbols are

$$\begin{aligned}
&\Gamma^t_{rr} = \frac{a\dot{a}}{1-kr^2}, \quad \Gamma^t_{\theta\theta} = a\dot{a}r^2, \quad \Gamma^t_{\phi\phi} = a\dot{a}r^2\sin^2\theta, \quad \Gamma^r_{tr} = \Gamma^\theta_{t\theta} = \Gamma^\phi_{t\phi} = \frac{\dot{a}}{a} \equiv H, \\
&\Gamma^r_{rr} = \frac{kr}{1-kr^2}, \quad \Gamma^r_{\phi\phi}\sin^2\theta, \quad \Gamma^r_{\theta\theta} = -r(1-kr^2), \\
&\Gamma^\theta_{r\theta} = \Gamma^\phi_{r\phi} = \frac{1}{r}, \quad \Gamma^\theta_{\phi\phi} = -\sin\theta\cos\theta, \quad \Gamma^\phi_{\theta\phi} = \frac{\cos\theta}{\sin\theta}.
\end{aligned} \tag{15}$$

[3] The line element is defined through the metric as $ds^2 = g_{\mu\nu} dx^\mu dx^\nu$. For convenience, from now on we will define the metric components through ds^2.

Here the subscripts and superscripts denoted by Greek letters run over the polar coordinates $\mu = t, r, \theta, \phi$ and denote the specific components of the tensors in polar coordinates. From the Christoffel symbols expressions we can compute the Einstein tensor $G_{\mu\nu} \equiv R_{\mu\nu} - \frac{1}{2} g_{\mu\nu} R$:

$$G_{tt} = 3H^2 + 3k, \quad G_{rr} = -\frac{k + a^2(2\dot{H} + 3H^2)}{1 - kr^2}, \tag{16}$$
$$G_{\theta\theta} = -r^2\big(k + a^2(2\dot{H} + H^2)\big), \quad G_{\phi\phi} = \sin^2\theta G_{\theta\theta}.$$

This gives the l.h.s. of Einstein equations for a homogeneous and isotropic universe. We now need to find a source that respects the cosmological principle in order to compute the r.h.s. of the Einstein equations. The stress-energy tensor for a perfect fluid is given by:

$$T_{\mu\nu} = (\rho + P) u_\mu u_\nu + P g_{\mu\nu}. \tag{17}$$

where ρ is the fluid energy density, P the fluid pressure and u_μ the fluid four-velocity. Since we want it to be isotropic it has to be at rest with the comoving observer, this implies:

$$T^\mu_\nu = \text{diag}(-\rho, P, P, P). \tag{18}$$

By using the conservation of the stress-energy tensor $\nabla_\mu T^\mu_\nu = 0$ we derive the continuity equation for the perfect fluid in a FLRW universe:

$$\dot{\rho} + 3H(\rho + 3P) = 0. \tag{19}$$

The *tt* and *rr* components of the Einstein equations give instead:

$$H^2 = \frac{\rho}{3} - \frac{k}{a^2}, \tag{20}$$
$$\dot{H} + H^2 = -\frac{1}{6}(\rho + 3P). \tag{21}$$

It can be shown by straightforward computations that the other components do not give independent equations. (20) and (21) are the First and Second Friedmann equations which together with (19) form a set of three equations that are not linearly independent. It is straightforward to show upon substitution that only two out of three are. The Hubble function $H(t)$ describes the expansion rate of the universe at coordinate time t which depends on the energy-matter content of the universe described by $\rho(t)$, $P(t)$. Notice that since we are assuming an homogeneous and isotropic universe all quantities are independent of the spatial coordinates and can only depend on the coordinate time t. In order to solve the system, it is necessary to assume an equation of state for the fluid which relates its pressure and energy density. On cosmological scales gravity is the only interaction, this makes safe to consider a barotropic equation of state for which pressure is proportional to the energy density

$$P = w\rho, \tag{22}$$

with w a constant. Setting the spatial curvature $k = 0$ in (20), for a general fluid with barotropic equation of state (22) and $-1 < w \leq 1$ the solution of the Friedmann equations can be derived by straightforwardly solving the system of differential equation (20),(21). We get:

$$a(t) = \left(\frac{t}{t_0}\right)^{\frac{2}{3(1+w)}}, \tag{23}$$
$$\rho(t) = \rho_0 \left(\frac{t_0}{t}\right)^2, \tag{24}$$

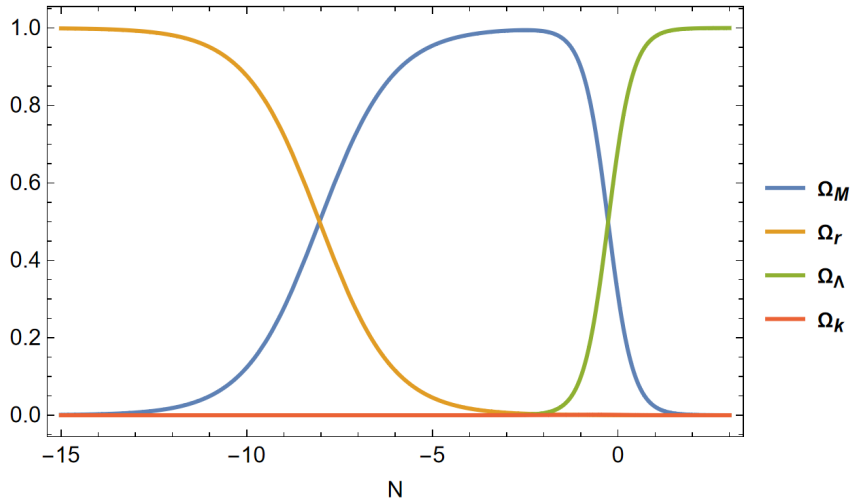

Figure 1: Evolution of the density parameters for the various types of energy density content in the Universe in terms of the number of e-folds $N = \ln(a)$. Assuming ΛCDM, the Universe started with radiation domination followed by matter domination $N \approx -8$ before the cosmological constant becomes the main source of energy density at $N \approx -0.27$. Given the current bound, curvature (if present) is always negligible during the whole evolution.

where ρ_0, t_0 are the present energy density of the fluid and present time respectively. This also implies

$$\rho(a) = \rho_0 a^{-3(1+w)}, \tag{25}$$

$$H(t) = \frac{2}{3(1+w)\,t_0}. \tag{26}$$

Instead, for the case $w = -1$ we find:

$$a(t) = e^{H_0(t-t_0)}, \tag{27}$$

$$\rho(t) = \rho_\Lambda = \text{const.}, \tag{28}$$

with $H(t) = H_0 = \text{const.}$

2.3 The ΛCDM model

Different types of matter are characterized by different equation of state parameters w defined by (22), as the ratio between the fluid pressure and energy density (sometimes it is referred as barotropic parameter in the literature, see for example Chapter 8 of [25]):

$w = 0$	Cold (Baryonic and Dark) Matter
$w = \frac{1}{3}$	Relativistic Matter
$w = -1$	Cosmological Constant
$w = -\frac{1}{3}$	Curvature

The ΛCDM model is currently the best fitting model we have to match the observation about the evolution of the Universe.

Let us now introduce the critical density $\rho_c = 3H^2$. If $\rho = \rho_c$ exactly, then the universe is spatially flat. If $\rho > \rho_c$ the universe is spatially closed i.e. it has spherical geometry, while if $\rho < \rho_c$ the universe is spatially open i.e. it has hyperbolic geometry. We then rewrite the first Friedmann equation as:

$$1 - \Omega_k = \Omega_M + \Omega_r + \Omega_\Lambda, \tag{29}$$

by dividing both sides of (20) by ρ_c. Here we have defined the density parameter $\Omega = \rho/\rho_c$ for each fluid and Ω_M, Ω_r, Ω_Λ, Ω_k are the density parameters associated respectively to matter, radiation, dark-energy and curvature [4]. The ΛCDM fits the observed density parameters today to be $\Omega_{\Lambda,0} \approx 0.69$ ($w_\Lambda = -1$) which drives the current accelerated expansion, $\Omega_{M,0} \approx 0.31$ ($w_M = 0$) of which $\Omega_{DM,0} \approx 0.26$ for Dark Matter and $\Omega_{BM,0} \approx 0.05$ for baryonic matter, $\Omega_{r,0} \approx 8 \cdot 10^{-5}$ ($w_r = 1/3$) which includes photons and neutrinos and $\Omega_{k,0} \leq 10^{-3}$ for curvature ($w = -1/3$) [4]. By assuming that the content of the Universe is correctly described by ΛCDM, we can reconstruct the full evolution of the density parameters from their present values as shown in Fig.1. Such a low value for $\Omega_{k,0}$ rises the problem of fine tuning for the ΛCDM model since this requires that ρ must be very close to the critical density ρ_c. This issue further worsen if one considers the evolution of the energy density, requiring an extremely fine-tuned value of ρ in the early Universe. This is the so called flatness problem that we are going to discuss in detail in the next chapter.

[4] In particular the sum $\Omega_{tot} = \Omega_M + \Omega_r + \Omega_\Lambda$ represents the total energy density of the universe and Ω_k is related to the spatial curvature of the universe through the relation $\Omega_k = -3k/(aH)^2$.

3 Inflation

In this chapter the author discusses in detail the inflationary paradigm, introduced to solve the issue of initial conditions implied by cosmological observations and in particular from the Cosmic Microwave Background. Moreover, it is discussed how to compute the main inflationary observables and how to test them through the observation of the CMB. Finally, the most popular and promising models for inflation are reviewed.

3.1 The Cosmic Microwave Background

The Cosmic Microwave Background (CMB) is the relic background radiation emitted at the time of the Last Scattering Surface, when the Universe became transparent to radiation. This happened when the Universe lifetime was about $t \approx 3 \cdot 10^5$ years and cold enough to let the hydrogen bound state to be formed i.e. after temperature dropped below $T \approx 13.6$ eV. At this temperature the average kinetic energy of electrons in the plasma became smaller than ioniziation energy of hydrogen and radiation was finally free to propagate without further scattering (this event is also sometimes referred as photon decoupling).
Let's now suppose we look at the sky in the direction indicated by $\hat{\mathbf{n}}$, a unit vector, and observe a temperature $T(\hat{\mathbf{n}})$. The average CMB temperature over the whole sky T_{CMB} is then computed as:

$$T_{\mathrm{CMB}} = \frac{1}{4\pi} \int T(\hat{\mathbf{n}}) d\Omega, \tag{30}$$

with $\mathrm{d}\Omega = \mathrm{d}\cos\theta \mathrm{d}\phi$ in polar coordinates θ, ϕ. Today the observed average CMB temperature is $T_{\mathrm{CMB}} = (2.7255 \pm 0.0006)$ K $\approx 2.35 \cdot 10^{-4}$eV [27]. Let's now consider the temperature fluctuations in direction $\hat{\mathbf{n}}$:

$$\frac{\delta T}{T}(\hat{\mathbf{n}}) \equiv \frac{T(\hat{\mathbf{n}}) - T_{\mathrm{CMB}}}{T_{\mathrm{CMB}}} = \sum_{lm} a_{lm} Y_{lm}(\hat{\mathbf{n}}), \tag{31}$$

where Y_{lm} are the spherical harmonics, with l, m integer numbers and $-l \leq m \leq l$. The coefficients a_{lm} are given by

$$a_{lm} = \int d\Omega\, Y^*_{lm}(\hat{\mathbf{n}}) \frac{\delta T}{T}(\hat{\mathbf{n}}), \tag{32}$$

which are the multipole moments of the CMB temperature fluctuations. The average of the fluctuations can be computed by decomposing the perturbations in spherical harmonics. From the multipole moments a_{lm} we can compute the angular power spectrum of temperature perturbations:

$$< a^*_{lm} a_{l'm'} >= C_l^{\mathrm{TT}} \delta_{ll'} \delta_{mm'} \tag{33}$$

which encodes the information of the CMB about temperature perturbations in the coefficients C_l^{TT}, where the superscript TT specifies that we are looking at temperature-temperature correlations (i.e. the correlation between the temperature of two different points in the sky) and $l = 0, 1, 2...$ correspond to the monopole, dipole, quadrupole ecc. moments. Probing a larger l multipole then implies probing a smaller scale in the CMB temperature field. These fluctuations can be related to the gravitational potential generated by density fluctuations of the plasma at the time of photon decoupling. In particular, they are generated by baryon acoustic oscillations: over-densities generate potential wells that attract more matter, while at the same time pressure acts against the gravitational pull. This oscillations have a characteristic size in the plasma and generate acoustic peaks

which can be observed in the CMB by plotting the coefficient C_l^{TT} against the multipole index l (see for example Fig.19 in [28]). Being able to probe those fluctuations with a better resolution implies being able to resolve those peaks with larger precision.
Temperature fluctuations are not the only observable in the CMB. Indeed we have the possibility of measuring its polarization as well. Since the CMB is relic radiation there can only be two possible polarization modes: the E-modes and the B-modes[5]. In particular we can compute the correlation coefficients of the polarization in the same way we did for temperature ones:

$$< a^*_{\mathrm{E},lm} a^*_{\mathrm{E},l'm'} >= C_l^{\mathrm{EE}} \delta_{ll'} \delta_{mm'}, \tag{34}$$

$$< a^*_{\mathrm{B},lm} a^*_{\mathrm{B},l'm'} >= C_l^{\mathrm{BB}} \delta_{ll'} \delta_{mm'}, \tag{35}$$

$$< a^*_{\mathrm{T},lm} a^*_{\mathrm{E},l'm'} >= C_l^{\mathrm{TE}} \delta_{ll'} \delta_{mm'}. \tag{36}$$

Where the superscripts EE, BB represent the polarization correlation and TE the cross-correlation between between temperature and E-modes. It can be shown that all the other combinations are zero [28]. In general these polarizations can be naturally induced by inflation. Indeed, as we are going to discuss in section 3.4, scalar perturbations generate E-modes, while tensor ones generate both E-modes and B-modes. In particular B-modes are extremely important for inflation as they can only be induced by primordial gravitational waves. The detection of B-modes would be considered a smoking gun for inflationary models and would confirm the inflationary paradigm (see section 3.2). In order to understand how we can relate temperature fluctuations, E-modes and B-modes to inflationary models we first need to briefly introduce the theory of cosmological perturbations. This will be done in section 3.4 after introducing the inflationary paradigm in section 3.2.

3.2 Homogeneity and flatness problem

Let us define the conformal time:

$$\tau \equiv \int_0^t \frac{dt'}{a(t')} = \int_0^a d\ln a \left(\frac{1}{aH}\right), \tag{37}$$

The quantity $(aH)^{-1}$ is the comoving Hubble radius and corresponds to the comoving distance that characterizes the Hubble horizon, i.e. the horizon which determines the observable universe at the present time. Any object at a distance larger than the Hubble horizon cannot be in causal contact with a comoving observer as its receding velocity is larger than the speed of light. In terms of conformal time τ the FLRW metric takes metric form:

$$ds^2 = a(\tau)^2 \left(-d\tau^2 + \frac{1}{1-kr^2} dr^2 + r^2 d\theta^2 + r^2 \sin^2\theta d\phi^2\right). \tag{38}$$

The standard Big Bang evolution comes with the problem of initial conditions. The periods of radiation and matter domination alone are not enough to explain the observed homogeneity and flatness of the Universe. The flatness issue is very easily understood by rewriting the first Friedmann equation (20) as:

$$1 - \Omega = -\frac{k}{(aH)^2}, \tag{39}$$

[5]The E, B superscripts are no coincidence. The E-modes are indeed curl-free polarization (radial polarization vectors), while the B-modes are the divergence-free polarization (polarization vectors have vorticity) of the electromagnetic field. (see for example Fig.21 of [28])

where again we divided (20) by $\rho_c = 3H^2$, and used $\Omega = \rho/\rho_c$. By solving the Friedmann equations (20),(21) in terms of a for a general fluid with barotropic equation of state (22) one can find that the comoving Hubble Radius is given by:

$$(aH)^{-1} = H_0^{-1} a^{\frac{1}{2}(1+3w)}. \tag{40}$$

For $w = 0$ and $w = 1/3$ the comoving Hubble radius is monotonically growing. This implies that the r.h.s. of (39) grows with the expansion of the universe. In order to reproduce the observed value of flatness today $\Omega_k < 0.001$, it is necessary for the energy density to be extremely fine tuned to the value of the critical density ρ_c in the early Universe. In other terms, flatness is an unstable fixed point for the universe evolution if we only assume $w = 0$ and $w = 1/3$ fluids were dominating in the early Universe. There is also one more issue, related to the almost perfect homogeneity observed in CMB. Since the comoving Hubble radius has been monotonically increasing, the size of the causally connected Universe is also increasing monotonically and it is the largest today. It is then impossible for different patches in the sky to be causally connected in the past. By computing it explicitly one can show [28] that the currently observable CMB was made of 10^5 causally disconnected patches at the time of recombination if we assume the standard Big Bang cosmology. However, the background radiation seems to be homogeneous up to order $\delta T/T_{\rm CMB} \approx 10^{-5}$ temperature fluctuations over the whole sky. This clearly seems to imply an extremely unlikely fine-tuning.
Both problems can be solved straightforwardly by the inflationary paradigm i.e. a period during which the comoving Hubble radius shrinks. This implies:

$$\frac{d}{dt}(aH)^{-1} < 0 \implies \frac{d^2a}{dt^2} > 0, \tag{41}$$

meaning we simply need an early phase during which the Universe expansion is accelerating. From the second Friedmann equation (21) this directly translates to having a fluid such that $\rho + 3P < 0$. For a barotropic fluid this implies $w < -\frac{1}{3}$. Modeling inflation correctly is however more delicate than this. First of all, a simple cosmological constant wouldn't work because it would lead to an eternal De-Sitter phase resulting in endless inflation. On the other hand, we want inflation to last sufficiently long to bring the whole observable Universe in causal contact at the time perturbations in the CMB were generated. This is achieved if inflation lasts for about $N \equiv \ln a \gtrsim 60$ e-folds after perturbations are produced. If we consider $H_{\rm end} \sim H_{\rm i} \sim$ const. during inflation, we can indeed estimate that inflation in terms of e-folds has to last:

$$e^N \equiv \frac{a_{\rm end}}{a_{\rm i}} \sim \frac{\dot{a}_{\rm end}}{\dot{a}_{\rm i}} \geq \frac{\dot{a}_{\rm end}}{\dot{a}_0}, \tag{42}$$

where the subscripts "end", "i","0" denote the quantities evaluated respectively at the end of inflation, at the beginning of inflation and today. By considering $\dot{a} \sim t^{-1/3}$ during matter domination and $\dot{a} \sim t^{-1/2}$ [6] during radiation domination we have from (42):

$$N \geq \ln\left(\frac{\dot{a}_{\rm end}}{\dot{a}_0}\right) = \ln\left(\frac{\dot{a}_{\rm end}}{\dot{a}_{\rm eq}}\frac{\dot{a}_{\rm eq}}{\dot{a}_0}\right) \sim \frac{1}{2}\ln\left(\frac{t_{\rm eq}}{t_{\rm end}}\right) + \frac{1}{3}\left(\frac{t_0}{t_{\rm eq}}\right) \approx 62, \tag{43}$$

where we have considered typical $t_{\rm end} \approx 10^{-38}$s, $t_{\rm eq} \approx 5\cdot 10^4$ years and $t_0 \approx 13.8\cdot 10^9$ years being respectively the time at the end of inflation, the time at radiation-matter equivalence and the life time of the Universe today. The actual total number depends on the exact times and is hence model dependent.

[6] This immediately follows from the continuity equation (19) and the first Friedmann equation (20) by considering a barotropic fluid with $w = 0$ and $w = 1/3$, respectively. See eq.(23).

3.3 Slow-roll inflation

In order to model inflation the simplest choice is considering a scalar field in the matter sector. Consider the following action:

$$S = \int d^4x\sqrt{-g}\left(\frac{1}{2}R - \frac{1}{2}g^{\mu\nu}\partial_\mu\phi\partial_\nu\phi - V(\phi)\right), \tag{44}$$

Since we are assuming the cosmological principle the scalar field can be a function of the time coordinate only, $\phi = \phi(t)$. Hence by deriving the equation of motion in a FLRW metric we get:

$$3H^2 = \frac{1}{2}\dot{\phi}^2 + V(\phi), \tag{45}$$

$$\ddot{\phi} + 3H\dot{\phi} + V'(\phi) = 0. \tag{46}$$

where the $'$ denotes derivative with respect to its argument. We can notice by inspection with (20),(21) that the scalar field can be interpreted as a fluid with:

$$\rho_\phi = \frac{1}{2}\dot{\phi}^2 + V(\phi), \tag{47}$$

$$P_\phi = \frac{1}{2}\dot{\phi}^2 - V(\phi), \tag{48}$$

which by using (22) gives the scalar field barotropic parameter:

$$w_\phi = \frac{\dot{\phi}^2 - 2V(\phi)}{\dot{\phi}^2 + 2V(\phi)}. \tag{49}$$

It is then clear that when $V(\phi) \gg \dot{\phi}^2$ i.e. the scalar field potential energy dominates over the kinetic one, we recover the necessary condition for accelerated expansion $w < -1/3$. It is useful to rewrite the second Friedmann equation for the scalar fluid in the following way:

$$\frac{\ddot{a}}{a} = H^2(1 - \epsilon_H) = -\frac{1}{6}(\rho_\phi + 3P_\phi), \tag{50}$$

where we defined the first Hubble slow-roll parameter (HSRP):

$$\epsilon_H \equiv -\frac{\dot{H}}{H^2} = -\frac{dH}{d\ln N}. \tag{51}$$

For the scalar field this reads

$$\epsilon_H = \frac{3}{2}(1 + w_\phi) = \frac{1}{2}\frac{\dot{\phi}^2}{H^2}. \tag{52}$$

It is straightoforward to see that whenever $\epsilon_H < 1$, we are satisfying the condition for inflation. When $\epsilon_H \ll 1$ we satisfy the first slow-roll condition i.e. the field is slowly varying during the evolution. Since we introduced inflation to solve the homogeneity and flatness problem it is not enough to have a period of accelerated expansion, we also want inflation to last sufficiently long to generate the observed CMB homogeneity $\delta T/T_{\text{CMB}} \approx 10^{-5}$ and present day flatness $\Omega_{k,0} \leq 0.001$. This is achieved by introducing the second HSRP:

$$\eta_H \equiv -\frac{\ddot{\phi}}{H\dot{\phi}} = \epsilon_H - \frac{1}{2\epsilon_H}\frac{d\epsilon_H}{dN}. \tag{53}$$

In the limit in which $\ddot{\phi} \ll 3H\dot{\phi} \sim V'(\phi)$ we satisfy the condition $\eta_H \ll 1$. This is equivalent to say that the fractional change of ϵ_H per e-fold is small, allowing inflation to last long enough. Due to the rapid expansion of the universe the term $3H\dot{\phi}$ acts as a damping term during the evolution of ϕ. This implies that slow-roll is an attractor solution of the KG equation for most potentials. From the slow-roll conditions it is possible to derive equivalent conditions in terms of the scalar field potential only. We define the first and second potential slow-roll parameters (PSRP):

$$\epsilon_V \equiv \frac{1}{2}\left(\frac{V'}{V}\right)^2, \tag{54}$$

$$\eta_V \equiv \frac{V''}{V}. \tag{55}$$

During slow-roll the relation between the HSRP and PSRP is [28]:

$$\epsilon_H \sim \epsilon_V, \tag{56}$$

$$\eta_H \sim \eta_V - \epsilon_V. \tag{57}$$

Inflation ends when the condition $\epsilon_H > 1$ is met. Slow-roll inflation ends whether either $\epsilon_V(\phi) = 1$ or $|\eta_V(\phi)| = 1$. In the slow-roll approximation it also possible to express the e-fold number in terms of the potential:

$$N(\phi) = \ln\left(\frac{a_{\text{end}}}{a}\right) = \int_a^{a_{\text{end}}} \frac{1}{\tilde{a}} d\tilde{a} = \int_t^{t_{\text{end}}} H dt = \int_\phi^{\phi_{\text{end}}} \frac{H}{\dot{\phi}} d\phi \sim \int_{\phi_{\text{end}}}^{\phi} \frac{V}{V'} d\phi. \tag{58}$$

where we performed straightforward change of variables and in the last passage we considered the slow-roll approximation $3H\dot{\phi} \sim V'(\phi)$ and $3H^2 \sim V(\phi)$. During inflation scalar and tensor perturbations are produced on top of the FLRW background. In order to test the inflationary paradigm we need to predict the amplitude of such perturbations and measure them by observing the fluctuations in the CMB. We are going to explicitly relate inflation generated amplitudes with the CMB observables in the next section.

3.4 Cosmological perturbation theory

It is possible to find very simple relations between the slow-roll parameters ϵ_V and η_V and observables in the CMB. In order to do so we need to compute the amplitude of quantum perturbations on the FLRW background. To do so we need to introduce perturbations on the FLRW background. The FLRW metric is maximally symmetric, this allows to use the Scalar-Vector-Tensor (SVT) decomposition of the metric and stress energy tensor. The goal is to compute the perturbed equation:

$$\delta G_{\mu\nu} = \delta T_{\mu\nu}. \tag{59}$$

We consider the metric and scalar perturbations, which at linear level evolve independently:

$$g_{\mu\nu}(t,\mathbf{x}) = \bar{g}_{\mu\nu}(t) + \delta g_{\mu\nu}(t,\mathbf{x}), \qquad \phi(t,\mathbf{x}) = \bar{\phi}(t) + \delta\phi(t,\mathbf{x}). \tag{60}$$

By using the SVT decomposition we have:

$$\delta g_{\mu\nu} = \delta g^S_{\mu\nu} + \delta g^V_{\mu\nu} + \delta g^T_{\mu\nu}, \tag{61}$$

with

$$\delta g^S_{\mu\nu} = a^2 \begin{pmatrix} -2\Phi & \partial_i B \\ \partial_i B & 2(\partial_i\partial_j E - \Psi\delta_{ij}) \end{pmatrix}, \tag{62}$$

$$\delta g^V_{\mu\nu} = a^2 \begin{pmatrix} 0 & -S_i \\ -S_i & \partial_j F_i + \partial_i F_j \end{pmatrix}, \tag{63}$$

$$\delta g^T_{\mu\nu} = a^2 \begin{pmatrix} 0 & 0 \\ 0 & h_{ij} \end{pmatrix}, \tag{64}$$

where Φ, B, E, Ψ are scalar perturbations, S_i, F_i are divergence free vectors, i.e. $\partial^i S_i = \partial^i F_i = 0$ and the tensor perturbation h_{ij} is transverse-traceless, i.e. $h^i_i = \partial^i h_{ij} = 0$. Vector perturbations S_i, F_i decay with the universe expansion, for this reason we will ignore them in what follows. In general introducing a perturbation on the background might generate some ambiguity due to the unfixed gauge choice (corresponding to the choice of a coordinate system). A coordinate change can in fact introduce unphysical perturbations on the background. At the same time one can also perform a gauge transformation so to "hide" a physical perturbation. The solution is to construct gauge invariant perturbations that are independent of the coordinate choice. In (64) the tensor perturbation h_{ij} is gauge invariant. Under gauge transformation

$$x^\mu \to x^\mu + \xi^\mu, \tag{65}$$

the scalar metric perturbations transform as:

$$\Phi \to \Phi - \frac{a'}{a}\xi^0 - \left(\xi^0\right)', \tag{66}$$

$$B \to B + \xi_0 - \xi', \tag{67}$$

$$E \to E - \xi, \tag{68}$$

$$\Psi \to \Psi + \frac{a'}{a}\xi^0, \tag{69}$$

where in this case the $'$ denotes derivatives with respect to the conformal time τ and $\xi^i \equiv \delta^{ij}\xi_{,j}$. The perturbed stress-energy tensor takes the form [28]:

$$\delta T^\mu_\nu = \begin{pmatrix} -\delta\rho & -\left(\bar\rho + \bar P\right)a^{-1}(v^i - B^{,i} + S^i) \\ \left(\bar\rho + \bar P\right)a v_i & -\delta P\delta^i_j + \Sigma^i_j \end{pmatrix}, \tag{70}$$

where $\bar\rho, \bar P$ are the background energy density and pressure, v_i the fluid velocity, Σ^i_j the anisotropic stress. It can be shown that:

$$\delta\rho \to \delta\rho - \bar\rho'\xi^0, \tag{71}$$

$$\delta P \to \delta P - \bar P'\xi^0. \tag{72}$$

From this, one can build gauge-invariant perturbations, which are combinations of metric and matter perturbation. For example the curvature perturbation on uniform-density hypersurfaces:

$$\zeta \equiv -\Psi - \frac{aH}{\bar\rho'}\delta\rho, \tag{73}$$

which during slow-roll inflation becomes:

$$\zeta = -\Psi - \frac{aH}{\bar{\phi}'}\delta\phi. \tag{74}$$

One can show that when crossing the horizon, the gauge invariant perturbation ζ is conserved until horizon re-entry [29]. By introducing the Fourier transform of ζ:

$$\zeta_{\mathbf{k}} = \frac{1}{\sqrt{2\pi^3}} \int d^3k \; \zeta(\mathbf{x}) e^{-i\mathbf{k}\,\mathbf{x}}, \tag{75}$$

the correlation function of scalar perturbations ζ is computed as:

$$< \zeta_{\mathbf{k}} \zeta_{\mathbf{k'}} >= (2\pi)^3 \delta(\mathbf{k} + \mathbf{k'}) P_\zeta(k), \tag{76}$$

where $P_\zeta(k)$ is a function of the modulus k of the wave vector **k**. We also define:

$$\Delta_s^2(k) \equiv \Delta_\zeta^2(k) = \frac{k^3}{2\pi^2} P_\zeta(k), \tag{77}$$

$$n_s \equiv 1 + \frac{d\ln\Delta_s^2}{d\ln k}, \tag{78}$$

respectively the power spectrum of the scalar perturbations and the spectral index, which determines the scale dependence of the power spectrum. The power spectrum is usually approximated by a power-law:

$$\Delta_s^2(k) = A_s(k_*)\left(\frac{k}{k_*}\right)^{n_s(k_*)-1}, \tag{79}$$

where $A_s(k)$ is the amplitude of the scalar perturbations and k_* an arbitrary reference scale. If ζ is gaussian, like in single field slow-roll [30, 31], then the power spectrum encodes all the statistical information about the perturbations. The same can be done for the two polarizations of the tensor perturbations h_{ij}:

$$< h_{\mathbf{k}} h_{\mathbf{k'}} >= (2\pi)^3 \delta(\mathbf{k} + \mathbf{k'}) P_h(k). \tag{80}$$

We also define:

$$\Delta_t^2(k) \equiv 2\Delta_h^2(k) = \frac{k^3}{\pi^2} P_h(k), \tag{81}$$

$$n_t \equiv \frac{d\ln\Delta_t^2}{d\ln k}, \tag{82}$$

$$\Delta_t^2(k) = A_t(k_*)\left(\frac{k}{k_*}\right)^{n_t(k_*)}, \tag{83}$$

where the tensor power spectrum Δ_t^2 counts the two independent polarizations of h_{ij}, n_t is the spectral index of the tensor power spectrum, and $A_t(k_*)$ is the amplitude of tensor perturbations evaluated at the pivot scale k_*. We also define the tensor-to-scalar ratio:

$$r \equiv \frac{\Delta_s^2(k_*)}{\Delta_t^2(k_*)}. \tag{84}$$

The quantities r, n_s, A_s, n_t, A_t represent the main observables for testing the inflationary scenario. In order to relate these quantities with slow-roll parameters, we start from the

Mukhanov equation (here we just show the results, for the full computation see for example section 11 of [28]):

$$v_k'' + \left(k^2 - \frac{z''}{z}\right) v_k = 0, \tag{85}$$

where $z = \frac{a\dot{\phi}}{H}$ and v_k is the Fourier transform of the Mukhanov variable $v = z\zeta$. After quantizing v_k one can compute the scalar power spectrum of the quantized field as:

$$\Delta_s^2 = \frac{H_*^4}{(2\pi)^2 \dot{\phi}_*^2}, \tag{86}$$

where quantities are evaluated at horizon crossing. The modes will freeze to this values until they re-enter the horizon [28] (of course different values of k will exit the horizon at different $k_* = a_* H_*$ values). A similar procedure can be followed to compute the tensor power spectrum:

$$\Delta_t^2 = \frac{2H_*^2}{\pi^2}. \tag{87}$$

The CMB coefficients of the angular power spectrum can be related to the computed power spectrums as [32]:

$$C_l^{\mathrm{TT}} = \frac{2}{\pi} \int dk k^2 P_\zeta(k) f_T^2(k), \tag{88}$$

where f_T is the transfer function that relates the invariant curvature perturbations ζ with the temperature fluctuations δT:

$$a_{lm} = 4\pi(-i)^l \int \frac{d^3k}{(2\pi)^3} f_T(k) \zeta_{\mathbf{k}} Y_{lm}(\hat{\mathbf{n}}). \tag{89}$$

Similar expressions can be obtained for the other coefficients, by using the appropriate transfer functions. While $C_l^{TT}, C_l^{TE}, C_l^{EE}$ all depend on P_ζ, the coefficients C_l^{BB} depend on $P_h(k)$ which then represents the only source of information about tensor modes generated during inflation.

Now that we related the background primordial fluctuations with observables quantities in the CMB, we can proceed with computing the relevant observables r, n_s, n_t in the single field slow-roll approximation. First of all we can explicitly compute from (86),(87) that:

$$r \equiv \frac{\Delta_s^2}{\Delta_t^2} = 16\epsilon(N_*), \tag{90}$$

where N_* is the number of e-folds between the time at which the pivot scale leaves the horizon and the end of inflation. One can compute as well:

$$n_s \equiv 1 + \frac{d\ln\Delta_s^2}{d\ln k} = 1 + 2\eta(N_*) - 4\epsilon(N_*), \tag{91}$$

$$n_t \equiv \frac{d\ln\Delta_t^2}{d\ln k} = -2\epsilon(N_*). \tag{92}$$

By recalling that $\epsilon \sim \epsilon_V$ and $\eta \sim \eta_V - \epsilon_V$ during slow-roll we recover that:

$$r = 16\epsilon_V(\phi_*), \tag{93}$$
$$n_s = 1 + 2\eta_V(\phi_*) - 6\epsilon_V(\phi_*), \tag{94}$$
$$A_s = \frac{V(\phi_*)}{24\pi^2\epsilon_V(\phi_*)}, \tag{95}$$
$$n_t = -2\epsilon_V(\phi_*), \tag{96}$$
$$A_t = \frac{2V(\phi_*)}{3\pi^2}, \tag{97}$$

with ϕ_* such that:

$$N_* = \int_{\phi_{\text{end}}}^{\phi_*} \frac{d\phi}{\sqrt{2\epsilon(\phi)}}.$$

Notice in particular the consistency relation $r = -8n_t$ holds for single field slow-roll inflation.
Let us now summarize. Equations (56),(55),(93)-(97) allow us to compute observables for inflation just from the scalar field potential $V(\phi)$. Those observables are related to the power spectra of scalar and tensor field perturbations (77),(81) generated during inflation. Those perturbations affect the temperature fluctuations δT and the E, B-modes in the CMB. By measuring those fluctuations in the CMB we can then directly constraint (90)-(92). All quantities have to be computed and measured at some pivot scale $\bar{k}$. For this thesis, for the Planck+Bicep/Keck and for the Planck+ACT dataset the chosen pivot scale is $\bar{k} = 0.05$ Mpc^{-1}. As of today there has no been direct observation of the tensor perturbations, only upper bounds have been found by CMB observations. The scalar perturbations have instead been measured. The latest combination of Planck+Bicep/Keck Array dataset gives [6, 5]:

$$r < 0.036, \tag{98}$$
$$n_s = 0.9651 \pm 0.0088, \tag{99}$$
$$A_s = (2.10 \pm 0.10) \cdot 10^{-9}, \tag{100}$$

at 2σ confidence level, the Planck+ACT dataset [8] gives[7]:

$$r < 0.047, \tag{101}$$
$$n_s = 0.9739 \pm 0.0068. \tag{102}$$

As a final remark notice that the inflationary observables are all dependent on the quantity N_* which depends on the inflationary energy, the reheating mechanism and the history of the evolution of the Universe. We will compute its value explicitly in the next section.

[7] Most of the results discussed in our papers were derived before the availability of the Planck+ACT dataset. In a recent paper the possibility of a BAO-CMB tension in the ACT analysis has been considered [33]. There, it is shown how the increase in n_s is a consequence of including the DESI BAO measurements in the analysis. Indeed there is currently a $\approx 3\sigma$ tension between the cosmological parameters inferred from CMB observations and the DESI BAO ones. Since with the current data it is not possible to resolve this tension, we consider in what follows both the Planck+Bicep/Keck Array dataset and the Planck+ACT dataset.

3.5 Number of e-folds

We saw in the previous section that the observables r, n_s, A_s ecc. all depend on the specific value of N_* i.e. the number of e-folds between the time at which the pivot scale $\bar{k} = 0.05$ Mpc^{-1} leaves the horizon and the end of inflation. It is then of fundamental importance to carefully compute the value N_* considering the full evolution of the Universe. Let's consider the comoving scale of the horizon $d_H(t)$ and remember that $d_H(t) \propto a$. We have that:

$$\frac{d_H(t_{\bar{k}})}{d_H(N_*)} = \frac{t_{\bar{k}}}{H_*^{-1}} = \frac{a_{\bar{k}}}{a_*} = \frac{a_{\rm end}}{a_*}\frac{a_{\rm reh}}{a_{\rm end}}\frac{a_{\rm eq}}{a_{\rm reh}}\frac{a_{\bar{k}}}{a_{\rm eq}}, \tag{103}$$

where $a_*, a_{\rm end}, a_{\rm reh}, a_{\rm eq}, a_{\bar{k}}$ are the scale factors respectively at horizon exit, at the end of inflation, at time of reheating, at time of radiation-matter equivalence and at horizon re-entry. The number of $e-$folds is then given by:

$$e^{N_*} \equiv \frac{a_{\rm end}}{a_*} = H_* t_{\bar{k}} \left(\frac{a_{\rm end}}{a_{\rm reh}}\right)\left(\frac{a_{\rm reh}}{a_{\rm eq}}\right)\left(\frac{a_{\rm eq}}{a_{\bar{k}}}\right). \tag{104}$$

Now considering $\rho \sim a^{-3(1+w)}$, $a(t) \sim 1/T$ during radiation domination and $a \sim t^{2/3}$ during matter domination we have:

$$N_* \equiv \ln\left(\frac{a_{\rm end}}{a_*}\right) = \ln\left(H_* t_{\bar{k}}\right) + \frac{1}{3(1+w)}\ln\left(\frac{\rho_{\rm reh}}{\rho_{\rm end}}\right) + \ln\left(\frac{T_{\rm eq}}{T_{\rm reh}}\right) + \frac{2}{3}\ln\left(\frac{t_{\rm eq}}{t_{\bar{k}}}\right). \tag{105}$$

We can compute $\rho_{\rm reh}$ using the well-known expression of the energy density for relativistic particles:

$$\rho_{\rm reh} = \frac{\pi^2 g_{\rm reh}}{30} T_{\rm reh}^4, \tag{106}$$

where $g_{\rm reh}$ is the number of relativistic degrees of freedom at reheating, and by considering that $\dot{\phi}^2 \ll V$ during inflation, while $\dot{\phi}^2 = V$ at the end of inflation [8] we can write:

$$\rho_{\rm end} = \frac{3}{2} V_{\rm end}, \quad 3H_*^2 \simeq V_*. \tag{107}$$

Using $t_{\rm eq} \approx 5 \cdot 10^4$ years, $T_{\rm eq} = 2.6$ eV we get:

$$N_* \simeq 55.5 + \frac{1-3w}{12(1+w)}\ln\left(\frac{\pi^2 g_{\rm reh}}{30}\right) - \frac{1-3w}{3(1+w)}\ln\left(\frac{V_{\rm end}^{1/4}}{T_{\rm reh}}\right) + \frac{1}{2}\ln\left(\frac{V_*}{V_{\rm end}}\right) + \ln\left(\frac{V_{\rm end}^{1/4}}{10^{16}{\rm GeV}}\right) \tag{108}$$

For typical inflation scenarios at scales $\approx 10^{16}$ GeV we get $N_* \approx 50 - 60$ if radiation domination starts right after inflation, while $N_* \approx 60 - 70$ if we have a period of kination (i.e. a period in which the scalar field kinetic term is the dominant source of energy density) before radiation domination (like in the case of quintessential inflation see, chapter 5).

3.6 Models of inflation

We finally have all the tools to compute the results of inflationary models. In this section we briefly review the most popular models. We start with the simplest models of inflation i.e. chaotic inflation and show its incompatibility with current observations. We then move to explore the most popular and minimalistic models: Starobinksy [21] and Higgs inflation [20].

[8] This follows from (49) by imposing $w_\phi = -1/3$ (we remind that a dominant barotropic fluid implies acceleration of the universe if $-1 < w < -1/3$ as a consequence of the Second Friedmann equation).

3.6.1 Chaotic inflation

The first attempt is to model inflation with a simple chaotic potential:

$$V(\phi) = \lambda_k \phi^k, \tag{109}$$

with k an integer number. In this case we have:

$$\epsilon_V = \frac{k^2}{2\phi^2}, \tag{110}$$

$$\eta_V = \frac{k(k-1)}{\phi^2}, \tag{111}$$

$$N = \frac{\phi^2}{2k} - \frac{\phi_{\text{end}}^2}{2k}, \tag{112}$$

and by neglecting the contribution of ϕ_{end} to the number of $e-$folds the CMB observables read:

$$r = \frac{4k}{N_*}, \tag{113}$$

$$n_s = 1 - \frac{k+2}{2N_*}, \tag{114}$$

$$A_s = \frac{(2k)^{\frac{k}{2}-1}}{3\pi^2} \lambda N_*^{\frac{k}{2}+1}. \tag{115}$$

This predicts $r = 0.267$, $n_s = 0.95$ for $k = 4$ and for $r = 0.134$, $n_s = 0.967$ for $k = 2$, which are excluded by current measurement as they predict a tensor-to-scalar ratio way above the current bounds. Since the simplest models do not work one could think of constructing more complicated actions to generate potentials that give viable predictions. Two popular options in the context of modified gravity are: 1) adding a non-minimal coupling between the scalar field and gravity, 2) add higher order contractions of the Riemann tensor in the gravitational sector. In the following we briefly review both cases through two of the most popular models: Higgs inflation e Starobinsky inflation.

3.6.2 Starobinsky inflation

The first option is to consider higher-order contractions of the Riemann tensor in the action. A popular model is Starobinsky inflation. Consider the Jordan frame action[9]:

$$S = \int d^4x \sqrt{-g} \left(\frac{1}{2} R + \alpha R^2 \right). \tag{116}$$

with α a dimensionless coupling. Although not manifestly, this action is equivalent to GR plus a scalar field. In order to see this, consider the dynamically equivalent action:

$$S = \frac{1}{2} \int d^4x \sqrt{-g} \big(F(\phi) + F'(\phi)(R - \phi) \big), \tag{117}$$

[9] The Jordan frame is the frame in which the original action is formulated. The frame in which the metric is minimally coupled to the matter action and gravity is described by an Einstein-Hilbert term is called instead Einstein frame. The two formulations are equivalent as long as it is possible to define the Einstein frame and proper inflationary observables. See for example [34] and references therein.

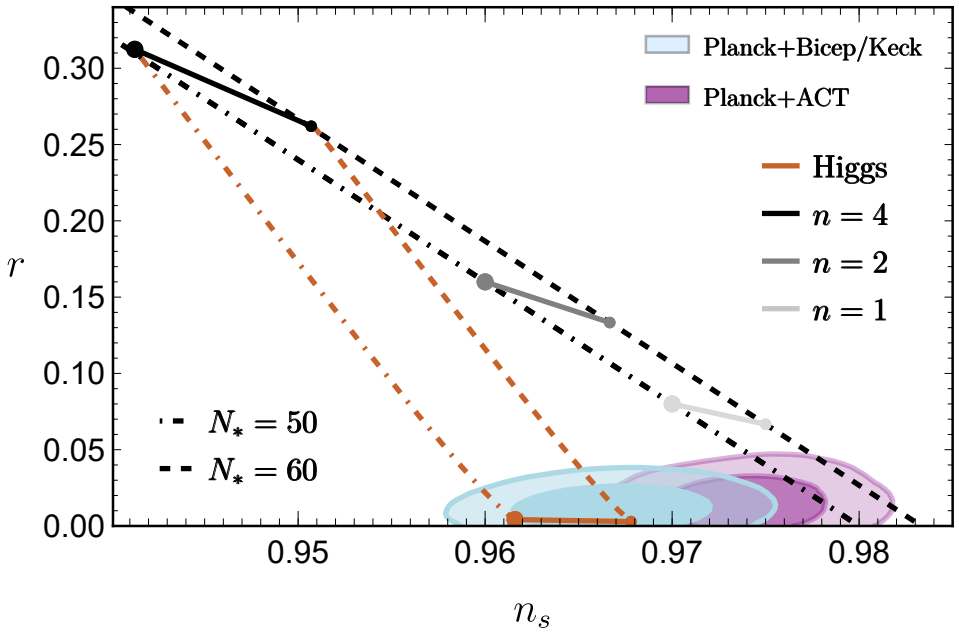

Figure 2: r vs. n_s for the chaotic model with general n at $N_* = 50$ (black dot-dashed line), $N_* = 60$ (black dashed line). Specific values are explicitly shown for $n = 4$ (black thick), $n = 2$ (gray) and $n = 1$ (light gray). The orange thick line is the prediction for Higgs (which is the specific case of non-minimally coupled quartic potential with $\lambda = 0.26$) and Starobinsky inflation between 50 and 60 $e-$folds. Moreover, the non-minimally coupled quartic model is shown for $N_* = 50$ (orange dot-dashed line), $N_* = 60$ (orange dashed line). Large dots correspond to $N_* = 50$, small dots to $N_* = 60$. We see that in that the strong coupling limit the quartic non-minimally coupled model matches Higgs and Starobinsky predictions. The light blue areas represent the $1,2\sigma$ allowed regions coming from the Planck+Bicep/Keck dataset. The purple areas represent the $1,2\sigma$ allowed regions coming from the Planck+ACT dataset. The Starobinsky/Higgs model is disfavored at $\gtrsim 2\sigma$ confidence level if we consider the Planck+ACT dataset.

with $F(\phi) = \phi + 2\alpha\phi^2$. By taking the variation with respect to ϕ we straightforwardly see that $F''(\phi)(R-\phi) = 0$, hence the actions are equivalent for $F''(\phi) \neq 0$. By performing a conformal transformation of the metric $g_{\mu\nu} \to \Phi g_{\mu\nu} = F'(\phi) g_{\mu\nu}$ we get:

$$S = \int d^4x\sqrt{-g}\left[\frac{R}{2} - \frac{3}{2}g^{\mu\nu}\frac{\partial_\mu\Phi\partial_\nu\Phi}{\Phi^2} - \frac{(\Phi-1)^2}{8\alpha\Phi^2}\right]. \tag{118}$$

We now define the canonical scalar field:

$$\frac{\partial\phi}{\partial\Phi} = \frac{\sqrt{3}}{\Phi}, \tag{119}$$

which implies the relation:

$$\phi = \sqrt{3}\ln\Phi. \tag{120}$$

In terms of the canonical scalar, the action takes the form:

$$S = \int d^4x\left[\frac{1}{2}R - \frac{1}{2}\partial^\mu\phi\partial_\mu\phi - U(\phi)\right], \tag{121}$$

with

$$U(\phi) = \frac{1}{8\alpha}\left(1 - e^{-\sqrt{2/3}\phi}\right)^2. \tag{122}$$

This potential predicts slow-roll parameters (in the large field $\phi \gg 1$ limit):

$$\epsilon_V \sim \frac{4}{3}e^{-2\sqrt{2/3}\phi}, \tag{123}$$

$$\eta_V \sim -\frac{4}{3}e^{-\sqrt{2/3}\phi}, \tag{124}$$

$$N \sim \frac{3}{4}e^{\sqrt{2/3}\phi} - \frac{3}{4}e^{2/3\phi_{\text{end}}}, \tag{125}$$

which, in the $N_* \gg 1$ approximation and neglecting the contribution from ϕ_{end}, give the CMB observables:

$$r \sim \frac{12}{N_*^2}, \tag{126}$$

$$n_s \sim 1 - \frac{2}{N_*}, \tag{127}$$

$$A_s \sim \frac{N_*^2}{144\alpha}. \tag{128}$$

The results are shown in Fig.2 It can be noticed how with the previous Planck+Bicep/Keck Array analysis Starobinsky inflation is extremely favored predicting both r, n_s well inside the 2σ bounds. This is not anymore the case if we include the latest DESI and ACT data for which Starobinsky inflation at 60 $e-$fold becomes disfavored at $\approx 2\sigma$ confidence level.

3.6.3 Higgs inflation

Consider the Standard Model action with a non-minimal coupling between the Higgs field and the Ricci scalar:

$$S_{\text{tot}} = \int d^4x\sqrt{-g}\left(\frac{M^2}{2}R + \xi H^+ HR + \mathscr{L}_{SM}\right), \tag{129}$$

where ξ is a dimensionless coupling. By choosing the unitary gauge and neglecting gauge interactions we can rewrite the simplified action as:

$$S = \int d^4x\sqrt{-g}\Big(\frac{M^2+\xi h^2}{2}R - \frac{1}{2}\partial_\mu h\partial_\nu h - \frac{\lambda}{4}(h^2-v^2)^2\Big), \tag{130}$$

where the condition $M_P^2 = M^2 + \xi v^2$ holds, with v the vacuum expectation value of the Higgs field. By setting $\xi = 0$ we do not get viable inflationary predictions since during inflation $h^2 \gg v^2$ and the potential reduces to quartic potential $k = 4$ of section 3.6.1. Let's see how the non-minimal coupling affects the predictions of tree-level Higgs inflation. By performing a conformal transformation $g_{\mu\nu} \to \Omega^2 g_{\mu\nu}$, $\Omega^2 = M^2 + \xi h^2$ we can rewrite the action in the so-called Einstein frame:

$$S = \int d^4x\sqrt{-g}\Big(\frac{1}{2}R - \frac{1}{2}g^{\mu\nu}\partial_\mu\chi\partial_\nu\chi - U(\chi)\Big), \tag{131}$$

where

$$U(\chi) = \frac{1}{\Omega^4(\chi)}\frac{\lambda}{4}\big(h^2(\chi)-v^2\big)^2, \tag{132}$$

$$\frac{d\chi}{dh} = \sqrt{\frac{\Omega^2+6\xi^2h^2}{\Omega^4}}. \tag{133}$$

In the large field limit, (or equivalently in the strong coupling limit) $h \gg 1/\sqrt{\xi}$ the Einstein frame potential $U(\chi)$ can be approximated by:

$$U(\chi) = \frac{\lambda}{4\xi^2}\Big(1 - e^{-\sqrt{2/3}\chi}\Big)^2. \tag{134}$$

After identification $4\xi^2/\lambda = 8\alpha$ the potential is the same as (122). By fixing λ to its observed value $\lambda \simeq 0.26$ [19], we recover the same observables (126)-(128) and again $r \approx 0.0034, n_s \approx 0.967$ at $N_* = 60$. If we instead leave λ unconstrained we obtain the result for a general non-minimally coupled quartic scalar potential. We show in Fig.2 the predictions for this case. The dot-dashed ($N_* = 50$) and dashed ($N_* = 60$) lines are obtained by varying ξ. We see that the case $\xi = 0$ coincides with the standard quartic chaotic inflation, while the strong coupling limit $\xi \to \infty$ is given by the Starobinsky/Higgs model. It can be noticed how with the previous Planck+Bicep/Keck Array analysis non-minimally coupled Higgs inflation is extremely favored predicting both r, n_s well inside the 2σ bounds. This is not anymore the case if we include the latest DESI and ACT data for which Higgs inflation at $60e-$fold becomes disfavored at a $\approx 2\sigma$ confidence level.

4 Quintessence

In this chapter a dynamical alternative to the cosmological constant is discussed, modeled in terms of a scalar field, which goes under the name of quintessence. First the general scalar field dynamics is discussed and later the most popular models of quintessence, i.e. exponential and inverse-power-law, are briefly reviewed.

ΛCDM represents the current cosmological Standard Model. As discussed in section 2.3 the model aims to describe the evolution of the Universe considering several contributions to the energy-density of the Universe: dark-energy represented by the cosmological constant Λ, Cold Matter further distinguished in dark matter and baryonic matter and a radiation component (see Fig.1). However, considering a cosmological constant rises the issue of fine tuning. Indeed, the so called cosmological constant problem requires a fine tuned cancellation of the contribution of the vacuum energy of quantum fields. This cancellation should leave a $\rho_\Lambda \approx 10^{-120}$ contribution that would represent the observed energy density of dark-energy today. For this reason one good option is to consider an unknown symmetry of nature such that $\Lambda = 0$ exactly. Then in order to predict the currently dominating source of energy density a dynamical source can be considered. A popular example is that of quintessence, a scalar field existing as a spectator field during the whole evolution of the Universe which starts dominating only at recent times. A viable quintessence model that aims to describe dark-energy needs to satisfy two conditions: the first is that $-1 \leq w_\phi < -\frac{1}{3}$ in order to ensure the Universe is accelerating, second it needs to become dominant at late times while being subdominant during radiation and matter domination. We now see how we can achieve these features by means of a scalar field.

4.1 Scalar field dynamics

Consider the action in (44). The scalar field obeys the Friedmann equation (45) and the Klein-Gordon equation (46). Its energy density ρ_ϕ, pressure P_ϕ and barotropic parameter w_ϕ are described by (47)-(49). In order to have a dark-energy phase we need the mass of the scalar field at present days to be very small and satisfy the condition $m^2 \equiv V''(\phi)$, $m \lesssim H_0 \approx 10^{-33}$ eV [35].
The first possible scenario is the case in which $m^2 \ll H_0^2$, where we recall H_0 is the Hubble parameter measured today. We will now prove that if this happens while the scalar field is subdominant then the field will freeze at value ϕ_F instead of slow-rolling (like during inflation) and only unfreeze when it becomes the dominant source of energy density in the recent past. This type of quintessence is called *thawing* quintessence. Indeed, consider a universe dominated by a background fluid such that $-1 < w_B < 1$. In the slow-roll limit, from the Klein-Gordon equation (46), we have $3H\dot{\phi} \sim -V'(\phi)$. If we Taylor expand around ϕ_F we can write $V'(\phi) \sim V''(\phi_F)\phi \equiv m^2\phi$. Hence, the scalar field equation (46) in a background dominated universe gives:

$$\frac{\dot{\phi}}{\phi} \sim -\frac{1+w_B}{2} m^2 t, \tag{135}$$

where we used that:

$$H(t) = \frac{2}{3(1+w_B)\,t}, \tag{136}$$

for a universe dominated by a background fluid with barotropic parameter w_B. By direct integration we get:

$$\phi(t) = \phi_F \; e^{-(1+w_B)\frac{m^2 t^2}{4}}, \tag{137}$$

where we are assuming $t \gg t_i$ with t_i being some initial time. Now since we are assuming the condition $V''(\phi_F) \ll H^2(t)$ we have that

$$\frac{1}{4}(1+w_B)m^2t^2 \ll \frac{1}{9(1+w_B)} < 1, \tag{138}$$

which implies from (137) $\phi \sim \phi_F$ as long as the scalar field is subdominant and $V''(\phi_F) \ll H(t)^2$. Notice that since $H(t)$ decreases with time it is sufficient to satisfy $V''(\phi_F) < H_0^2$ to enforce $m^2 < H(t)$ at all times. Of course the scalar field value ϕ_F has to be justified somehow, so to solve the coincidence problem i.e. the requirement that the scalar field energy density predicts the observed value the dark-energy energy density [4]:

$$\rho_\phi \sim V(\phi_0) \sim V(\phi_F) = (7.15 \pm 0.19) \cdot 10^{-121} \approx 7 \cdot 10^{-121}. \tag{139}$$

This can be done for example by models of quintessential inflation which we will consider in chapter 5.

There is however another possibility. The field might have been steadily slow-rolling down the potential, which becomes shallower at late times, while satisfying the condition $V'' \sim H^2(t)$ at all times. This type of quintessence is called *freezing*. In order to have a satisfying model we would like our scalar field to behave as dark-energy at late times independently of the specific choice of initial conditions. This can indeed be achieved by freezing models. In this case, the evolution of the field gradually slows down as the potential becomes shallower at late times and the scalar field follows an attractor behavior. To understand how this behavior emerges for a subdominant quintessence field, it is useful to introduce two dimensionless parameters (we recall that $M_P = 1$):

$$\lambda = -\frac{V'}{V}, \qquad \gamma = \frac{V''V}{(V')^2}. \tag{140}$$

Consider now the time derivative of λ written in terms of λ and γ:

$$\dot{\lambda} = -\dot{\phi}\lambda^2(\gamma - 1). \tag{141}$$

Now consider a general potential V. If $V' < 0$ then $\dot{\phi} > 0$ while the field ϕ moves to higher values in order to minimize the potential. In this case then $\lambda > 0$, but $\dot{\phi} > 0$ implying $\dot{\lambda} < 0$, leading to $\lambda \to 0$ if $\gamma > 1$. Alternatively, if $V' > 0$, then $\dot{\phi} < 0$ as the field ϕ moves to lower values in order to minimize the potential. In this case then $\lambda < 0$, but $\dot{\phi} < 0$ implies $\dot{\lambda} > 0$, which leads to $\lambda \to 0$, if we have again $\gamma > 1$. The case in which $\gamma > 1$ is called *tracking freezing* quintessence. The limiting case for which $\gamma = 1$ is called *scaling freezing* quintessence. We now show how having a tracking quintessence automatically leads to a scalar field dominated universe at late times. By computing the time derivative of (49) and using (140) we can compute:

$$\dot{w}_\phi = \frac{2V}{\rho_\phi^2}\left(\dot{\phi}\ddot{\phi} + \frac{1}{2}\lambda\dot{\phi}^3\right), \tag{142}$$

then by considering (46) we have:

$$\dot{w}_\phi = (1 - w_\phi)\dot{\phi}\left(\lambda - \frac{3H\dot{\phi}}{\rho_\phi}\right). \tag{143}$$

Finally, using the First Friedmann equation for the scalar field (45) we can get the expression:

$$\dot{w}_\phi = H(1 - w_\phi)\left(-3(w_\phi + 1) + \lambda\sqrt{3\Omega_\phi(w_\phi + 1)}\right), \tag{144}$$

where

$$\Omega_\phi = \frac{\rho_\phi}{\rho}, \tag{145}$$

is the scalar field density parameter and ρ, ρ_ϕ the total energy density of the universe and the energy density of the scalar field respectively. Since we are discussing attractor solutions, we require $-1 < w_\phi < 1$ to be a constant, i.e. $\dot{w}_\phi \approx 0$. This implies:

$$\Omega_\phi = \frac{3}{\lambda^2}(w_\phi + 1). \tag{146}$$

Clearly for tracking quintessence as $\lambda \to 0$ we will end up with a scalar field dominated solution. By taking the time derivative of (145) and using the continuity equation (19) for the scalar field and the background fluid we compute that

$$\dot{\Omega}_\phi = 3H(w_\phi - w_B)\Omega_\phi(\Omega_\phi - 1), \tag{147}$$

while we have from (140)

$$\dot{\Omega}_\phi = -\frac{2\dot{\lambda}}{\lambda}\Omega_\phi, \tag{148}$$

which substituted into (147) implies:

$$(w_\phi - w_B)(\Omega_\phi - 1) = 2(1 + w_\phi)(\gamma - 1). \tag{149}$$

In particular considering that quintessence is subdominant during most the evolution of the Universe (i.e. $\Omega_\phi \ll 1$) we have from the equation above that:

$$w_\phi = \frac{w_B - 2(\gamma - 1)}{2\gamma - 1}. \tag{150}$$

From (149) we see that, in general, when the scalar field finally starts dominating ($\Omega_\phi \approx 1$), it will have $w_\phi \approx -1$. In the case of scaling quintessence $\gamma = 1$, we see from (141) that λ is constant, which implies that, in general, the scalar field will remain subdominant with a constant Ω_ϕ and $w_\phi = w_B$ mimicking the background fluid. This is the case of exponential quintessence which we are going to analyze in the next section.
Notice the difference between freezing and thawing quintessence. In the former case the field is steady-rolling and eventually follows the attractor behavior independently of the choice of initial conditions. In the latter, the frozen field never hits the attractor behavior and only starts evolving when quintessence becomes dominating and the field slow-rolls along the potential. Unlike freezing models, thawing quintessence needs to be fine tuned to solve the coincidence problem i.e. initial conditions needs to be explained. In the following we will explicitly discuss examples for all those types of quintessence focusing on the two most popular models: exponential and inverse power-law quintessence.

4.2 Exponential quintessence

Consider an action in the form (44) with a scalar potential given by:

$$V(\phi) = V_0 e^{-\lambda\phi}, \tag{151}$$

with V_0, λ positive constants. Let's first consider the case in which the scalar field is dominant. For this potential, the attractor solution is given by:

$$V = \frac{2(6 - \lambda^2)}{\lambda^2}\frac{1}{\lambda^2 t^2}, \tag{152}$$

$$\frac{1}{2}\dot{\phi}^2 = \frac{2}{\lambda^2 t^2}, \tag{153}$$

which is an exact solution for the Klein-Gordon equation as it can be verified by inspection, plugging the expressions in (46). From (20), it follows immediately that $H(t) = 2\lambda^{-2}t^{-1}$ and $\omega_\phi = -1 + \lambda^2/3$ which implies that accelerated expansion happens for $\lambda < \sqrt{2}$. By using the First Friedmann equation (20) and (152),(153) we compute that:

$$\frac{V''}{H^2} = \frac{1}{2}\lambda^2(6-\lambda^2), \tag{154}$$

which is a constant, i.e. the field is steady-rolling along the potential. Now consider the case in which the background is dominant and the scalar behaves as a spectator field. In this case the attractor solution is given by:

$$V = \frac{2(1-w_B)}{1+w_B}\frac{1}{\lambda^2 t^2}, \tag{155}$$

$$\frac{1}{2}\dot{\phi}^2 = \frac{2}{\lambda^2 t^2}. \tag{156}$$

From (47),(48), one then immediately computes:

$$\rho_\phi = \frac{4}{1+w_B}\frac{1}{\lambda^2 t^2}, \tag{157}$$

$$\rho = \frac{4}{3(1+w_B)^2}\frac{1}{t^2}, \tag{158}$$

which straightforwardly gives:

$$\Omega_\phi = \frac{3(1+w_B)}{\lambda^2}, \tag{159}$$

and we notice immediately that, since λ is constant, this case corresponds to the scaling freezing quintessence model mentioned in the previous section. From (155), (156) we can immediately notice that also in the subdominant case the field is steady-rolling along the potential since:

$$\frac{V''}{H^2} = \frac{9}{2}(1-w_B^2). \tag{160}$$

Comparing (146) with (159) we see that $w_\phi = w_B$ and Ω_ϕ remains always a fraction of the total energy density. This means that the exponential potential (151) can never successfully describe dominant dark-energy. A simple solution can be obtained by considering a double exponential [36]:

$$V(\phi) = V_1 e^{-\lambda_1\phi} + V_2 e^{-\lambda_2\phi}, \tag{161}$$

with $\lambda_1 > \lambda_2$. The first term will be important in early evolution, while the second will dominate at late times. Initially, the behavior will be driven by the attractor solution of the first exponential behaving as scaling freezing quintessence with $w_\phi = w_B$. The scaling behavior is then abandoned as soon as the second exponential term becomes important. This will terminate the scaling behavior and finally lead to scalar field domination with $w = -1+\lambda_2^2/3$. The current bounds from BBN [4] constrain $\Omega_\phi < 0.045$ at the time of primordial nucleosynthesis, while the observational bounds on dark-energy give $w < -0.95$ at 2σ confidence level [4]. This translates to $\lambda_1 > 9.4$ and $\lambda_2 < 0.4$. The main issue with this scenario is that V_1 still needs to be fine-tuned to a scale which is close to the cosmological constant energy in order to match the observed energy density of the Universe. This might be considered unsatisfying given the whole purpose of introducing a scalar field was to solve the coincidence problem. Exponential quintessence can however still work for $\lambda \ll \sqrt{2}$ if the field evolution never hits the attractor. This happens if the field freezes at a

value ϕ_F and only unfreezes when becoming dominant. In this case we will have thawing quintessence which, we recall, needs to have an explanation for the initial condition ϕ_F (which can be done for example with models of quintessential inflation as we are going to discuss in chapter 5).

4.3 Inverse Power-Law quintessence

An alternative to exponential quintessence is the inverse-power law potential given by:

$$V(\phi) = \frac{M^{q+4}}{\phi^q}, \tag{162}$$

with $q, M > 0$ constants. By using the definition of γ in (140), we see that we recover a tracking quintessence model if:

$$\gamma = \frac{q+1}{q} > 1, \tag{163}$$

which is trivially always true for any $q > 0$. The general attractor solution is given by:

$$V = \left(\frac{4(q+2) - 2q(1+w_B)}{q(q+2)^2(1+w_B)}\right)^{\frac{q}{q+2}} M^{\frac{2(q+4)}{q+2}} t^{-\frac{2q}{q+2}}, \tag{164}$$

$$\frac{\dot\phi^2}{2} = \frac{2}{(q+2)^2}\left(\frac{4(q+2) - 2q(1+w_B)}{q(q+2)^2(1+w_B)}\right)^{-\frac{q}{q+2}} M^{\frac{2(q+4)}{q+2}} t^{-\frac{2q}{q+2}}, \tag{165}$$

which can be straightforwardly checked to be an exact solution of the Klein-Gordon equation (46). From (164),(165) and using the First Friedmann equation one can straightforwardly compute that the tracker obeys:

$$\frac{V''}{H^2} = \frac{9(q+1)(1+w_B)\big(4(q+2) - 2q(1+w_B)\big)}{4(q+2)^2}, \tag{166}$$

which of course is a constant, implying as expected that steady-roll is happening on the attractor solution. Unfortunately, as we see from (150), (163) the model also predicts:

$$w_\phi = \frac{q w_B - 2}{q+2}, \tag{167}$$

which is in general not good for reasonable potentials. In order to satisfy the observational bound $w_\phi < -0.95$ and match the observed value of energy density of dark-energy we would in fact need $q < 0.1$ and $M < 10^{-11}$GeV for a matter dominated background $w_B = 0$. This makes the tracking model not very realistic and unlikely to bring to a viable dark-energy scenario.
Inverse power-law can however work in case of thawing quintessence. In this case in fact the field will unfreeze only after it becomes dominant and will start slow-rolling along the potential. From the slow-roll KG equation $3H\dot\phi \sim -V'$ and plugging in (164),(165) we get:

$$\dot\phi^2 \phi^{q+2} \sim \frac{q^2}{3} M^{q+4}, \tag{168}$$

and by using the expression of the barotropic parameter (49) we have:

$$w_\phi = \frac{q^2 - 6\phi^2}{q^2 + 6\phi^2}, \tag{169}$$

implying $\phi_0 > 2.55q$ today, if we want to satisfy the observational constraint $w_\phi < -0.95$. At the same time if we want to solve the coincidence problem, we require that $V(\phi_0) = M^{q+4}\phi_0^{-q} \sim M^{q+4}\phi_F^{-q} \approx 7 \cdot 10^{-121}$.
This happens only if the tracker is never reached which in turns requires fine tuning on the choice of ϕ_F. Again we will see in the next chapter how quintessential inflation can fix the value to ϕ_F through inflation.

5 Quintessential inflation

In this chapter the author considers quintessential inflation as a way to model both early and late time acceleration of the Universe expansion. We first describe the general features going from inflation to kination, passing through reheating and radiation domination and finally to matter domination and dark-energy. Later, the focus is moved to two popular models of quintessential inflation: the Peebles-Vilenkin potential [37] and the quintessential α-attractors [38].

We saw in chapter 3 and 4 that inflation and dark-energy can be both described in terms of a scalar field. Indeed both phases describe an accelerating expansion of the Universe which is driven by the potential of the scalar field. It is only natural then to try explaining both phenomena with a single scalar degree of freedom. The main difference and main obstacle are the energy scales at which the two take place. Inflation has a typical energy scale of $\approx 10^{16}$ GeV while dark-energy in the present day has an energy-density $\approx 10^{-12}$ GeV. This is a gap of almost 30 orders of magnitude that needs to be explained if one wants to adopt a single scalar field to predict both early and late Universe acceleration. This is the aim of models of quintessential inflation. The great advantage of this kind of models is that they only need one set of initial conditions at inflation. The quintessential behavior, will be naturally determined by the inflationary attractor properties.
We show a typical example of evolution of the barotropic parameter (Fig. 3) and the energy densities (Fig. 4) for the scalar, radiation and matter fluid. In the early Universe the scalar field is dominated by the potential $V(\phi)$ and drives inflation. While the scalar field slow-rolls it will acquire kinetic energy by moving down the potential and inflation will eventually end. At this point standard inflationary models usually provide an oscillatory reheating mechanism. The inflaton reaches the minimum of the potential and starts oscillating around it. Its energy is transferred through a direct coupling between the inflaton and the SM particles. This cannot happen in models of quintessential inflation as the scalar field needs to survive until present days to behave as dark-energy. Hence, in the case of quintessential models an alternative reheating mechanism needs to be provided (e.g. Ricci reheating [39], curvaton reheating[40], etc. [41, 42, 43, 44]). At the end of inflation, radiation is produced while the scalar field is still dominating. In this period the scalar field energy density is driven by its kinetic energy. This leads to a period of kination right after the end of inflation which is absent in the Standard Cosmological Model. Kination is characterized by a barotropic parameter $w_{\text{kin}} = 1$ and lasts until t_{reh} the time at which radiation becomes dominating. This always happens since energy density during kination scales as $\rho_{\text{kin}} \sim a^{-6}$ while $\rho_r \sim a^{-4}$ (since $w_r = 1/3$ for radiation and $\rho \sim a^{-3(1+w)}$ as a consequence of the continuity equation (19)). Radiation and matter domination are standard. In the meanwhile the energy density of the scalar field is depleted by expansion until the scalar field freezes at some value ϕ_F. After that, the energy density of the scalar field will become a constant, $V(\phi_F)$. A constant energy density doesn't deplete with expansion and eventually it will start dominating again in the late Universe since matter ($w_M = 0$) scales as $\rho_M \sim a^{-3}$, which will become subdominant at the time of matter-dark energy equivalence. After the scalar field is once again the dominating source of energy-density, it will unfreeze and slow-roll along the potential exactly as it happens in thawing quintessence model. The important difference here is that ϕ_F is now fixed by the inflationary attractor so its specific value is explained.
In the following we will consider the general setup of quintessential inflation and explain the general features of this framework, the predictions and the shortcomings.

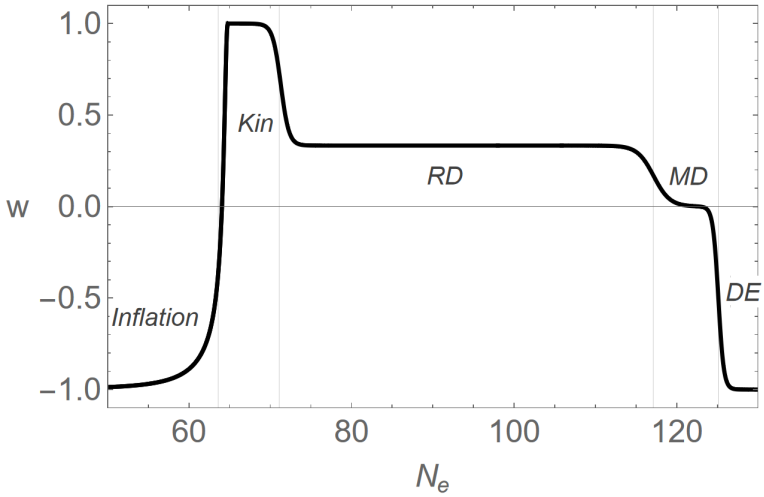

Figure 3: A typical example of evolution of the barotropic parameter of the Universe and the energy densities for the scalar, radiation and matter fluid in quintessential inflation models. Notice the appearance of kination, absent in the Standard Cosmological Model. The figure can also be found in [III].

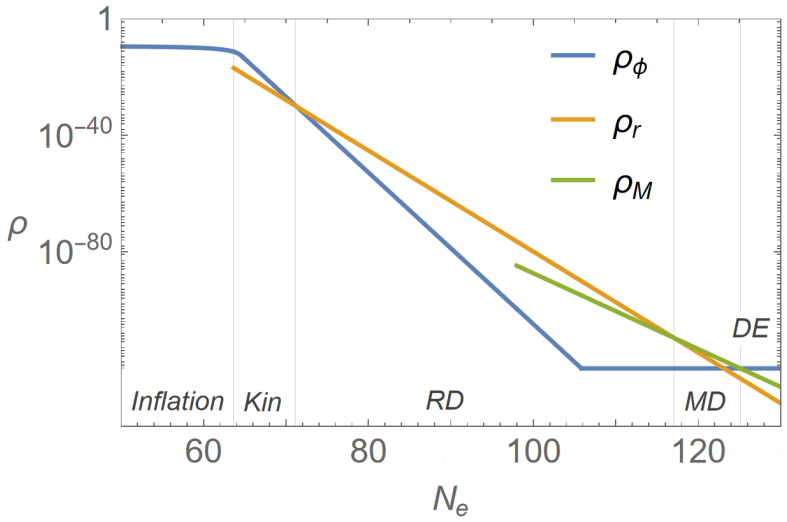

Figure 4: A typical example of evolution of the barotropic parameter of the Universe and the energy densities for the scalar, radiation and matter fluid in quintessential inflation models. Notice the appearance of kination, absent in the Standard Cosmological Model. The figure can also be found in [III].

5.1 Inflation

Inflationary computations proceed in a standard way as explained in section 3.3. In general quintessential inflation, the scalar field starts with an energy density $\approx 10^{16}$GeV and it will last until $w_\phi < -1/3$. This period has to last $N_* \approx 60-70$ e-folds since the comoving scale leaves the horizon. This is larger than the usual number of e-folds expected in the Standard Cosmological Model $N_* \approx 50-60$ e-folds. This is due to kination which is a key feature of quintessential inflation. The extra contribution to the number of e-folds can be computed by using (108):

$$\Delta N = \frac{1-3w}{12(1+w)} \ln\left(\frac{\rho_{\rm end}}{\rho_{\rm reh}}\right) \sim \frac{1}{3}\ln\left(\frac{V_{\rm end}^{1/4}}{T_{\rm reh}}\right) \tag{170}$$

where in the last line we used $w=1$ during kination, $\rho_{\rm end} \sim 3/2 V_{\rm end}$ at the end of inflation and $\rho_{\rm reh} \sim T_{\rm reh}^4$ from (106). For typical inflation energy $\approx 10^{16}$GeV and reheating temperatures ≈ 1 TeV we have indeed $\Delta N \approx 10$ which justifies the larger number of e-folds.

5.2 Kination and overproduction of gravitational waves

Inflation finally ends when $\dot\phi^2 \sim V$. Since the scalar field has to survive until present days its energy cannot be converted into radiation and reheating needs to happen by other mechanisms which do not involve the scalar field. During kination the scalar field obeys the equation:

$$\ddot\phi + 3H\dot\phi \sim 0. \tag{171}$$

This implies

$$\dot\phi = \sqrt{\frac{2}{3}}\frac{1}{t}, \tag{172}$$

$$\rho_\phi \sim \dot\phi^2/2 \sim a^{-6}, \tag{173}$$

with $w=1$ and $a \sim t^{2/3(1+w)} = t^{1/3}$. Notice that since the energy density is dominated by kinetic energy, kination is model independent and unaffected by the choice of the potential. By integrating (172) we find:

$$\phi(t) = \phi_{\rm end} + \sqrt{\frac{2}{3}}\ln\left(\frac{t}{t_{\rm end}}\right), \tag{174}$$

where $\phi_{\rm end}$ and $t_{\rm end}$ are the respectively the field value and time at the end of inflation. Such a period is a key feature of quintessential inflation. It is a well-known fact (see [45] and references therein) that if such a period is introduced in the evolution of the Universe, we might not satisfy the bounds coming from Big Bang Nucleosynthesis. In fact, during kination, due to having $w=1$, a spike is produced in the spectrum of gravitational waves that might induce the aforementioned issue [4]. The upper bound on the density of the produced gravitational waves is sensitive to the number of degrees of freedom and can be computed as [46]:

$$h_0^2\Omega_{\rm peak} \equiv \int_{k_{\rm BBN}}^{k_{\rm end}} h_0^2\Omega_{\rm GW}(k)\,d\ln k \leq \frac{7}{8}\left(\frac{4}{11}\right)^{4/3} h_0^2\Omega_{r,0}\Delta N_{\rm eff} \leq 5.6\cdot 10^{-6}\Delta N_{\rm eff}, \tag{175}$$

where $\Omega_{\rm GW}(k)$ is the spectrum of GWs, k is the mode the re-enters the horizon at a given time, $k_{\rm BBN}$ the modes re-entering at nucleosynthesis, $k_{\rm end}$ the modes re-entering at the end of inflation, $h_0^2\Omega_{r,0}$ is the density radiation measured today, and $\Delta N_{\rm eff} \equiv N_{\rm eff} - 3$ the

effective number of relativistic degrees of freedom at nucleosynthesis. Notice that the gravitational waves background can contribute to the relativistic degrees of freedom if present at the time of BBN. At the same time we have that the modes re-entering the horizon $k = a_k H_k \sim a^{-(1+3w)/2}$, which implies:

$$\Omega_{\rm GW}(k) = \frac{\rho_{\rm GW}(k)}{\rho(k)} \sim k^{2\frac{w-1/3}{w+1/3}}. \tag{176}$$

This means that modes re-entering during radiation domination $w = 1/3$ will have a flat spectrum while the ones re-entering during kination will have $\Omega(k) \sim k$. In general we have:

$$\Omega_{\rm GW}(k) = \Omega_{\rm GW}^{\rm rd} \begin{cases} k/k_{\rm reh}, & k_{\rm reh} < k < k_{\rm end} \\ 1, & k_{\rm eq} < k < k_{\rm reh} \\ (k/k_{\rm eq})^{-2}, & k_0 < k < k_{\rm eq} \end{cases} \tag{177}$$

with $\Omega_{\rm GW}^{\rm rd}$ is the density parameter for gravitational waves during radiation domination. We have $\Omega_{\rm GW}^{\rm rd} \propto H_{\rm end}^2 \approx 10^{-17}$ for inflation happening around 10^{16} GeV [46]. From (177) we have that $\Omega_{\rm peak} \equiv \Omega_{\rm GW}(k_{\rm end})$ hence from integral (175) we can constraint $\Omega_{\rm GW}^{\rm rd}(k_{\rm end}/k_{\rm reh})$. This is equivalent to put a constraint on the reheating temperature $T_{\rm reh}$ as we will explicitly show in the next section.

5.3 Reheating

Kination finally ends in order to allow for the Hot Big Bang. If we want to reproduce the correct abundances of primordial nuclei generated during BBN, we need this to happen at energy scales > 1MeV. This has to be true for any reheating model independently of the context. Let's now see what the lower bound is in the case of quintessential inflation. Since during kination we have $\rho_\phi \sim a^{-6}$ eventually radiation (which scales as $\rho_r \sim a^{-4}$) will start dominating as the Universe expands. The moment at which this happens is called *re-heating* and marks the beginning of radiation domination. Reheating must happen before BBN. Let's define the density parameter for radiation at the end of inflation as:

$$\Omega_r^{\rm end} \equiv \frac{\rho_r^{\rm end}}{\rho_{\rm end}}, \tag{178}$$

where $\rho_r^{\rm end}$ is the energy density of radiation produced at the end of inflation and $\rho_{\rm end}$ is the total energy density of the Universe at the end of inflation. The specific value of $\Omega_r^{\rm end}$ will depend on the choice of the reheating mechanism which is bounded between:

$$\Omega_{r,\rm grav}^{\rm end} \leq \Omega_r^{\rm end} \leq 1, \tag{179}$$

where the upper bound is obtained by choosing maximum efficiency of the reheating process, while the lower bound $\Omega_{r,\rm grav}^{\rm end}$ is obtained by choosing gravitational reheating i.e. the less efficient reheating mechanism [44]. Radiation becomes the dominant source of energy density when the Hot Big Bang takes place, at the time of reheating:

$$t_{\rm reh} = \frac{t_{\rm end}}{(\Omega_r^{\rm end})^{3/2}}. \tag{180}$$

where we used the definition of (178) and (23), (25) to compute the equality time between radiation and scalar field energy density. By using the expression above and plugging it in (174) we get:

$$\phi_{\rm reh} = \phi_{\rm end} - \sqrt{\frac{3}{2}} \ln\left(\Omega_r^{\rm end}\right). \tag{181}$$

If we assume further that radiation has enough time to thermalize during kination, then the reheating temperature can be computed as [38]:

$$T_{\rm reh} = \left(\frac{30}{\pi^2 g_{\rm reh}} (\Omega_r^{\rm end})^3 \rho_\phi^{\rm end}\right)^{1/4}, \tag{182}$$

where $g_{\rm reh}$ is the number of relativistic degrees of freedom at time of reheating. We are now in a position to compute the lower bound on the reheating temperature $T_{\rm reh}$ using the constrains on the overproduction of gravitational waves described in the previous section. Given that

$$k_{\rm end} = a_{\rm end} H_{\rm end}, \tag{183}$$

$$k_{\rm reh} = a_{\rm reh} H_{\rm reh}, \tag{184}$$

we can compute from the First Friedmann equation that in general:

$$H_{\rm end} = \sqrt{\frac{V_{\rm end}}{2}}, \tag{185}$$

$$H_{\rm reh} = \pi \sqrt{\frac{g_{\rm reh}}{90}} T_{\rm reh}^2. \tag{186}$$

where we used $\rho_{\rm end} \sim 3/2 V_{\rm end}$ (see eq.(107)) at the end of inflation and $\rho_{\rm reh}$ given by (106). Using the above equations, we can finally compute:

$$\Omega_{\rm peak} = \Omega_{\rm GW}^{\rm rd} \frac{k_{\rm end}}{k_{\rm reh}} = \Omega_{\rm GW}^{\rm rd} \frac{a_{\rm end} H_{\rm end}}{a_{\rm reh} H_{\rm reh}} = \Omega_{\rm GW}^{\rm rd} \left(\frac{H_{\rm end}}{H_{\rm reh}}\right)^{2/3}. \tag{187}$$

where in the last equality we considered kination domination. For typical inflation scenarios $\sim 10^{16}$GeV we have $H_{\rm end} \approx 10^{-5}$. From (175), considering $g_{\rm reh} \approx 100$ and $N_{\rm eff} \lesssim 0.2$ we finally have our bound on the reheating temperature:

$$T_{\rm reh} \gtrsim 10^7 \text{GeV}. \tag{188}$$

This bound can be partially relaxed if inflation happens at energies lower than 10^{16} GeV, since $\Omega_{\rm GW}^{\rm rd}$ scales with $H_{\rm end}^2$. This is indeed the case when the tensor-to-scalar ratio r is very small as the energy scale of inflation is directly related to r as [28]:

$$U(N_*) \approx \left(\frac{r}{0.01}\right)^{\frac{1}{4}} 10^{16} \text{GeV}. \tag{189}$$

5.4 Quintessence

Radiation domination and matter domination are standard in quintessential inflation models. After kination is over the scalar field becomes subdominant and its kinetic energy is depleted by the friction term in the First Friedmann equation. The scalar field will eventually freeze at the value ϕ_F. Let us compute it. During radiation domination the scalar field is still described by the Klein-Gordon equation (171). By solving the Friedmann equations for a radiation fluid we have that $H(t) = \frac{3}{2t}$, which implies:

$$\dot{\phi} = \left(\frac{2 t_{\rm reh}}{3 t^3}\right)^{1/2}, \tag{190}$$

which after integration leads to:

$$\phi(t) = \phi_{\rm reh} + 2\sqrt{\frac{2}{3}}\left(1 - \frac{t_{\rm reh}}{t}\right), \tag{191}$$

which allows to compute the value at which freezes. In fact for $t \gg t_{\rm reh}$ we get

$$\phi_F = \phi_{\rm end} + \sqrt{\frac{2}{3}}\left(2 - \frac{3}{2}\ln\Omega_r^{\rm end}\right). \tag{192}$$

We see that the freezing value ϕ_F only depends on the inflationary attractor and the reheating mechanism through $\phi_{\rm end}$ and $\Omega_r^{\rm end}$. In order for the model to predict a viable dark-energy era we need to satisfy two more constraints. First the model has to address the coincidence problem i.e.

$$V(\phi_F) = \rho_{\rm DE,0} \approx 7 \cdot 10^{-121}. \tag{193}$$

Second the barotropic parameter $w_{DE} < -0.95$ according to the Planck observations [4]. In order to do so we have to make sure that the field does not hit the tracker (see Section 4.1). In this way the field will unfreeze only at t_{DE} i.e. the time at which dark-energy starts dominating. The field will then start slow-rolling along the quintessence tail and behave as dark-energy.

5.5 Popular models of quintessential inflation

In this section we briefly review two popular models: the first model of quintessential inflation, the Peebles-Vilenkin potential, and the case of quintessential α-attractors.

5.5.1 Peebles-Vilenkin potential

The Peebles-Vilenkin potential was first introduced in [37] as an attempt to describe a model of quintessential inflation, where the scalar field drives both early and late Universe acceleration. The potential takes the form:

$$V(\phi) = \begin{cases} \lambda(\phi^4 + M^4) & \phi \leq 0 \\ \lambda \frac{M^8}{\phi^4 + M^4} & \phi > 0. \end{cases} \tag{194}$$

Notice that although being defined piecewise, the potential is smooth in $\phi = 0$. Inflation is driven by the quartic potential for $\phi < 0$, while the quintessence tail $\phi > 0$ describes the dark-energy acceleration. Nowadays, it is clear that this potential fails to predict the inflationary observables. Indeed the model predicts:

$$n_s \approx 0.95, \quad r \approx 0.26, \quad A_s = 2.1 \cdot 10^{-9}, \tag{195}$$

which does not fit the current observed bounds on r, n_s. The constraint on the reheating temperature $T_{\rm reh} \gtrsim 10^7$ GeV constraints the number of e-folds through (108) in the range $N_* \approx 57.5 - 67.5$ (instead of the typical 50-60 estimated in section 3.5.). The model however successfully predicts a quintessence tail with $w_{DE} \approx -1$, solving the coincidence problem for $M \approx 10^5$ GeV. Details can be found in [37].

5.5.2 Quintessential inflation and $\alpha-$attactors

The Lagrangian of the scalar field is given by [38]:

$$\mathscr{L} = -\frac{1}{2}\frac{\partial_\mu\phi\partial^\mu\phi}{(1-\phi^2/6\alpha)^2} + V_0 e^{-\kappa\phi} - \Lambda, \tag{196}$$

with $\alpha, \kappa, \Lambda, V_0$ constants. By choosing $\Lambda = V_0 e^{-k\sqrt{6\alpha}}$ we can set the total vacuum energy to zero (we assume this is the case due to some unknown symmetry). By means of a

field redefinition $\phi = \sqrt{6\alpha}\tanh\frac{\varphi}{\sqrt{\alpha}}$, we get the scalar potential in terms of the canonically normalized field i.e. the kinetic term in terms of φ is simply $-\frac{1}{2}\partial_\mu\varphi\partial^\mu\varphi$:

$$V(\phi) = e^{-\kappa\sqrt{6\alpha}}V_0\left(e^{\kappa\sqrt{6}\alpha\left(1-\tanh\frac{\varphi}{\sqrt{6\alpha}}\right)}-1\right). \tag{197}$$

For $\varphi \to -\infty$ the potential becomes:

$$V(\varphi) \sim e^{-k\sqrt{6\alpha}}V_0\exp\left(-2\kappa\sqrt{6\alpha}e^{\frac{2\varphi}{\sqrt{6\alpha}}}\right). \tag{198}$$

This function has a plateau $V(-\infty) = e^{-k\sqrt{6\alpha}V_0}$ for $\phi \to -\infty$. Inflation takes place on this plateau and predicts the observables [38]:

$$r = \frac{12\alpha}{(N_* + \sqrt{3\alpha/2})^2}, \quad n_s \sim 1 - \frac{2}{N_*}. \tag{199}$$

In particular by fixing $A_s \approx 2.1\cdot10^{-9}$ we find the range $2.4\cdot10^{15}\text{GeV} \lesssim M \lesssim 3.8\cdot10^{16}\text{GeV}$ for $10^{-2} \lesssim \alpha \lesssim 10^2$, with $M^4 \equiv V_0 e^{\kappa\sqrt{6\alpha}}$. By constraining the reheating temperature T_{reh} one can also get the bounds on the number of e-folds in the range $N_* \approx 56 - 66$. The model can fit both the Planck+Bicep/Keck and the Planck+ACT dataset between the 2σ bounds. The quintessence tail is obtained by taking the limit $\varphi \to \infty$:

$$V(\varphi) = V_t e^{-\lambda\varphi}, \tag{200}$$

with $V_t = 2\kappa\sqrt{6\alpha}e^{-\kappa\sqrt{6\alpha}}V_0$ and $\lambda = 2/\sqrt{6\alpha}$. Therefore, this behaves as the exponential quintessence discussed in chapter 4. Since the scalar field is subdominant during the evolution of the Universe, it will follow the scaling attractor and mimic the dominant fluid i.e. cold matter with $w = 0$. However, it can be shown [47] that if $\sqrt{2} < \lambda \lesssim 2\sqrt{6}$ the field after unfreezing can still predict a transient accelerated expansion. This will happen because the numerical solution will not follow the scaling solution immediately, but it will oscillate around it giving an effective barotropic parameter which is temporary $w < -\frac{1}{3}$. This further constraints $0.03 \lesssim \alpha < 0.33$. Finally, imposing the solution for the coincidence problem one can further constraint κ, after choosing a reheating mechanism and fixing ϕ_F. See [38] for the details.

6 Palatini formulation

In this section the Palatini formulation of gravity is finally introduced, representing an alternative approach with respect to metric theories. The main formalism is discussed and the attention focused on a specific class of Palatini theories, in particular those whose gravitational action is described by an $F(R)$ term. Differences between metric and Palatini $F(R)$ are compared and a few examples of viable inflationary models for this class explicitly reviewed.

Up to now we discussed inflation and quintessence in the context of General Relativity. GR is a metric theory of gravity meaning that the metric encodes all the gravitational dynamics and fully describes all the geometrical properties of the spacetime. The affine connection has a fixed relation to the metric which is given by the Levi-Civita connection (5). The curvature Riemann tensor then takes the form (3) which can be expressed in terms of the metric and its first and second derivative $g, \partial g$ and $\partial^2 g$.
In the Palatini formulation[10] the metric field $g_{\mu\nu}$ and the affine connection $\Gamma^\sigma_{\mu\nu}$ are a priori independent. The metric field $g_{\mu\nu}$ appears in the action as an auxiliary field without kinetic terms, while the Riemann tensor is defined solely from the affine connection. The relation between them is fixed at the level of equation of motion after taking the variation with respect to the independent connection. Let's consider the following action:

$$S = \int d^4x\sqrt{-g}\left(R + \mathscr{L}_m(g_{\mu\nu}, \Gamma^\sigma_{\mu\nu}, \Phi, \nabla_\mu\Phi)\right), \tag{201}$$

where $R = g^{\mu\nu}R_{\mu\nu}(\Gamma)$ is the Ricci scalar constructed by contracting the metric-independent Ricci tensor with the metric. Matter fields and their derivatives are collectively denoted by Φ and $\nabla_\mu\Phi$. Notice that in this case the Ricci tensor is still derived from the contraction of the Riemann tensor (3), and it is independent from the metric. Moreover in principle, the matter Lagrangian also explicitly depends on $\Gamma^\sigma_{\mu\nu}$ and not just on the metric $g_{\mu\nu}$. It was shown in [50, 51] that this class of theories is phenomenologically equivalent to GR plus matter fields only in the case $\mathscr{L}_m = \mathscr{L}_m(g_{\mu\nu}, \Phi, \nabla_\mu\Phi)$ i.e. only when matter is minimally coupled to the metric, at least at the classical level. In general by taking the variation of the action with respect to the independent fields we get the following set of equations of motion:

$$R_{\mu\nu} - \frac{1}{2}g_{\mu\nu}R = T_{\mu\nu}, \tag{202}$$

$$-\nabla_\lambda(\sqrt{-g}g^{\mu\nu}) + \delta^\nu_\lambda\nabla_\rho(\sqrt{-g}g^{\mu\rho}) + 2\sqrt{-g}(g^{\mu\nu}S^\sigma_{\sigma\lambda} - \delta^\nu_\lambda g^{\mu\rho}S^\sigma_{\sigma\rho} + g^{\mu\sigma}S^\nu_{\lambda\sigma}) = \Delta^{\nu\mu}_\lambda, \tag{203}$$

where we have defined the torsion tensor (4):

$$T_{\mu\nu} \equiv -\frac{2}{\sqrt{-g}}\frac{\partial\left(\sqrt{-g}\mathscr{L}_m\right)}{\partial g^{\mu\nu}}, \tag{204}$$

$$\Delta^{\nu\mu}_\lambda \equiv -\frac{\partial\mathscr{L}_m}{\partial\Gamma^\lambda_{\nu\mu}}, \tag{205}$$

where $T_{\mu\nu}$ is the usual stress-energy tensor, and $\Delta^{\mu\nu}_\lambda$ is known as hypermomentum tensor. These are the general equations of motion for a theory containing an Einstein-Hilbert term and general matter fields, when considering an independent connection. In the most general approach, the connection is left completely unconstrained. This is a wide framework

[10] Despite the name, the original idea was first presented by Einstein [48, 49].

known in literature as Metric-Affine Gravity. In the Palatini approach instead the connection is still assumed to be torsion free i.e. the connection is antisymmetric in the lower indices $2S^{\sigma}_{\mu\nu} = \Gamma^{\sigma}_{\mu\nu} - \Gamma^{\sigma}_{\nu\mu} = 0$. In this case, when the matter Lagrangian is independent of Γ, it is straightforward to compute that (203) reduces to

$$\nabla_{\lambda}(\sqrt{-g}g^{\mu\nu}) = 0, \tag{206}$$

which implies that the affine connection can be identified with the Levi-Civita connection of General Relativity (5).

6.1 F(R) gravity: Metric vs. Palatini

Unless the action is given by a Ricci scalar term plus a connection-independent matter Lagrangian, the connection will differ from the one in General Relativity and the two formulations will give phenomenologically different results [51, 52]. In particular this will be true when considering higher order terms in the action describing the gravitational sector. It is in fact possible to extend the Einstein-Hilbert action by including higher order contractions of the Riemann tensor in the action. One popular case is that of $F(R)$ theories, where $F(R)$ is a general function of the Ricci scalar. A particular case of this class is the Staorbinsky model discussed in section 3.6.2 for which $F(R)$ is quadratic. We start by considering the metric case. Consider the action:

$$S = \frac{1}{2}\int d^4x\sqrt{-g}F(R), \tag{207}$$

in metric gravity the equations of motion for the gravitational sector are derived by taking the variation with respect to $g_{\mu\nu}$. This yields:

$$F'(R)R_{\mu\nu} - \frac{1}{2}F(R)g_{\mu\nu} - \nabla_{\mu}\nabla_{\nu}F'(R) + g_{\mu\nu}\Box F'(R) = 0, \tag{208}$$

This equations are fourth-order in $g_{\mu\nu}$ and only reduce to second order for $F(R) = R$. As in 3.6.2 let us define a new scalar field ϕ such that:

$$S = \int d^4x\sqrt{-g}\left(\frac{1}{2}F(\phi) + \frac{1}{2}F'(\phi)(R-\phi)\right), \tag{209}$$

by taking the variation with respect to ϕ, we get the condition $F''(\phi)(R-\phi) = 0$, which gives $R = \phi$ for $F''(R) \neq 0$. This implies that (207) gives the same equations of motion of (209). Let us now perform the conformal transformation:

$$g_{\mu\nu} \to F'(\phi)g_{\mu\nu}, \tag{210}$$

to obtain the Einstein frame action:

$$S = \int d^4x\sqrt{-g}\left(R - \frac{3}{2\Phi^2}\partial_{\mu}\Phi\partial^{\mu}\Phi - \frac{V(\Phi)}{\Phi^2}\right), \tag{211}$$

where we have defined:

$$\Phi = F'(\phi), \tag{212}$$

$$V(\Phi) = \phi(\Phi)\Phi - F\big(\Phi(\phi)\big). \tag{213}$$

This implies that Φ is dynamical, hence the theory contains a new scalar gravitational degree of freedom (exactly as it happens in the quadratic Starobinsky case).

The situation is different in the case of Palatini gravity. Consider once again action (207). This time however consider $R = g^{\mu\nu}R_{\mu\nu}(\Gamma)$ where the Ricci tensor is defined as a function of the connection only. The metric and the affine connection are independent, therefore we need to vary with respect to both fields. This gives the equations of motion:

$$F'(R)R_{\mu\nu} - \frac{1}{2}g_{\mu\nu}F(R) = 0, \tag{214}$$

$$-\nabla_\lambda(\sqrt{-g}F'(R)g^{\mu\nu}) + \delta^\nu_\lambda\nabla_\rho(\sqrt{-g}F'(R)g^{\mu\rho}) = 0. \tag{215}$$

The theory can be brought to the Einstein frame by defining an auxiliary field ζ such that:

$$S = \frac{1}{2}\int d^4x\big[F(\zeta) + F'(\zeta)(R-\zeta)\big], \tag{216}$$

where again we see that the equation of motion for ζ gives $\zeta = R$ for $F''(\zeta) \neq 0$. As usual we define the conformal transformation $g_{\mu\nu} \to F'(\zeta)g_{\mu\nu}$. This time however the Ricci tensor is independent of $g_{\mu\nu}$ and the conformal transformation straightforwardly gives:

$$S = \frac{1}{2}\int d^4x\sqrt{-g}\left(R - \frac{\zeta F'(\zeta) - F(\zeta)}{F'(\zeta)^2}\right), \tag{217}$$

and we can see explicitly that the field ζ is not dynamical. This is a crucial difference and it implies that there is no extra scalar field in Palatini formulation of $F(R)$ gravity. Instead, the above action is equivalent to GR plus a cosmological constant. Attempts to fit the observations with ad hoc choices of the $F(R)$ actions have been made, however the proposed models do not manage to solve the Cosmological Constant problem (see [53],[54] and references therein). On the other hand this has very interesting consequences of the phenomenology of inflation: the same Jordan frame actions formulated in metric and Palatini formalism correspond to different Einstein frame actions.

6.2 Inflation in Palatini gravity

The recent results from the Atacama Telescope (ACT) [8] provided a shift in the measured value of n_s. The latest Planck+Bicep/Keck analysis [5] gives $n_s = 0.9649 \pm 0.0042$ at 68% confidence level, when combined with DESI and ACT the new prediction for the spectral index is shifted to $n_s = 0.9743 \pm 0.0034$ representing a 2σ shift with respect to the previous results. This makes the predictions for Higgs inflation and the Starobinsky model disfavored at a $\gtrsim 2\sigma$ confidence level (see Fig.2). While statistically not significant this still hints at the necessity of considering alternatives to popular inflationary models. The recent results from ACT has further increased the interest in Palatini inflation since many model of this class can predict a value for n_s compatible with the observed one [55, 56, 57]. Palatini theories have proven to have many interesting features for inflation model building which are worth to be briefly reviewed, considering two separate cases. First, the case in which the gravitational sector is given by the Einstein-Hilbert term and the matter action is non-minimally coupled to the Ricci scalar, including the relevant case of Palatini Higgs inflation, as opposed to the metric Higgs inflation discussed in section 3.6.3 [58, 59, 60, 61, 62, 63, 64]. Second, the case in which the matter action is minimally coupled but the gravitational sector contains higher order terms [65, 66, 67, 68, 69].

6.2.1 Non-minimally coupled theories

Consider the following Jordan frame action in the Palatini formulation:

$$S = \int d^4x\sqrt{-g}\left[\frac{1}{2}\big(1 + f(\phi)\big)R - \frac{1}{2}g^{\mu\nu}\partial_\mu\phi\partial_\nu\phi - V(\phi)\right], \tag{218}$$

where $f(\phi)$, $V(\phi)$ are general functions of the scalar field. This action admits an equivalent Einstein-frame formulation. Notice that now the Ricci scalar is given by $R = g^{\mu\nu}R_{\mu\nu}(\Gamma)$ where the Ricci tensor $R_{\mu\nu}(\Gamma)$ is dependent of $\Gamma^{\sigma}_{\mu\nu}$ only, therefore the conformal redefinition:

$$g_{\mu\nu} \to \big(1 + f(\phi)\big) \equiv \Omega^2(\phi) g_{\mu\nu}, \tag{219}$$

leaves the Ricci tensor unaffected. Another way to see this is to consider the on-shell transformation of the Ricci scalar:

$$R \to R - \frac{1}{2} g^{\mu\nu} \frac{\frac{3}{2}(\partial_\phi \Omega^2)^2 + \Omega^2}{\Omega^4} \partial_\mu\phi\partial_\nu\phi, \tag{220}$$

where R is still constructed from the affine connection $\Gamma^{\lambda}_{\mu\nu}$. The connection equation then gives:

$$\Gamma^{\lambda}_{\mu\nu} = \bar{\Gamma}^{\lambda}_{\mu\nu} + \delta^{\lambda}_{\mu}\partial_\nu\omega(\phi) + \delta^{\lambda}_{\nu}\partial_\mu\omega(\phi) - g_{\mu\nu}\partial^{\lambda}\omega(\phi), \tag{221}$$

with $\bar{\Gamma}^{\lambda}_{\mu\nu}$ the Levi-Civita connection and $\omega(\phi) \equiv \ln\Omega(\phi)$. By substituting this into the expression for R one can show that it exactly cancels out the extra kinetic term in (220) giving $R \to \bar{R}$ where $\bar{R}$ is the Einstein frame metric dependent Ricci scalar. In order to avoid cumbersome notation, we drop the overbar in what follows. Whether we are working in the Jordan or Einstein frame will be specified in the text. By performing the conformal transformation we get the equivalent Einstein frame action:

$$S = \int d^4x\sqrt{-g}\left[\frac{R}{2} - \frac{1}{2\Omega^2(\phi)} g^{\mu\nu}\partial_\mu\phi\partial_\nu\phi - \frac{V(\phi)}{\Omega^4(\phi)}\right]. \tag{222}$$

By means of a field redefinition $\frac{\partial\phi}{\partial\chi} = \Omega(\phi)$ we can rewrite the action in terms of the canonically normalized field χ:

$$S = \int d^4x\sqrt{-g}\left(\frac{R}{2} - \frac{1}{2} g^{\mu\nu}\partial_\mu\chi\partial_\nu\chi - U(\chi)\right), \tag{223}$$

where:

$$U(\chi) = \frac{V\big(\phi(\chi)\big)}{\Omega(\phi(\chi))^4}, \tag{224}$$

is the Einstein frame potential. From this potential we can compute the inflationary observables in the slow-roll approximation by taking derivatives with respect to the canonical field χ exactly as in section 3.3. Several models have been studied including Higgs inflation, Coleman-Weinberg inflation, and chaotic models [70, 71, 72, 73, 74, 75]. In light of the recent ACT analysis it is interesting to highlight that introducing a non minimal coupling in the form $f(\phi) = \xi\phi^n$, $V(\phi) = \lambda\phi^{2n}$ restores compatibility with data of the chaotic model with $n = 1$. We show in Fig.5 the observables r vs. n_s for the non-minimally coupled chaotic model with $n = 1$ (blue) and $n = 2$ (green), at $N_* = 50$ (dot-dashed line), $N_* = 60$ (dashed line). The orange thick line is the prediction for metric Higgs and Starobinsky inflation between 50 and 60 $e-$folds. Large dots correspond to $N_* = 50$, small dots to $N_* = 60$. The Palatini prediction for Higgs inflation corresponds to the $r \to 0$ limit of the $n = 2$ case (i.e. the strong coupling limit). The light blue areas represent the $1, 2\sigma$ allowed regions coming from the Planck+Bicep/Keck dataset. The purple areas represent the $1, 2\sigma$ allowed regions coming from the Planck+ACT dataset. The Palatini Higgs model is disfavored at $\gtrsim 2\sigma$ confidence level if we consider the Planck+ACT dataset, while the $n = 1$ case is favored for non-minimal coupling $\xi \gtrsim 0.1$.

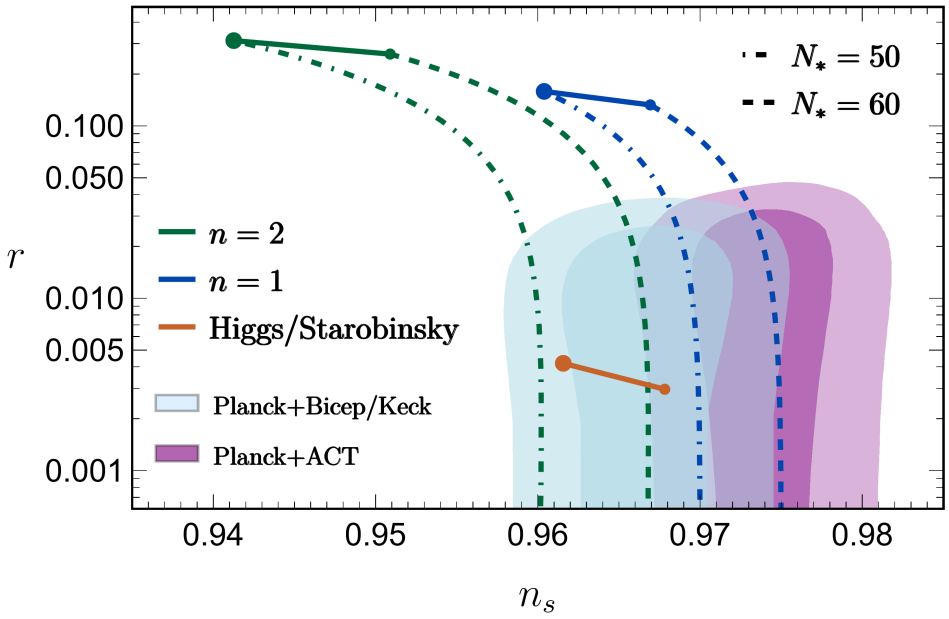

Figure 5: r vs. n_s for the non-minimally coupled chaotic model with $n = 1$ (blue) and $n = 2$ (green), at $N_* = 50$ (dot-dashed line), $N_* = 60$ (dashed line). The orange thick line is the prediction for metric Higgs and Starobinsky inflation between 50 and 60 $e-$folds. Large dots correspond to $N_* = 50$, small dots to $N_* = 60$. The Palatini prediction for Higgs inflation corresponds to the $r \to 0$ limit of the $n = 2$ case (i.e. the strong coupling limit). The light blue areas represent the $1, 2\sigma$ allowed regions coming from the Planck+Bicep/Keck dataset. The purple areas represent the $1, 2\sigma$ allowed regions coming from the Planck+ACT dataset. The Palatini Higgs model is disfavored at $\gtrsim 2\sigma$ confidence level if we consider the Planck+ACT dataset, while the $n = 1$ case is favored for non-minimal coupling $\xi \gtrsim 0.1$.

6.2.2 Higher-order theories

As an example of higher order theory let us consider the following action where we add a quadratic Ricci scalar term to the Einstein-Hilbert action coupled to a scalar field:

$$S = \int d^4x\sqrt{-g}\left[\frac{1}{2}R + \frac{\alpha}{2}R^2 - \frac{1}{2}g^{\mu\nu}\partial_\mu\phi\partial_\nu\phi - V(\phi)\right], \tag{225}$$

where $V(\phi)$ is general function of the scalar field. In order to compute the equivalent Einstein frame action we define an auxiliary field ζ in such a way that:

$$S = \int d^4x\sqrt{-g}\left[\frac{1}{2}F(\zeta) + \frac{1}{2}F'(\zeta)(R-\zeta) - \frac{1}{2}g^{\mu\nu}\partial_\mu\phi\partial_\nu\phi - V(\phi)\right], \tag{226}$$

where $F(\zeta) = \zeta + \alpha\zeta^2$. Notice that this action gives the same equations of motions of the original action since ζ is algebraically related to R as one can see by taking the variation of the action in ζ (as long as $F''(\zeta) \neq 0$). By means of a conformal redefinition:

$$g_{\mu\nu} \to F'(\zeta)g_{\mu\nu}, \tag{227}$$

we get the Einstein frame equivalent action:

$$S = \int d^4x\sqrt{-g}\left[\frac{1}{2}R - \frac{1}{2F'(\zeta)}g^{\mu\nu}\partial_\mu\phi\partial_\nu\phi - U(\zeta,\phi)\right], \tag{228}$$

where

$$U(\zeta,\phi) = \frac{V(\phi) + \zeta F'(\zeta) - F(\zeta)}{2F'(\zeta)}. \tag{229}$$

By taking the variation with respect to ζ one can provide the algebraic relation between ζ and ϕ and substitute it back in the action to eliminate the auxiliary field ζ. The equation of motion for ζ gives:

$$2F(\zeta) - \zeta F'(\zeta) - F'(\zeta)\partial^\mu\phi\partial_\mu\phi = 4V(\phi). \tag{230}$$

By considering $F(\zeta) = \zeta + \alpha\zeta^2$, we can explicitly compute the solution:

$$\zeta = \frac{\partial^\mu\phi\partial_\mu\phi + 4V(\phi)}{1 - 2\alpha\partial^\mu\phi\partial_\mu\phi}. \tag{231}$$

Putting it back into (228) we get:

$$S = \int d^4x\sqrt{-g}\left[\frac{1}{2}R - \frac{1}{2}\partial_\mu\chi\partial^\mu\chi + \frac{1}{4}\frac{1}{1+8\alpha U(\chi)}\left(\partial_\mu\chi\partial^\mu\phi\chi\right)^2 + U(\chi)\right], \tag{232}$$

where we have defined a canonical scalar field such that $\frac{\partial\phi}{\partial\chi} = \sqrt{F'(\zeta)}$ and:

$$U(\chi) = \frac{V(\phi(\chi))}{1 + 8\alpha V(\phi(\chi))}. \tag{233}$$

This model has been extensively studied in [65, 66, 67, 68, 69]. Its appealing property is to generate asymptotically flat potentials for $\alpha \to \infty$ and/or $V(\phi) \to \infty$ independently of the choice of the Jordan frame potential. Indeed it is straightforward to check $U \to 1/8\alpha$ in this limit. It is interesting to explicitly compute the slow-roll parameters for this models in terms of the slow-roll parameters in absence of the higher-order quadratic term i.e.

$\alpha = 0$. In the slow-roll approximation the higher order kinetic term can be neglected and we can compute:

$$\epsilon_U(\chi) = \frac{1}{2}\left(\frac{U'(\chi)}{U(\chi)}\right), \tag{234}$$

$$\eta_U(\chi) = \frac{U''(\chi)}{U(\chi)}, \tag{235}$$

$$N(\chi) = \int_{\chi}^{\chi_{\text{end}}} \frac{U'}{U} d\chi, \tag{236}$$

If we neglect the contribution from χ_{end} we can compute the CMB observables:

$$r = r^0\left(1 + 8\alpha U(\chi_*)\right)^{-1}, \tag{237}$$

$$n_s = n_s^0, \tag{238}$$

$$A_s = A_s^0, \tag{239}$$

where r^0, n_s^0, A_s^0 are the observables computed in the case $\alpha = 0$, i.e. when $U(\phi) = V(\phi)$. We see that all observables are unchanged except the tensor to scalar ratio which is suppressed for $\alpha \to \infty$. Since we never specify the form of the original Jordan frame potential $V(\phi)$, this behavior is model independent. This is particularly interesting in light of the recent Planck+ACT results. It has been studied in [72] that a wide class of models in Palatini gravity possess an attractor solution which corresponds to linear inflation i.e. $V(\phi) = \lambda\phi$. As it was highlighted in [55] linear inflation predicts a $n_s = 0.975$ at $N_* = 60$ e-folds which lays close to the current central value of the Planck+ACT dataset. Linear inflation however predicts a value of the tensor-to-scalar ratio, currently outside the 2σ bound. By embedding the model in a quadratic theory of gravity (240) we then recover compatibility with data for $\alpha \gtrsim 10^8$ (see for example Fig. 2 of [55]).

6.2.3 Quintessential inflation

We also mention for completeness that $F(R)$ Palatini gravity has been studied also in the context of quintessential inflation. Relevant examples are [76],[77], where the $F(R)$ is chosen to be in the quadratic form. As we see in the action (232), the scalar field kinetic term takes a more complicated form with the appearance of an higher order term. Moreover, it is a well-known fact that the matter sector in the Einstein frame is also modified due to the conformal transformation. However, as shown in [76] these features only have a negligible influence on the scalar field dynamics during the evolution of the universe.
In particular in [76] a viable model can be obtained using the Peebles-Vilenkin potential; the model satisfies indeed the bounds on the CMB observables and solves the coincidence problem by introducing a mass scale $M \approx 10$ GeV.
In [77] both a quadratic choice of the $F(R)$ and the introduction of a running non-mininimal coupling allow to build viable quintessential inflation scenarios by considering an exponential potential as in (151), and satisfying the observational bounds within a large choice of the model parameters.

Summary and Conclusions

The goal of this thesis is to address the issue of inflation and dark-energy in the context of Palatini gravity, an alternative formulation with respect to the standard metric formulation of General Relativity which predicts different phenomenology. The focus is on extended models of gravity, in particular $F(R)$ theories. The thesis discusses the phenomenology of inflation and quintessence in this framework.
Here the main results of the selected papers are briefly summarized and the discussion updated in light of the ACT dataset.

In paper I we considered an action in the form:

$$S = \int d^4x\sqrt{-g}\left[\frac{1}{2}F(R) - k(\phi)\frac{1}{2}g^{\mu\nu}\partial_\mu\phi\partial_\nu\phi - V(\phi)\right], \tag{240}$$

with $F(R)$ a general function of the Ricci scalar and $k(\phi), V(\phi)$ general functions of the scalar field. The action admits an Einstein frame equivalent formulation:

$$S = \int d^4x\sqrt{-g}\left[\frac{1}{2}R - \frac{1}{2}g^{\mu\nu}\partial_\mu\chi\partial_\nu\chi - U(\chi,\zeta)\right], \tag{241}$$

with ζ an auxiliary field and:

$$\left(\frac{d\chi}{d\phi}\right)^2 = \frac{k(\phi)}{F'(\zeta)}, \tag{242}$$

$$U(\chi,\zeta) = \frac{V(\phi(\chi)) - \zeta F'(\zeta) + F(\zeta)}{2F'(\zeta)}. \tag{243}$$

The auxiliary field ζ is not dynamical and can be eliminated by using the equation of motion for ζ (230). This is not always possible because of the complicated dependence on ζ and $\partial_\mu\phi$. However, since we are interested in slow-roll inflation we can neglect the inflaton kinetic term in (230) and write:

$$G(\zeta) \equiv \frac{1}{4}\big(2F(\zeta) - \zeta F'(\zeta)\big) = V(\phi(\chi)). \tag{244}$$

Notice that if $F(\zeta)$ diverges faster than quadratic, then $G(\zeta)$ always has a maximum for $\zeta > 0$. By substituting (244) back into the action we obtain:

$$S = \int d^4x\sqrt{-g}\left[\frac{1}{2}R - \frac{1}{2}g^{\mu\nu}\partial_\mu\chi\partial_\nu\chi - U(\zeta)\right], \tag{245}$$

with

$$U(\zeta) = \frac{\zeta}{F'(\zeta)}. \tag{246}$$

The computations can now proceed in a standard way by using the slow-roll formalism of section 3.3, by taking the derivatives of (246) with respect to the canonical field χ (using the chain rule for derivatives). Outside of slow-roll the evolution of the system is determined by:

$$\dot{\zeta} = \frac{3H\dot{\phi}^2F'(\zeta)k(\phi) + 3V'(\phi)\dot{\phi}}{2G'(\zeta) + \frac{3}{2}\dot{\phi}^2F''(\zeta)k(\phi)}. \tag{247}$$

It was proven in [78] that $F(R)_{>2}$ functions i.e. those that diverge faster then quadratic do not lead to graceful exit from inflation due to the appearance of a pole in (247) unless the

potential is positive definite for every ϕ. However even in this case, the potential needs to be fine tuned so that the absolute maximum of $V(\phi)$ is lower than the maximum of $G(\zeta)$ for the map between ζ and ϕ to be well-defined. This means that $V(\phi)$ must have an upper bound. In all other cases the $F(R)_{>2}$ class can only be considered an effective theory under the slow-roll approximation. To overcome this issue the class of $F(R,X)$ theories was introduced, with $X \equiv -g^{\mu\nu}\partial_\mu\phi\partial_\nu\phi$ the inflaton kinetic term. In this way starting from:

$$S = \int d^4x\sqrt{-g}\left[\frac{1}{2}F(R,X) - \frac{1}{2}g^{\mu\nu}\partial_\mu\phi\partial_\nu\phi - V(\phi)\right], \tag{248}$$

and restricting our attention to the class $F(R_X) \equiv F(R+X)$, we get the Einstein frame formulation:

$$S = \int d^4x\sqrt{-g}\left[\frac{1}{2}R - \frac{1}{2}g^{\mu\nu}\partial_\mu\phi\partial_\nu\phi - U(\zeta)\right], \tag{249}$$

with $U(\zeta)$ still given by (246). However, there are two crucial differences with respect to the action in (245). First of all equation (244) is now exact and not just an approximation valid during slow-roll. Second, the inflaton ϕ is already canonically normalized, so that we can use the slow-roll formalism by taking derivatives of $U(\zeta)$ with respect to ϕ.
The quadratic choice $F(R_X) = 2\Lambda + \omega R_X + \alpha R_X^2$ was explicitly studied in II. This class only admits two combinations of the coefficients Λ, ω, α such that the Einstein frame potential is positive and bounded from below. In particular the two configurations produce the class of *tailed fractional attractors* and *canonical fractional attractors*. The tailed fractional attractors are obtained by setting $\Lambda > 0$, $\omega < 0$, $\alpha > 0$ and considering a Jordan frame potential $V(\phi) < 0$. This has to be so to ensure that the Einstein frame potential is positive and bounded from below. Indeed, by doing so one obtains:

$$U(\phi) = \frac{\Lambda - V(\phi)}{8\alpha(\Lambda - V(\phi)) - \omega^2}, \tag{250}$$

which is always positive as long as $8\alpha\Lambda > \omega^2$. By choosing a potential in the monomial form $V(\phi) = -\lambda\phi^k$ one gets the predictions for CMB observables (see attached paper for the details):

$$r \sim 0, \tag{251}$$

$$n_s = 1 - \frac{k-1}{k-2}\frac{2}{N_*}. \tag{252}$$

It was proven in [78] that tailed attractors represent the strong coupling limit for all the $F(R_X)_{>2}$, independently of the specific choice of the $F(R_X)$ function. Steeper potentials (i.e. large k) are in better agreement with the Planck+Bicep/Keck Array dataset, with the best fit obtained for the case $k \to \infty$. However, if we consider the Planck+ACT dataset the tailed attractors are disfavored at $\gtrsim 2\sigma$ confidence level.
The canonical fractional attractors are obtained by setting $\Lambda \leq 0, \omega > 0, \alpha > 0$ and considering a Jordan frame potential $V(\phi) > 0$. In this case the Einstein frame potential takes the form:

$$U(\phi) = \frac{V(\phi) - \Lambda}{8\alpha(V(\phi) - \Lambda) + \omega^2}, \tag{253}$$

by choosing a potential in the monomial form $V(\phi) = \lambda\phi^k$ one gets the predictions for CMB observables (see the attached paper for the details):

$$r \sim 0, \tag{254}$$

$$n_s = 1 - \frac{k+1}{k+2}\frac{2}{N_*}. \tag{255}$$

As remarked in [56] canonical attractors fit very well the Planck+ACT dataset for simple choices of $k = 2, 4$, with the former being favored. If instead one considers the Planck+ Bicep/Keck Array dataset only, steeper potential are favored, as for the tailed attractors. Given the success of this framework in providing inflationary setups we decided to study a scenario for quintessential inflation in III. In particular we embedded the generalized Peebles-Vilenkin potential (see eq. 8 of paper III) $k = 2, 4, 8$ and $q = 4$ in a quadratic $F(R, X) = R_X + \alpha R_X^2$ (i.e. in the form of canonical attractors) with $\Lambda = 0$, $\omega = 1$. The free parameters of the model are α, λ and M. Moreover, since we do not constraint the reheating mechanism the reheating temperature T_{reh} is also considered a free parameter. The parameter α is constrained through the inflationary observables r, n_s, which give $\alpha \gtrsim 10^8$. The parameter λ is fixed by requiring $A_s = 2.1 \cdot 10^{-9}$ (see Fig.2 of paper III). The model in order to provide a viable mechanism for quintessence needs to behave as thawing quintessence (see section 4.1). In order to do so, it requires the scalar to unfreeze only in recent times. This happens if $M > M_{\text{min}}$, to be computed numerically. At the same time we can constraint the reheating temperature T_{reh} by considering the bound on the overproduction of gravitational waves discussed in section 5.2. Unfortunately doing so makes the model not viable as the coincidence problem cannot be solved. However, by assuming the production of heavy particles in the early Universe with a characteristic mass of order 10^{15} GeV (which later decay in the Standard Model particles) [79] we can relax the constraint on T_{reh}. This makes the model parameter space viable. In particular we find that $M \sim 10^3 - 10^5$ GeV and $T_{\text{reh}} \sim 0.1 - 10^3$ GeV solve the coincidence problem and provide an experimentally viable quintessential inflation model for $k = 4, q = 4$. A similar analysis was carried for an higher order $F(R, X)$ by choosing a suitable exponential version of the Peebles-Vilenkin potential. See the attached paper for the details.

List of Figures

(if needed)

References

[1] Christian Dioguardi, Antonio Racioppi, and Eemeli Tomberg. Slow-roll inflation in Palatini F(R) gravity. *JHEP*, 06:106, 2022.

[2] Christian Dioguardi and Antonio Racioppi. Palatini F(R,X): A new framework for inflationary attractors. *Phys. Dark Univ.*, 45:101509, 2024.

[3] Konstantinos Dimopoulos, Christian Dioguardi, Gert Hütsi, and Antonio Racioppi. Quintessential inflation in palatini F(R,X) gravity. *The European Physical Journal Plus*, 140(11), November 2025.

[4] N. Aghanim et al. Planck 2018 results. VI. Cosmological parameters. *Astron. Astrophys.*, 641:A6, 2020. [Erratum: Astron.Astrophys. 652, C4 (2021)].

[5] Y. Akrami et al. Planck 2018 results. X. Constraints on inflation. *Astron. Astrophys.*, 641:A10, 2020.

[6] P. A. R. Ade et al. Improved Constraints on Primordial Gravitational Waves using Planck, WMAP, and BICEP/Keck Observations through the 2018 Observing Season. *Phys. Rev. Lett.*, 127(15):151301, 2021.

[7] Adame et al. Desi 2024 vi: cosmological constraints from the measurements of baryon acoustic oscillations. *Journal of Cosmology and Astroparticle Physics*, 2025(02):021, February 2025.

[8] Erminia Calabrese et al. The Atacama Cosmology Telescope: DR6 Constraints on Extended Cosmological Models. 3 2025.

[9] F. Donato, G. Gentile, P. Salucci, C. Frigerio Martins, M. I. Wilkinson, G. Gilmore, E. K. Grebel, A. Koch, and R. Wyse. A constant dark matter halo surface density in galaxies. *Mon. Not. Roy. Astron. Soc.*, 397:1169–1176, 2009.

[10] David Harvey, Richard Massey, Thomas Kitching, Andy Taylor, and Eric Tittley. The non-gravitational interactions of dark matter in colliding galaxy clusters. *Science*, 347:1462–1465, 2015.

[11] Marco Cirelli, Alessandro Strumia, and Jure Zupan. Dark Matter. 6 2024.

[12] E. Aprile et al. The XENONnT dark matter experiment. *Eur. Phys. J. C*, 84(8):784, 2024.

[13] M. F. Albakry et al. A Strategy for Low-Mass Dark Matter Searches with Cryogenic Detectors in the SuperCDMS SNOLAB Facility. In *Snowmass 2021*, 3 2022.

[14] M. G. Aartsen et al. The IceCube Neutrino Observatory: Instrumentation and Online Systems. *JINST*, 12(03):P03012, 2017. [Erratum: JINST 19, E05001 (2024)].

[15] Alan H. Guth. The Inflationary Universe: A Possible Solution to the Horizon and Flatness Problems. *Phys. Rev. D*, 23:347–356, 1981.

[16] Andrei D. Linde. A New Inflationary Universe Scenario: A Possible Solution of the Horizon, Flatness, Homogeneity, Isotropy and Primordial Monopole Problems. *Phys. Lett. B*, 108:389–393, 1982.

[17] Andreas Albrecht and Paul J. Steinhardt. Cosmology for Grand Unified Theories with Radiatively Induced Symmetry Breaking. *Phys. Rev. Lett.*, 48:1220–1223, 1982.

[18] Peter W. Higgs. Broken symmetries and the masses of gauge bosons. *Phys. Rev. Lett.*, 13:508–509, Oct 1964.

[19] Georges Aad et al. Observation of a new particle in the search for the Standard Model Higgs boson with the ATLAS detector at the LHC. *Phys. Lett. B*, 716:1–29, 2012.

[20] Javier Rubio. Higgs inflation. *Front. Astron. Space Sci.*, 5:50, 2019.

[21] Alexei A. Starobinsky. A New Type of Isotropic Cosmological Models Without Singularity. *Phys. Lett. B*, 91:99–102, 1980.

[22] E. Allys et al. Probing Cosmic Inflation with the LiteBIRD Cosmic Microwave Background Polarization Survey. *PTEP*, 2023(4):042F01, 2023.

[23] Kevork Abazajian et al. Snowmass 2021 CMB-S4 White Paper. 3 2022.

[24] Jian-Ping Hu and Fa-Yin Wang. Hubble Tension: The Evidence of New Physics. *Universe*, 9(2):94, 2023.

[25] Sean Carroll. *Spacetime and Geometry: An Introduction to General Relativity*. Benjamin Cummings, 2003.

[26] Wendy L. Freedman. The Hubble constant and the expansion age of the universe. *Phys. Rept.*, 333:13–31, 2000.

[27] D. J. Fixsen. The temperature of the cosmic microwave background. *The Astrophysical Journal*, 707(2):916–920, November 2009.

[28] Daniel Baumann. Tasi lectures on inflation, 2012.

[29] David Wands, Karim A. Malik, David H. Lyth, and Andrew R. Liddle. A New approach to the evolution of cosmological perturbations on large scales. *Phys. Rev. D*, 62:043527, 2000.

[30] Juan Martin Maldacena. Non-Gaussian features of primordial fluctuations in single field inflationary models. *JHEP*, 05:013, 2003.

[31] Viviana Acquaviva, Nicola Bartolo, Sabino Matarrese, and Antonio Riotto. Second order cosmological perturbations from inflation. *Nucl. Phys. B*, 667:119–148, 2003.

[32] Scott Dodelson. *Modern Cosmology*. Academic Press, Amsterdam, 2003.

[33] Elisa G. M. Ferreira, Evan McDonough, Lennart Balkenhol, Renata Kallosh, Lloyd Knox, and Andrei Linde. The BAO-CMB Tension and Implications for Inflation. 7 2025.

[34] Antonio Racioppi and Martin Vasar. On the number of e-folds in the Jordan and Einstein frames. *Eur. Phys. J. Plus*, 137(5):637, 2022.

[35] Shinji Tsujikawa. Quintessence: A Review. *Class. Quant. Grav.*, 30:214003, 2013.

[36] T. Barreiro, Edmund J. Copeland, and N. J. Nunes. Quintessence arising from exponential potentials. *Phys. Rev. D*, 61:127301, 2000.

[37] P. J. E. Peebles and A. Vilenkin. Quintessential inflation. *Phys. Rev. D*, 59:063505, 1999.

[38] Konstantinos Dimopoulos and Charlotte Owen. Quintessential Inflation with α-attractors. *JCAP*, 06:027, 2017.

[39] Toby Opferkuch, Pedro Schwaller, and Ben A. Stefanek. Ricci reheating. *Journal of Cosmology and Astroparticle Physics*, 2019(07):016, jul 2019.

[40] Bo Feng and Mingzhe Li. Curvaton reheating in non-oscillatory inflationary models. *Physics Letters B*, 564(3):169–174, 2003.

[41] Md Riajul Haque, Essodjolo Kpatcha, Debaprasad Maity, and Yann Mambrini. Primordial black hole reheating. *Phys. Rev. D*, 108:063523, Sep 2023.

[42] Gary Felder, Lev Kofman, and Andrei Linde. Instant preheating. *Phys. Rev. D*, 59:123523, May 1999.

[43] Konstantinos Dimopoulos and Leonora Donaldson-Wood. Warm quintessential inflation. *Physics Letters B*, 796:26–31, 2019.

[44] E.J. Chun, S. Scopel, and I. Zaballa. Gravitational reheating in quintessential inflation. *Journal of Cosmology and Astroparticle Physics*, 2009(07):022, jul 2009.

[45] Jaume de Haro and Llibert Aresté Saló. A Review of Quintessential Inflation. *Galaxies*, 9(4):73, 2021.

[46] Chao Chen, Suruj Jyoti Das, Konstantinos Dimopoulos, and Anish Ghoshal. Flipped Rotating Axion Non-minimally Coupled to Gravity: Baryogenesis and Dark Matter. 2 2025.

[47] Urbano França and Rogerio Rosenfeld. Fine tuning in quintessence models with exponential potentials. *JHEP*, 10:015, 2002.

[48] Attilio Palatini. Deduzione invariantiva delle equazioni gravitazionali dal principio di Hamilton. *Rendiconti del Circolo Matematico di Palermo*, 43.1:203–212, 1919.

[49] Albert Einstein. Einheitliche Feldtheorie von Gravitation und Elektrizitat. *Verlag der Koeniglich-Preussichen Akademie der Wissenschaften*, 22:414–419, 1925.

[50] Florian Bauer and Durmus A. Demir. Inflation with Non-Minimal Coupling: Metric versus Palatini Formulations. *Phys. Lett. B*, 665:222–226, 2008.

[51] Tomi Koivisto and Hannu Kurki-Suonio. Cosmological perturbations in the palatini formulation of modified gravity. *Class. Quant. Grav.*, 23:2355–2369, 2006.

[52] Thomas P. Sotiriou and Valerio Faraoni. f(R) Theories Of Gravity. *Rev. Mod. Phys.*, 82:451–497, 2010.

[53] Morad Amarzguioui, O. Elgaroy, D. F. Mota, and T. Multamaki. Cosmological constraints on f(r) gravity theories within the palatini approach. *Astron. Astrophys.*, 454:707–714, 2006.

[54] Thomas P. Sotiriou. Constraining f(R) gravity in the Palatini formalism. *Class. Quant. Grav.*, 23:1253–1267, 2006.

[55] Christian Dioguardi and Alexandros Karam. Palatini linear attractors are back in action. *Phys. Rev. D*, 111(12):123521, 2025.

[56] Christian Dioguardi, Antonio J. Iovino, and Antonio Racioppi. Fractional attractors in light of the latest ACT observations. *Phys. Lett. B*, 868:139664, 2025.

[57] Ioannis D. Gialamas, Alexandros Karam, Antonio Racioppi, and Martti Raidal. Has ACT measured radiative corrections to the tree-level Higgs-like inflation? 4 2025.

[58] Syksy Rasanen and Pyry Wahlman. Higgs inflation with loop corrections in the Palatini formulation. *JCAP*, 11:047, 2017.

[59] Antonio Racioppi. Coleman-Weinberg linear inflation: metric vs. Palatini formulation. *JCAP*, 12:041, 2017.

[60] Tommi Markkanen, Tommi Tenkanen, Ville Vaskonen, and Hardi Veermäe. Quantum corrections to quartic inflation with a non-minimal coupling: metric vs. Palatini. *JCAP*, 03:029, 2018.

[61] Laur Järv, Antonio Racioppi, and Tommi Tenkanen. Palatini side of inflationary attractors. *Phys. Rev. D*, 97(8):083513, 2018.

[62] Antonio Racioppi. Non-Minimal (Self-)Running Inflation: Metric vs. Palatini Formulation. *JHEP*, 21:011, 2020.

[63] Ioannis D. Gialamas, Alexandros Karam, and Antonio Racioppi. Dynamically induced Planck scale and inflation in the Palatini formulation. *JCAP*, 11:014, 2020.

[64] Laur Järv, Alexandros Karam, Aleksander Kozak, Angelos Lykkas, Antonio Racioppi, and Margus Saal. Equivalence of inflationary models between the metric and Palatini formulation of scalar-tensor theories. *Phys. Rev. D*, 102(4):044029, 2020.

[65] Vera-Maria Enckell, Kari Enqvist, Syksy Rasanen, and Lumi-Pyry Wahlman. Inflation with R^2 term in the Palatini formalism. *JCAP*, 02:022, 2019.

[66] Tommi Tenkanen. Minimal Higgs inflation with an R^2 term in Palatini gravity. *Phys. Rev. D*, 99(6):063528, 2019.

[67] I. Antoniadis, A. Karam, A. Lykkas, T. Pappas, and K. Tamvakis. Rescuing Quartic and Natural Inflation in the Palatini Formalism. *JCAP*, 03:005, 2019.

[68] I. Antoniadis, A. Karam, A. Lykkas, and K. Tamvakis. Palatini inflation in models with an R^2 term. *JCAP*, 11:028, 2018.

[69] Ioannis D. Gialamas, Alexandros Karam, Thomas D. Pappas, and Vassilis C. Spanos. Scale-invariant quadratic gravity and inflation in the Palatini formalism. *Phys. Rev. D*, 104(2):023521, 2021.

[70] Kristjan Kannike, Aleksei Kubarski, Luca Marzola, and Antonio Racioppi. Pseudo-Goldstone dark matter in a radiative inverse seesaw scenario. *JHEP*, 12:166, 2023.

[71] Luca Marzola and Antonio Racioppi. Minimal but non-minimal inflation and electroweak symmetry breaking. *JCAP*, 10:010, 2016.

[72] Antonio Racioppi. New universal attractor in nonminimally coupled gravity: Linear inflation. *Phys. Rev. D*, 97(12):123514, 2018.

[73] Kristjan Kannike, Aleksei Kubarski, Luca Marzola, and Antonio Racioppi. A minimal model of inflation and dark radiation. *Phys. Lett. B*, 792:74–80, 2019.

[74] Ioannis D. Gialamas, Alexandros Karam, Thomas D. Pappas, Antonio Racioppi, and Vassilis C. Spanos. Scale-invariance, dynamically induced Planck scale and inflation in the Palatini formulation. *J. Phys. Conf. Ser.*, 2105(1):012005, 2021.

[75] Antonio Racioppi, Jürgen Rajasalu, and Kaspar Selke. Multiple point criticality principle and Coleman-Weinberg inflation. *JHEP*, 06:107, 2022.

[76] Konstantinos Dimopoulos and Samuel Sánchez López. Quintessential inflation in Palatini $f(R)$ gravity. *Phys. Rev. D*, 103(4):043533, 2021.

[77] Konstantinos Dimopoulos, Alexandros Karam, Samuel Sánchez López, and Eemeli Tomberg. Palatini R ^{2} quintessential inflation. *JCAP*, 10:076, 2022.

[78] Christian Dioguardi, Antonio Racioppi, and Eemeli Tomberg. Beyond (and back to) Palatini quadratic gravity and inflation. *JCAP*, 03:041, 2024.

[79] Jaume de Haro. Reheating formulas in quintessential inflation via gravitational particle production. *Phys. Rev. D*, 109(2):023517, 2024.

[80] Christian Dioguardi and Massimiliano Rinaldi. A note on the linear stability of black holes in quadratic gravity. *Eur. Phys. J. Plus*, 135(11):920, 2020.

[81] N. Bostan, R. H. Dejrah, C. Dioguardi, and A. Racioppi. Natural inflation in Palatini F(R,X). *JCAP*, 07:082, 2025.

Acknowledgements

My greatest thanks go to Dr. Antonio Racioppi for his guidance and patience during my early days as a PhD student and junior researcher. I am also grateful for the valuable discussions and conversations throughout these years — both the serious and the less serious ones. Thanks to you, I've learned a great deal on a professional level and have grown both as a physicist and as a person. Thank you for being not just a supervisor, but also a friend.

Thanks to all the colleagues and friends I have had the pleasure of meeting, talking and working with: the former PhD fellows Kristjan, Ruiwen, Nico and Antonio (now grown-up researchers), and my current PhD colleagues Juan, Martin, Vini, Gala and Sasha, to whom I wish all the best for their future in the jungle that academia is today. Most importantly, thanks to them (and actually to Alex and Ioannis as well) for the table football matches — after years of constant daily training, we are all proudly semi-pros now.

Thanks as well to my co-supervisor Gert Hütsi and to the rest of the KBFI group. I truly believe this is the best group I could have done my PhD in, not only for its impressive scientific productivity but also for the warm and welcoming environment, which made these years smooth and relatively stress-free (an impressive achievement, considering the average PhD experience!).

A huge thank you also goes to the people and friends outside the office walls — all those who made my daily life a lighter experience. A special thanks to Guru, who has put up with me the longest.

But my deepest thanks go to Sofia, who found me almost two years ago and has decided to stick with me ever since. Thank you for your day-to-day support, for your patience on my moody days, and for standing by me in every decision I make. I wish the best for our future.

E infine grazie alla mia famiglia. Grazie per aver sempre stimato le mie scelte, in qualunque fase della mia vita, e per avermi spronato e incoraggiato nei momenti in cui io stesso ne dubitavo. Senza voi non sarei mai arrivato qui. Senza il vostro supporto concreto, morale ed emotivo non avrei combinato proprio nulla. Sono felice e orgoglioso di sapere di poter sempre contare su di voi e di poter ricambiare quando posso, nel modo in cui posso.

E un piccolo grazie va anche al me stesso del passato, perché se sei qui oggi, è anche grazie a te.

This work was supported by the Estonian Research Council Grant PRG1055.

Abstract
Inflation in F(R) Palatini gravity and beyond

The recent cosmological observations, challenge the Standard Cosmological Model. The new data coming from DESI seems to prefer a dynamical nature for dark-energy, over a cosmological constant, in order to describe the current accelerated expansion of the universe. Measurements of the current Universe expansion rate H_0 coming from SuperNovae Type1a are now in strong tension at $> 5\sigma$ confidence level with H_0 measurements coming from the Cosmic Microwave Background. Moreover, the recent Planck+ACT dataset, shows a $\approx 2\sigma$ tension with the previous Planck and Bicep/Keck Array observations which strongly favored the most popular inflationary models such as Higgs and Starobinsky inflation. If further confirmed by future observations these results could open a crisis for Modern Cosmology.

Within this thesis the author wants to address inflation and dark-energy in the context of Palatini gravity, an alternative formulation with respect to standard General Relativity, that predicts different phenomenology. In particular the author focuses on a specific class of extended models of gravity, the $F(R)$ theories, and discusses the phenomenology of inflation to model early universe expansion, and quintessence to describe the late time acceleration. In this work a detailed understanding of inflation in $F(R)$ Palatini gravity beyond the quadratic order it is achieved for the first time, developing a new method for the the computation of the CMB observables, and using it to study the features and the limitations of these models.

In this context, in the first paper I, it is proven that theories that contain terms diverging faster than R^2, do not have a graceful exit of inflation if the potential is positive and unbounded from above. It was also proven that theories with an $F(R)$ in the form $F(R) = R + \alpha R^n$ that diverges slower than R^2 can predict viable inflation according to the observations for $n \to 2$, if a simple monomial potential in the form $V(\phi) = \lambda\phi^k$ is considered.

In the second work II, the class of $F(R)$ models is extended to the class of $F(R, X)$, where X is the inflation kinetic term. There, it was proven that this class of models can easily overcome all the issues and pathologies of the standard $F(R)$ theories. The predictions for the class of quadratic $F(R, X)$ models are derived and classified based on their inflationary attractor behavior. In this paper it was further shown that for the quadratic $F(R)$s, almost any form of the potential $V(\phi)$ allows to predict viable CMB observables according to the observations.

Finally, in the third paper III the issue of the late time acceleration of the universe is considered. A quintessential inflation scenario was built in the context of $F(R, X)$ models, unifying the descriptions of inflation and dark-energy through the dynamics of a single scalar field. It was moreover shown that the $F(R, X)$ framework can provide viable quintessential inflation scenarios given specific assumptions on the particle physics in the early universe.

Kokkuvõte
Inflatsioon F(R) Palatini gravitatsioonis ja laiemalt

Hiljutised kosmoloogilised vaatlused on seadnud kosmoloogilise standardmudeli kehtivuse kahtluse alla. DESI uued andmed viitavad sellele, et universumi praeguse kiireneva paisumise kirjeldamiseks sobib pigem dünaamiline tumeenergia, mitte kosmoloogiline konstant. 1a tüüpi supernoovade mõõtmistel saadud praegune universumi paisumiskiirus H_0 on nüüd tugevas vastuolus (üle $> 5\sigma$ usaldusnivoo) kosmilise taustkiirguse mõõtmisel saadud H_0 väärtusega. Peale selle näitab uus Planck+ACT andmestik $\approx 2\sigma$ tasemel vastuolu varasemate Plancki ja Bicep/Keck Array vaatlustega, mis toetasid tugevalt kõige populaarsemaid inflatsioonimudeleid nagu Higgsi ja Starobinsky inflatsioon. Kui need tulemused leiavad kinnitust tuleviku vaatlustes, võib see tähendada tänapäevase kosmoloogia kriisi. Käesolevas väitekirjas käsitleme inflatsiooni ja tumeenergiat Palatini gravitatsiooni raames: see on standardse üldrelatiivsusteooria alternatiivne formuleering, mis ennustab teistsugust fenomenoloogiat. Eelkõige keskendume kindlale klassile laiendatud gravitatsioonimudelitele, $F(R)$ teooriatele, ja kasutame varajase universumi paisumise kirjeldamiseks inflatsiooni fenomenoloogiat ning hilise universumi kiireneva paisumise kirjeldamiseks kvintessentsi. Käesolevas töös jõuame esmakordselt inflatsiooni lähemale mõistmisele $F(R)$ Palatini gravitatsiooni üle teise järgu lahendite, arendame välja uue meetodi kosmilise taustkiirguse vaadeldavate suuruste arvutamiseks ning kasutame seda nende mudelite omaduste ja piiride uurimiseks.

Esimeses artiklis I tõestame, et teooriates, mis sisaldavad liikmeid, mis hajuvad kiiremini kui R^2, ei lõpe inflatsioon sujuvalt, kui potentsiaal on positiivne ja ülevalt tõkestamata. Samuti tõestame, et teooriad, kus $F(R)$ hajub aeglasemalt kui R^2, võivad ennustada vaatlustega kooskõlas olevat inflatsiooni $n \to 2$ korral, kui kasutame lihtsat monomiaalset potentsiaali kujul $V(\phi) = \lambda\phi^k$.

Teises artiklis II laiendame $F(R)$ mudelite klassi $F(R, X)$ mudeliteks, kus X on inflatoni kineetiline liige. Näitame, et see mudelite klass suudab vältida kõiki tavaliste $F(R)$ teooriate probleeme ja patoloogiaid, ning tuletame teist järku $F(R, X)$ mudelite ennustused, mida me klassifitseerime vastavalt nende inflatsioonilise atraktori käitumisele. Samuti näitame, et teist järku mudelite jaoks lubab peaaegu iga potentsiaali $V(\phi)$ kuju ennustada vaatlustega kooskõlas olevaid kosmilise taustkiirguse vaadeldavaid.

Viimases artiklis III käsitleme hilise universumi kiireneva paisumise probleemi. $F(R, X)$ mudelite raames konstrueerime kvintessents-inflatsiooni stsenaariumi, mis ühendab inflatsiooni ja tumeenergia kirjeldusi üheainsa skalaarvälja kaudu. Näitame, et sobivate eelduste korral võib $F(R, X)$ raamistik pakkuda vaatlustega kooskõlas olevaid kvintessents-inflatsiooni stsenaariume, kui teha varajase universumi osakesteefüüsika kohta teatud eeldusi.

Appendix

Publication I

Christian Dioguardi, Antonio Racioppi, and Eemeli Tomberg. Slow-roll inflation in Palatini F(R) gravity. *JHEP*, 06:106, 2022

Published for SISSA by Springer

Received: *February 14, 2022*
Revised: *May 6, 2022*
Accepted: *May 18, 2022*
Published: *June 20, 2022*

JHEP06(2022)106

Slow-roll inflation in Palatini $F(R)$ gravity

Christian Dioguardi,[a,b] **Antonio Racioppi**[b] **and Eemeli Tomberg**[b]

[a] *Tallinn University of Technology, Akadeemia tee 23, 12618 Tallinn, Estonia*
[b] *National Institute of Chemical Physics and Biophysics, Rävala 10, 10143 Tallinn, Estonia*
E-mail: christian.dioguardi@kbfi.ee, antonio.racioppi@kbfi.ee, eemeli.tomberg@kbfi.ee

Abstract: We study single field slow-roll inflation in the presence of $F(R)$ gravity in the Palatini formulation. In contrast to metric $F(R)$, when rewritten in terms of an auxiliary field and moved to the Einstein frame, Palatini $F(R)$ does not develop a new dynamical degree of freedom. However, it is not possible to solve analytically the constraint equation of the auxiliary field for a general $F(R)$. We propose a method that allows us to circumvent this issue and compute the inflationary observables. We apply this method to test scenarios of the form $F(R) = R + \alpha R^n$ and find that, as in the previously known $n = 2$ case, a large α suppresses the tensor-to-scalar ratio r. We also find that models with $F(R)$ increasing faster than R^2 for large R suffer from numerous problems.

Keywords: Cosmology of Theories BSM, Early Universe Particle Physics

ArXiv ePrint: 2112.12149

https://doi.org/10.1007/JHEP06(2022)106

Contents

JHEP06(2022)106

1 Introduction

Past and recent observations of the cosmic microwave background radiation (CMB) support the flatness and homogeneity of the Universe at large scales. Such properties can be explained by assuming an accelerated expansion during the very early Universe [1–4]. This inflationary era is also able to generate and preserve the primordial inhomogeneities which generated the subsequent large-scale structure that we observe. In its minimal version, inflation is usually formulated by adding to the Einstein-Hilbert action one scalar field, the inflaton, whose energy density induces the near-exponential expansion.

Recently, the BICEP/Keck Array experiment [5] has reduced even more the available parameter space, disfavoring most of the minimal inflationary models. On the other hand, the maybe most popular inflationary setup, the Starobinsky model [1], still lies in the allowed region. Such a model involves non-minimal gravity and it can be equivalently described by the addition of a R^2 term to the Einstein-Hilbert action or by a scalar field non-minimally coupled to gravity (e.g. [6] and references therein).

However, in the context of non-minimally coupled theories there is more than one *choice* of the dynamical degrees of freedom. In the common metric formulation, the metric tensor is the only dynamical degree of freedom, while the connection is fixed to be the Levi-Civita one. On the other hand, in the Palatini formulation, both the metric and the connection are independent variables. Their corresponding equations of motion (EoMs) will dictate

the eventual relation between the two variables. When the action is linear in the curvature scalar, the two formalisms lead to equivalent theories (i.e. the Levi-Civita connection arises from the solution of one EoM), otherwise the theories are completely different [7] and lead to different phenomenological predictions, as recently investigated in e.g. [8–52].

In particular, there is a dramatic difference between the metric and the Palatini formulations when an R^2 term is added to a single scalar field inflationary action. In the metric case, we obtain a bi-field inflationary setup (e.g. [53, 54] and references therein), while in the Palatini case we still obtain a single field scenario [19]. In the latter case, it is remarkable that the presence of the R^2 term leaves essentially unchanged all the phenomenological parameters except for the tensor-to-scalar ratio r, which can be arbitrarily lowered by increasing the coupling in front of the R^2 term. Motivated by the results of [19], one wonders if any other $F(R)$ in the Palatini formulation can produce analogous results. However, such models are more complicated to study than $F(R) = R+\alpha R^2$. When studying $F(R)$ theories, it is common to use a representation via an auxiliary field and move the problem to the Einstein frame. In Palatini $F(R) = R + \alpha R^2$ the EoM for the auxiliary field is independent of α and quite simple to solve [19]. Unfortunately, the same does not happen for any generic $F(R)$, where the EoM for the auxiliary field may not be analytically solvable at all. The purpose of our work is to present a method that allows the computation of inflationary predictions even in such a case.

The article is organized as follows. In section 2, we introduce the theory of a single field inflaton in the presence of Palatini $F(R)$ gravity and develop a new method that allows slow-roll computations even when it is not possible to solve exactly the EoM of the auxiliary field. In section 3, we apply our method to test scenarios of the form $F(R) = R + \alpha R^n$ with arbitrary $n > 1$. Finally, in section 4, we check the behaviour of the aforementioned scenarios beyond the slow-roll approximation, in particular in the high R limit. We present our conclusions in section 5. In appendix A, we compare our results to an earlier work [55] that discussed similar models.

2 Slow-roll computations

We start by considering the following action for a real scalar inflaton ϕ minimally coupled to a $F(R)$ gravity (in Planck units: $M_{\rm P} = 1$):

$$S_J = \int \mathrm{d}^4x\sqrt{-g_J}\left[\frac{1}{2}F(R(\Gamma)) - \frac{1}{2}k(\phi)g_J^{\mu\nu}\partial_\mu\phi\partial_\nu\phi - V(\phi)\right] , \tag{2.1}$$

where $k(\phi) > 0$ is the non-minimal kinetic function for the inflaton and $V(\phi)$ its positive scalar potential.[1] We stress that we are considering the Palatini formulation of gravity by using the notation $R(\Gamma)$, where R is the curvature scalar and $\Gamma^\rho_{\mu\nu}$ is the connection in the Jordan frame. As is customary, we rewrite the $F(R)$ term using the auxiliary field ζ

$$S_J = \int \mathrm{d}^4x\sqrt{-g_J}\left[\frac{1}{2}\left(F(\zeta) + F'(\zeta)\left(R(\Gamma) - \zeta\right)\right) - \frac{1}{2}k(\phi)g_J^{\mu\nu}\partial_\mu\phi\partial_\nu\phi - V(\phi)\right] , \tag{2.2}$$

[1] The study applies also to theories with ϕ non-minimally coupled to gravity, if it is possible to perform a frame transformation and cast the action in the form of (2.1) (or equivalently (2.2) e.g. [6, 40]). The cases where this is not possible need to be investigated separately. We postpone such a study to a future work.

JHEP06(2022)106

where $F'(\zeta) = \partial F/\partial\zeta$. Then, we move the theory to the Einstein frame via the Weyl transformation

$$g_{E\,\mu\nu} = F'(\zeta)\; g_{J\,\mu\nu}\,, \tag{2.3}$$

which leads to the action

$$S_E = \int \mathrm{d}^4x\sqrt{-g_E}\left[\frac{M_\mathrm{P}^2}{2}R_E - \frac{1}{2}g_E^{\mu\nu}\partial_\mu\chi\partial_\nu\chi - U(\chi,\zeta)\right], \tag{2.4}$$

where the canonically normalized scalar χ is defined by

$$\frac{\partial\chi}{\partial\phi} = \sqrt{\frac{k(\phi)}{F'(\zeta)}}\,, \tag{2.5}$$

and the full scalar potential is

$$U(\chi,\zeta) = \frac{V(\phi(\chi))}{F'(\zeta)^2} - \frac{F(\zeta)}{2F'(\zeta)^2} + \frac{\zeta}{2F'(\zeta)}\,. \tag{2.6}$$

By varying (2.4) with respect to ζ, we get its EoM in the Einstein frame,

$$2F(\zeta) - \zeta F'(\zeta) - k(\phi)\,\partial^\mu\phi\partial_\mu\phi\,F'(\zeta) - 4V(\phi) = 0\,, \tag{2.7}$$

where we assumed $F'(R), F''(R) \neq 0$. The standard procedure would be now to solve (2.7), determine the solution for the auxiliary field as $\zeta(\phi, \partial^\mu\phi\partial_\mu\phi)$ and insert it back into the action (2.4). However, for a generic $F(R)$, we cannot expect (2.7) to be explicitly solvable, even though it should still be satisfied. On the other hand, we might still be able to perform inflationary computations in the slow-roll approximation. Assuming that slow-roll conditions are satisfied (i.e. $g_J^{\mu\nu}\partial_\mu\phi\partial_\nu\phi \ll V(\phi)$),[2] we can write the EoM (2.7) as

$$G(\zeta) = V(\phi)\,, \tag{2.8}$$

with

$$G(\zeta) \equiv \frac{1}{4}\left[2F(\zeta) - \zeta F'(\zeta)\right]. \tag{2.9}$$

In the slow-roll approximation we still cannot always provide explicit solutions for ζ for a given $F(R)$. However, it is possible to perform inflationary computations by using the auxiliary field as a computational variable and using (2.8) as a constraint. First of all, by using (2.8), we replace $V(\phi)$ with $G(\zeta)$ in (2.6), obtaining a scalar potential[3] that depends only on the auxiliary field ζ:

$$U(\chi,\zeta) = \frac{1}{4}\frac{2F(\zeta) - \zeta F'(\zeta)}{F'(\zeta)^2} - \frac{F(\zeta)}{2F'(\zeta)^2} + \frac{\zeta}{2F'(\zeta)} = \frac{1}{4}\frac{\zeta}{F'(\zeta)} \equiv U(\zeta)\,. \tag{2.10}$$

We stress that the last result implies that $\zeta > 0$ in the slow-roll regime, since both the potential $U(\zeta)$ and $F'(\zeta)$ (controlling the signs of the Weyl transformation and the

[2] We will go back to the full evolution of the system in section 4 and discuss the slow-roll conditions in more detail.

[3] Note that $U(\zeta)$ is an actual scalar potential only when the kinetic term of ϕ is negligible like in slow-roll.

JHEP06(2022)106

kinetic term) should be positive there. It was shown in [19] that $F(R) = R + \alpha R^2$ gives an asymptotically flat potential, regardless of the initial $V(\phi)$. We can easily deduce from (2.10) that no other asymptotic form of $F(R)$ than $F(R) \sim R^2$ can give such a result.

Let us proceed and perform inflationary computations. We need to compute the first derivative of $U(\zeta)$ with respect to χ, the canonically normalized scalar field in the Einstein frame:

$$\frac{\partial}{\partial\chi}U(\zeta) = \frac{\partial\phi}{\partial\chi}\frac{\partial\zeta}{\partial\phi}\frac{\partial}{\partial\zeta}U(\zeta) = \sqrt{\frac{F'(\zeta)}{k(V^{-1}(G))}}\left(\frac{\partial G}{\partial\zeta}\frac{\partial V^{-1}}{\partial G}\right)^{-1}\frac{\partial U}{\partial\zeta}\,, \tag{2.11}$$

where we used the chain rule for the derivative of composite functions together with (2.5), and $V^{-1}(G)$ is the inverse function of $V(\phi)$ defined via (2.8). In the end, after using (2.9) for G, we have a function of ζ only. Similarly, for a general function $f(\zeta)$, we have:

$$\frac{\partial}{\partial\chi}f(\zeta) = g(\zeta)\frac{\partial f(\zeta)}{\partial\zeta}\,, \tag{2.12}$$

where

$$g(\zeta) \equiv \frac{\partial\zeta}{\partial\chi} = \sqrt{\frac{F'(\zeta)}{k(V^{-1}(G))}}\left(\frac{\partial G}{\partial\zeta}\frac{\partial V^{-1}}{\partial G}\right)^{-1}\,. \tag{2.13}$$

This derivative can be explicitly computed as long as V is invertible. This allows us to easily express higher order derivatives:

$$\frac{\partial^2}{\partial\chi^2}U(\zeta) = g(\zeta)\frac{\partial}{\partial\zeta}\left(g(\zeta)\frac{\partial U}{\partial\zeta}\right) = gg'U' + g^2U''\,,\ \ldots \tag{2.14}$$

From (2.11) and (2.14) we can derive the slow-roll parameters straightforwardly:

$$\epsilon(\zeta) = \frac{1}{2}\left(\frac{\partial U/\partial\chi}{U}\right)^2 = \frac{1}{2}g^2\left(\frac{U'}{U}\right)^2\,, \tag{2.15}$$

$$\eta(\zeta) = \frac{\partial^2 U/\partial\chi^2}{U} = \frac{gg'U' + g^2U''}{U}\,. \tag{2.16}$$

Hence, the equations for the CMB observables r, n_s, A_s read:

$$r(\zeta) = 16\epsilon(\zeta) = 8g^2\left(\frac{U'}{U}\right)^2\,, \tag{2.17}$$

$$n_s(\zeta) = 1 + 2\eta(\zeta) - 6\epsilon(\zeta) = 1 + \frac{2g}{U^2}\left(g'U'U + gU''U - 24gU'^2\right)\,, \tag{2.18}$$

$$A_s(\zeta) = \frac{U}{24\pi^2\epsilon(\zeta)} = \frac{U^3}{12\pi^2g^2U'^2}\,, \tag{2.19}$$

where A_s has to satisfy [56]

$$\ln\left(10^{10}A_s\right) = 3.044 \pm 0.014 \tag{2.20}$$

at the CMB scale. Analogously, the number of e-folds becomes

$$N_e = \int_{\chi_f}^{\chi_N}\frac{U}{\partial U/\partial\chi}\mathrm{d}\chi = \int_{\zeta_f}^{\zeta_N}\frac{U}{g^2\,\partial U/\partial\zeta}\mathrm{d}\zeta\,, \tag{2.21}$$

JHEP06(2022)106

where value at the end of inflation, ζ_f, is determined by[4] $\epsilon(\zeta_f) = 1$. Equation (2.21) determines the auxiliary field value ζ_N at the time a given scale leaves the horizon, corresponding to N_e. In our examples below, we take $N_e \in [50, 60]$ at CMB.

Before proceeding to examples, we will briefly comment on the mandatory requirements of our procedure in the following subsection.

2.1 Requirements

First of all we need to satisfy the usual requirements of any non-minimal gravity model, i.e. reproducing Einstein gravity as a low energy limit and having the correct positive sign in the Weyl transformation (2.3) (i.e. $F'(R) > 0$). Then, we need to satisfy the constraint in eq. (2.8). This induces several additional conditions. First, $V(\phi)$ needs to be an invertible function, so that we can define the function $g(\zeta)$ in eq. (2.13). The function $g(\zeta)$ must also be uniquely defined, therefore $G(\zeta)$ must be a bijective function, at least in a smaller domain that satisfies eq. (2.8). Last but not least, since $V(\phi)$ is positive everywhere, the same must be true also for $G(\zeta)$ in the region of validity of the slow-roll approximation, i.e. $\zeta > 0$. As we can see from eq. (2.9), this is not, in general, true for an arbitrary $F(R)$. The problem lies in the fact that $G(\zeta)$ is the difference of two generally positive terms $F(\zeta)$ and $\zeta F'(\zeta)$. Assuming that $F(\zeta) \sim \zeta^n$ for very large positive ζ, we can see from (2.9) that $G(\zeta)$ is positive in this limit only when $n \leq 2$. If that is the case, since G is continuous and behaves linearly around 0, G will take all possible positive values ensuring the existence of a ζ that satisfies (2.8) (and also (2.7)). We can easily extend the same reasoning to functions F that do not possess a monomial asymptotic behaviour, leading to the following summary of requirements for successful scenarios:

$$F(R) \sim R \quad \text{when } R \sim 0\,, \tag{2.22}$$

$$F'(R) > 0\,, \tag{2.23}$$

$$V(\phi) \quad \text{invertible}\,, \tag{2.24}$$

$$G(\zeta) \quad \text{bijective}\,, \tag{2.25}$$

$$G(\zeta) > 0 \text{ when } \zeta > 0 \Rightarrow \lim_{R\to+\infty} \frac{F(R)}{R^2} \to \text{positive or null constant}\,. \tag{2.26}$$

While it is relatively easy to satisfy the first four constraints, the last condition reduces noticeably the number of available $F(R)$ models. However, when (2.26) is not satisfied, it is still possible to perform some inflationary computations if some additional constraints are realized. When (2.26) does not hold but (2.22) and (2.23) do, $G(\zeta)$ is a function bounded from above (in the real positive domain) with at least one local maximum. This means that (2.8) can be satisfied only for the $V(\phi)$ values that lie within the upper limit of $G(\zeta)$. In this case, inflationary computations can still make sense if slow-roll is realized within such a region and $G(\zeta)$ is treated as an effective description.

[4] The careful reader might notice that $|\eta| = 1$ could trigger the end of slow-roll before the actual end of the inflationary phase. However, this is never the case in our example scenarios below, at least for the parameter space that we considered.

JHEP06(2022)106

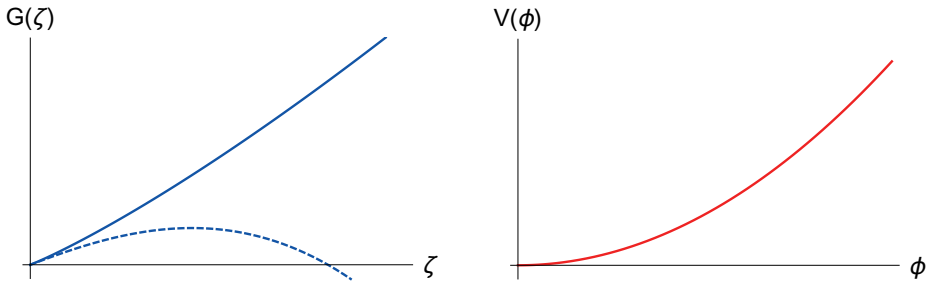

Figure 1. Reference plots of $G(\zeta)$ (left) and $V(\phi) = \phi^2$ (right) for $F(R) = R + R^n$ with $n = 3/2$ (continuous) and $n = 5/2$ (dashed).

In figure 1, we present a visual example of the issue. In the left panel we show a reference plot of $G(\zeta)$ for $F(R) = R + R^n$ with $n = 3/2$ (continuous) and $n = 5/2$ (dashed), while in the right panel we show a reference plot of $V(\phi) = \phi^2$. As we can see in the right panel, V is covering all positive values in the y-axis as expected. The same happens in the left panel for $n = 3/2$ i.e. when (2.26) is satisfied. Therefore, a ζ that satisfies (2.8) always exists. On the other hand, for $n = 5/2$ i.e. when (2.26) is not satisfied, G presents a local maximum and then decreases towards negative values. Therefore, when the V value is high enough, there is no real solution for ζ that can satisfy (2.8). Hence, an effective description is the only available working option. The positivity and bijectivity of G (together with condition (2.22)) can be still realized within the origin and the local maximum of G. Therefore slow-roll must be realized within this interval in order to have at least a feasible inflationary model.

In the following section, we will present a numerical study considering test scenarios in both $n < 2$ and $n > 2$ configurations. After that, we will comment on the beyond slow-roll behaviour and see in more detail the problems that arise if (2.26) is not satisfied for large ζ.

3 Test scenarios

In this section we test our method with

$$F(R) = R + \alpha R^n\,, \quad k(\phi) = 1\,, \quad V(\phi) = \frac{m^2}{2}\phi^2\,. \tag{3.1}$$

We consider two different scenarios,[5] $n < 2$ and $n > 2$. We stress that, during slow-roll, the positivity of both $U(\zeta)$ and $F'(\zeta)$ implies $\zeta > 0$ and $\alpha > 0$. Before proceeding, we also check that our procedure reproduces the results of [19] with $F(R) = R + \alpha R^2$ for any kind of $V(\phi)$.

[5] In the limit $\alpha \to \infty$, our results should agree with those of [55], where the authors considered slow-roll in Palatini $F(R)$ models with $F(R) \sim R^n$. However, this does not happen because of a sign error in [55]. We discuss the differences between our computation and theirs in appendix A.

JHEP06(2022)106

3.1 $n = 2$

We can easily verify that for the $F(R) = R + \alpha R^2$ we get the same results as in [19]. These results can be cast in the following form:

$$U = \frac{V}{1 + 8\alpha V} = \frac{U^0}{1 + 8\alpha U^0}\,, \tag{3.2}$$

$$r = \frac{r^0}{1 + 8\alpha U^0}\,, \tag{3.3}$$

$$n_s = n_s^0\,, \qquad N_e = N_e^0\,, \qquad A_s = A_s^0\,, \tag{3.4}$$

where $\ldots^0$ means that the quantity is computed for $\alpha = 0$. First of all, we check the scalar potential. Eq. (2.9) becomes

$$\begin{aligned} G(\zeta) &= \frac{1}{4}\left[2F(\zeta) - \zeta F'(\zeta)\right] = \frac{1}{4}\left[2\zeta + 2\alpha\zeta^2 - \zeta(1 + 2\alpha\zeta)\right] \\ &= \frac{1}{4}\zeta = V(\phi) = U^0\,, \end{aligned} \tag{3.5}$$

which leads to

$$U = \frac{1}{4}\frac{\zeta}{F'(\zeta)} = \frac{\zeta}{4 + 8\alpha\zeta} = \frac{U^0}{1 + 8\alpha U^0}\,, \tag{3.6}$$

in agreement with eq. (3.2). Let us check now the inflationary parameters, starting with r. First of all, we need to evaluate the g function:

$$g = \sqrt{F'(\zeta)}\left(\frac{\partial G}{\partial\zeta}\frac{\partial V^{-1}}{\partial G}\right)^{-1} = \sqrt{1 + 2\alpha\zeta}\left(\frac{\partial V^{-1}}{\partial\zeta}\right)^{-1}\,. \tag{3.7}$$

Therefore, the tensor-to-scalar ratio becomes

$$r(\zeta) = 8g^2\left(\frac{U'}{U}\right)^2 = \left(\frac{\partial V^{-1}}{\partial\zeta}\right)^{-2}\frac{8}{\zeta^2}\left(\frac{1}{1 + 2\alpha\zeta}\right) = \frac{r^0}{1 + 8\alpha U^0}\,, \tag{3.8}$$

again in agreement with the result of [19] in eq. (3.3). Analogously we can prove the validity of the remaining results in eq. (3.4).

3.2 $n < 2$

In this subsection we apply our method on the model in (3.1) for $1 < n < 2$. Such a scenario satisfies all the requirements listed in (2.22)–(2.26). Applying (2.17), (2.18) and (2.19) we can compute the phenomenological parameters:

$$N_e = \left[\frac{\zeta\,(n - (n-1))}{8m^2}\,{}_2F_1\left(1, \frac{1}{n-1}; \frac{n}{n-1}; (n-2)\alpha\zeta^{n-1}\right)\right]_{\zeta=\zeta_f}^{\zeta=\zeta_N}\,, \tag{3.9}$$

$$r(\zeta_N) = \frac{64m^2}{\zeta_N}\frac{1 + \alpha(2-n)\zeta_N^{n-1}}{1 + \alpha n\zeta_N^{n-1}}\,, \tag{3.10}$$

$$n_s(\zeta_N) = 1 - \frac{8m^2}{\zeta_N}\frac{2 + \alpha(n-2)(n-3)\zeta_N^{n-1}}{1 + \alpha(2-n)n\zeta_N^{n-1}}\,, \tag{3.11}$$

$$A_s(\zeta_N) = \frac{1}{384\pi^2 m^2}\frac{\zeta_N^2}{1 + \alpha(2-n)\zeta_N^{n-1}}\,, \tag{3.12}$$

JHEP06(2022)106

where we used the hypergeometric function

$$ {}_2F_1(a,b,c,z) = \sum_{k=0}^{\infty} \frac{(a)_n (b)_n}{(c)_n} \frac{z^n}{n!} \tag{3.13} $$

with $(q)_n$ the (rising) Pochhammer symbol. Notice that the $n = 2$ case is also described by eqs. (3.9)–(3.12). We can also derive more readable expressions in the limit $|n-2|\alpha \to \infty$ (which automatically excludes the $n = 2$ configuration). In such a limit we can approximate the number of e-folds as

$$ N_e \sim \frac{n}{8m^2} \zeta_N \,, \tag{3.14} $$

obtaining

$$ r(\zeta_N) \simeq \frac{8(2-n)}{N_e} \,, \tag{3.15} $$

$$ n_s(\zeta_N) \simeq 1 - \frac{3-n}{N_e} \,, \tag{3.16} $$

$$ A_s(\zeta_N) \simeq \frac{2^{2-3n} \left(\frac{n}{N_e}\right)^{n-3}}{3\pi^2(2-n)} \frac{(m^2)^{2-n}}{\alpha} \,. \tag{3.17} $$

We show in figure 2 a more detailed numerical analysis, where we plot r vs. n_s (a), r vs. α (b), α vs. n_s (c) and m vs. α (d) for $n = 3/2$ (green), $n = 7/4$ (red), $n = 31/16$ (blue) with $N_e = 50$ (dashed) and $N_e = 60$ (dotted), while A_s is fixed to the observed value (2.20). For reference we also plot the predictions for $N_e \in [50, 60]$ of the corresponding asymptotic solutions in eqs. (3.15)–(3.17) (same color code, continuous line), of quadratic inflation (black) and for $n = 2$ with $N_e = 50$ (black, dashed) and $N_e = 60$ (black, dotted). The orange areas represent the $1,2\sigma$ allowed regions coming from the latest combination of Planck, BICEP/Keck and BAO data [5]. The numerical results in figure 2(a) were obtained by varying the parameter m from $m = 6.98 \cdot 10^{-6}$ ($N_e = 50$) and $m = 5.82 \cdot 10^{-6}$ ($N_e = 60$) to $m = 1.6 \cdot 10^{-5}$ (both $N_e = 50, 60$). This is equivalent to increase the parameter α since the relation between the two parameters is fixed by the amplitude of the power spectrum (cf. eqs. (2.19) and (3.17)), as shown in figure 2(d). From figure 2(b) we notice that the net effect of the αR^n term is to lower the tensor-to-scalar ratio r. As we get closer to $n = 2$ we see that this effect is enhanced, as expected, approaching the asymptotic value (3.15) for $\alpha \to \infty$. A similar discussion also applies to n_s in figure 2(c). In this case, n_s increases until α is big enough, and then n_s approaches the asymptotic value (3.16).

To conclude, we stress that the limits for $\alpha \to +\infty$ with $n = 2$ and $n \neq 2$ are two completely different configurations. However, as can be deduced from figure 2, keeping n fixed, it is always possible to identify a maximum value for α so that the results between $n = 2$ and $n \neq 2$ are indistinguishable and this maximum value increases with n getting closer to 2. Then, for α values above such a maximum, the results for $n = 2$ and $n \neq 2$ depart, converging towards two different asymptotic configurations. In particular, eqs. (3.10) and (3.11) with $n = 2$ are asymptotic limits, approached when n is very close to 2, but never reached. Our results show that at a given $\alpha \gg 1$, a slight variation from $n = 2$ might completely jeopardize the inflationary predictions of the $n = 2$ case. This happens when $\alpha \gg \frac{1}{|n-2|}$.

JHEP06(2022)106

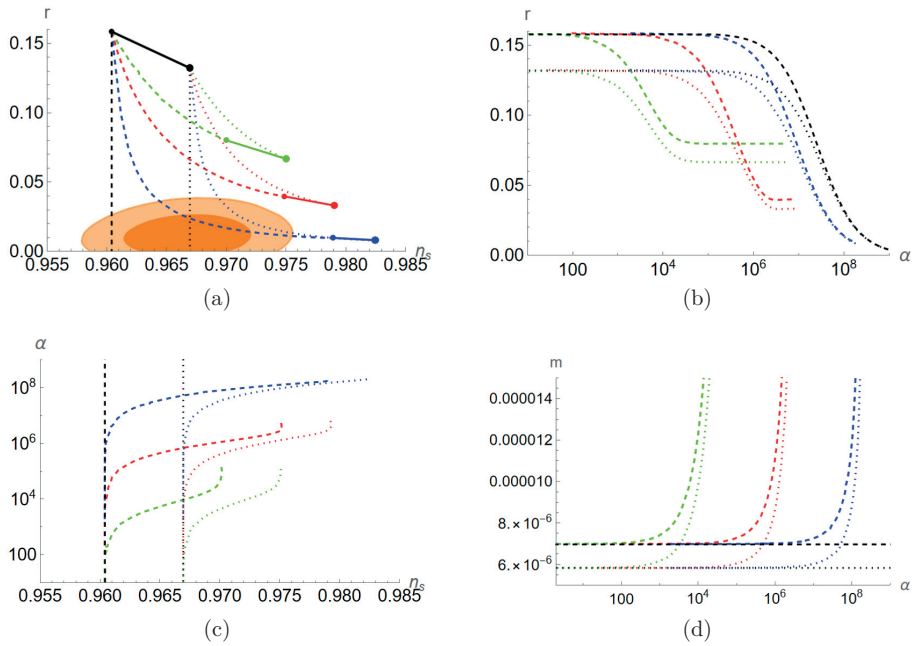

Figure 2. The observables r vs. n_s (a), r vs. α (b), α vs. n_s (c) and m vs. α (d) for the model in (3.1) with $n = 3/2$ (green), $n = 7/4$ (red), $n = 31/16$ (blue) and $n = 2$ (black) for $N_e = 50$ (dashed) and $N_e = 60$ (dotted). The scalar amplitude A_s is fixed to its observed value. For reference, we also plot the predictions for $N_e \in [50, 60]$ of the corresponding asymptotic solutions in eqs. (3.15)–(3.17) (same color code, continuous line) and of quadratic inflation (black). The orange areas represent the 1,2σ allowed regions coming from the latest combination of Planck, BICEP/Keck and BAO data [5].

3.3 $n > 2$

In this subsection, we test our method with the setup of eq. (3.1) but for $n > 2$. Such a scenario satisfies the requirements (2.22)–(2.24), but not (2.26). Moreover also (2.25) requires additional care. We start by checking the constraint (2.8):

$$G(\zeta) = \frac{1}{4}\left[\zeta - \alpha(n-2)\zeta^n\right] = V(\phi)\,. \tag{3.18}$$

For $n > 2$, $G(\zeta)$ is a function unbounded from below and exhibits a local maximum at $\zeta_{\max} = [\alpha\, n\, (n-2)]^{\frac{1}{1-n}}$. Therefore (2.26) is not satisfied, but we can still treat the model as an effective theory if slow-roll is realized between 0 and $\zeta_{\max}$. In such a domain we also manage to satisfy (2.25).

In the region of validity of the model the inflationary parameters are still given by (3.9)–(3.12). We show in figure 3 a more detailed numerical analysis, where we plot r vs. n_s (a), r vs. α (b), α vs. n_s (c) and m vs. α (d) for $n = 3$ (blue), $n = 5/2$ (red), $n = 9/4$ (green) with $N_e = 50$ (dashed) and $N_e = 60$ (dotted). For reference we also plot the results for $n = 2$ with $N_e = 50$ (black, dashed) and $N_e = 60$ (black, dotted). The scalar amplitude A_s is fixed

JHEP06(2022)106

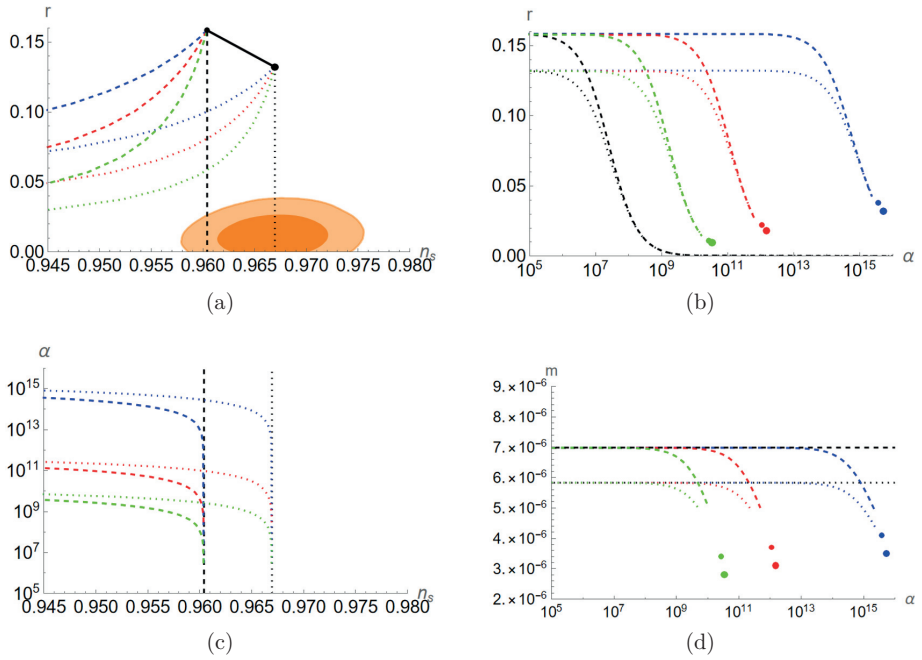

Figure 3. The observables r vs. n_s (a), r vs. α (b), α vs. n_s (c) and m vs. α (d) for the model in (3.1) with $n = 3$ (blue), $n = 5/2$ (red), $n = 9/4$ (green) and $n = 2$ (black) for $N_e = 50$ (dashed) and $N_e = 60$ (dotted). In the same color code, we show the limit values $r_{\bar{\alpha}}$ (eq. (3.21)) and $m_{\bar{\alpha}}$ (eq. (3.19)) for $N_e = 50$ (small dot) and $N_e = 60$ (large dot). The scalar amplitude A_s is fixed to its observed value. The orange areas represent the 1,2σ allowed regions coming from the latest combination of Planck, BICEP/Keck and BAO data [5].

to its observed value. The orange areas again represent the 1,2σ allowed regions coming from the latest combination of Planck, BICEP/Keck and BAO data [5]. The numerical results were obtained by varying the parameter m in the range $3.95 \cdot 10^{-6} < m < 5.82 \cdot 10^{-6}$ ($N_e = 60$) and $4.44 \cdot 10^{-6} < m < 6.98 \cdot 10^{-6}$ ($N_e = 50$). Once again the net effect of the αR^n term is to lower r, and this effect is more enhanced as n approaches 2. However, the effect on n_s and m is the opposite with the respect to the $n < 2$ case. In fact, now, by increasing α both n_s and m are decreasing.

We can also see that, for a given n, there is an upper limit on α. Since slow-roll inflation happens between 0 and $\zeta_{\max}$, the possible number of e-folds is bounded from above in a given model. In order to get the required amount of e-folds, we need $\zeta_N < \zeta_{\max}$ at $N_e \in [50, 60]$. However, by increasing α, $\zeta_{\max}$ decreases and the distance between ζ_N and $\zeta_{\max}$ decreases as well. We can set a rough upper limit for α when $\zeta_N = \zeta_{\max}$. The limit is only rough because η has a pole at $\zeta = \zeta_{\max}$ meaning the loss of validity of the slow-roll approximation. Such a pole is reflected in figure 3(c) with the appearance of horizontal asymptotes with n_s pointing towards $-\infty$. Therefore the actual upper limit $\bar{\alpha}$ takes place

JHEP06(2022)106

for ζ_N not equal, but slightly smaller than $\zeta_{\max}$. Nevertheless, we can still provide useful estimates for the limit values of r, m and α by using $\zeta_N = \zeta_{\max}$. First of all, we impose such a condition on the amplitude of the power spectrum (3.12), obtaining a limit for m^2:

$$m^2_{\bar{\alpha}} \simeq \frac{n(\bar{\alpha}(n-2)n)^{-\frac{2}{n-1}}}{384\pi^2(n-1)A_s}\,, \tag{3.19}$$

where A_s satisfies (2.20). We can now compute the number of e-folds (3.9) till $\zeta_{\max}$, obtaining

$$N_e \sim (\bar{\alpha}(n-2)n)^{\frac{1}{n-1}}\,\frac{48\pi^2(n-1)A_s}{n}\left[n + (1-n)\,{}_2F_1\left(1, \frac{1}{n-1}; \frac{n}{n-1}; \frac{1}{n}\right)\right]. \tag{3.20}$$

We can use (3.20) as a definition for $\bar{\alpha}$. Using the previous results, we obtain the limit value for r

$$r_{\bar{\alpha}} \simeq \frac{(n-2)(\bar{\alpha}(n-2)n)^{\frac{1}{1-n}}}{6\pi^2(n-1)A_s}\,. \tag{3.21}$$

The limit values $r_{\bar{\alpha}}$ and $m_{\bar{\alpha}}$ are shown respectively in figure 3(b) and figure 3(d) for $n = 3$ (blue), $n = 5/2$ (red) and $n = 9/4$ (green). The small (large) dot stands for $N_e = 50$ (60) e-folds. As we can see, the numerical values for r approach closely the limit ones, but cannot reach them because that would imply a violation of the slow-roll approximation. Analogously, $m_{\bar{\alpha}}$ and the actual limit of m have the same order of magnitude.

4 Beyond slow-roll approximation

To gain a sense of the global dynamics of our models, it is interesting to solve their evolution numerically without the slow-roll approximation, in particular for the problematic $n > 2$ case. Starting from the action (2.4), after some manipulations, the full Einstein frame EoMs read:

$$\ddot{\phi} + 3H\dot{\phi} + \frac{V'(\phi)}{F'(\zeta)k(\phi)} = \frac{\dot{\phi}\dot{\zeta}F''(\zeta)}{F'(\zeta)} - \frac{1}{2}\frac{k'(\phi)}{k(\phi)}\dot{\phi}^2\,, \tag{4.1}$$

$$3H^2 = \frac{1}{2}\frac{\dot{\phi}^2}{F'(\zeta)}k(\phi) + U(\phi,\zeta)\,, \tag{4.2}$$

$$-\frac{1}{2}\dot{\phi}^2F'(\zeta)k(\phi) + 2V(\phi) - 2G(\zeta) = 0\,. \tag{4.3}$$

These can be used to also derive

$$\dot{H} = -\frac{1}{2}\frac{\dot{\phi}^2}{F'(\zeta)}k(\phi)\,, \tag{4.4}$$

$$\epsilon_H \equiv -\frac{\dot{H}}{H^2} = \frac{12V(\phi) - 6F(\zeta) + 3\zeta F'(\zeta)}{6V(\phi) - 3F(\zeta) + 2\zeta F'(\zeta)}\,. \tag{4.5}$$

Again, solving the constraint equation (4.3) may be problematic, but it can be replaced with its time derivative which, using (4.1) and (4.3), reads

$$\dot{\zeta} = \frac{3H\dot{\phi}^2F'(\zeta)k(\phi) + 3V'(\phi)\dot{\phi}}{2G'(\zeta) + \frac{3}{2}\dot{\phi}^2F''(\zeta)k(\phi)}\,. \tag{4.6}$$

JHEP06(2022)106

To solve the full time evolution, one only needs to solve (4.3) once to get the initial condition of ζ; after that, it is simple to follow the time evolution of ζ through (4.6). The constraint (4.3) can later be used to check the accuracy of the result.

Let us check the slow-roll limit of the full equations. There, the potential terms dominate over the kinetic ones. The Hubble constraint becomes $3H^2 = U$ as usual. The constraint (4.3) becomes (2.8), $G(\zeta) = V(\phi)$, fixing a one-to-one correspondence between ϕ and ζ and the new canonical field χ, which in this limit can be defined through (2.5). Since in this limit, $\partial_\zeta U(\phi, \zeta) = 0$ (by construction), we have

$$\frac{\mathrm{d}U}{\mathrm{d}\chi} = \frac{\mathrm{d}\phi}{\mathrm{d}\chi}\partial_\phi U(\phi,\zeta) = \frac{V'(\phi)}{F'(\zeta)^{3/2}k(\phi)^{1/2}}\,, \tag{4.7}$$

and the field equation becomes

$$3H\dot\phi = -\frac{V'(\phi)}{F'(\zeta)k(\phi)} \qquad \Rightarrow \qquad 3H\dot\chi = -\frac{\mathrm{d}U}{\mathrm{d}\chi}\,, \tag{4.8}$$

as expected. In practice, the goodness of the slow-roll approximation can be estimated by comparing the extra terms in (4.1), (4.2), and (4.3) to the leading slow-roll terms.

4.1 $n < 2$

In this subsection, we study the time evolution beyond the slow-roll approximation for the test scenario in (3.1) with $n < 2$. In particular, we consider the following benchmark point:[6,7]

$$n = 3/2\,, \quad \alpha = 8710\,, \quad m = 1.15\cdot 10^{-5}\,. \tag{4.9}$$

The corresponding time evolution given by (4.3), (4.6) in the (ζ, ϕ) plane is depicted in the flow chart of figure 4. The darker orange region corresponds to inflation with $\epsilon_H < 1$. As expected, inflation takes place only when $\zeta > 0$ (cf. eq. (2.10)). The grey areas represent excluded regions either because $F'(\zeta)$ turns negative and $\dot\phi$ diverges[8] (for $\zeta < -5.9\cdot 10^{-9}$), or because $V(\phi) < G(\zeta)$ and the constraint equation (4.3) does not have real solutions for $\dot\phi$ (for small ϕ, large ζ). Slow-roll happens at the edge of this region, where $V(\phi) \approx G(\zeta)$, as explained above. The blue dot denotes the CMB scale with $N_e = 50$, and has $A_s = 2.1\cdot 10^{-9}$, $n_s = 0.967$, $r = 0.096$.

In figure 4, it was assumed that $H > 0$ and $\dot\phi < 0$. This is only one branch of the possible solutions. However, from the EoMs and symmetry of the potential V we see that the system stays invariant under the transformations $\dot\phi \leftrightarrow -\dot\phi$, $\phi \leftrightarrow -\phi$ (in particular, $\dot\zeta$ does not change). Thus, the $\dot\phi > 0$ branch is obtained by mirroring figure 4 with respect to the x-axis. The system can only jump from one branch to the other when $\dot\phi = 0$, that is, at the slow-roll edge of the right hand side grey region. In figure 4, trajectories with $\phi < 0$ end up on the lower edge and switch to the $\dot\phi > 0$ branch: the field rolls up the potential, slows down, stops, and turns around, entering slow-roll on the other branch. Trajectories with

[6] To deal with the fractional exponent for negative ζ, we take $F(R) = R + \alpha|R|^{3/2}$.

[7] We remind the reader that all parameters and field values are in Planck units, $M_\mathrm{P} = 1$.

[8] At the same limit, the Weyl transformation (2.3) becomes singular.

JHEP06(2022)106

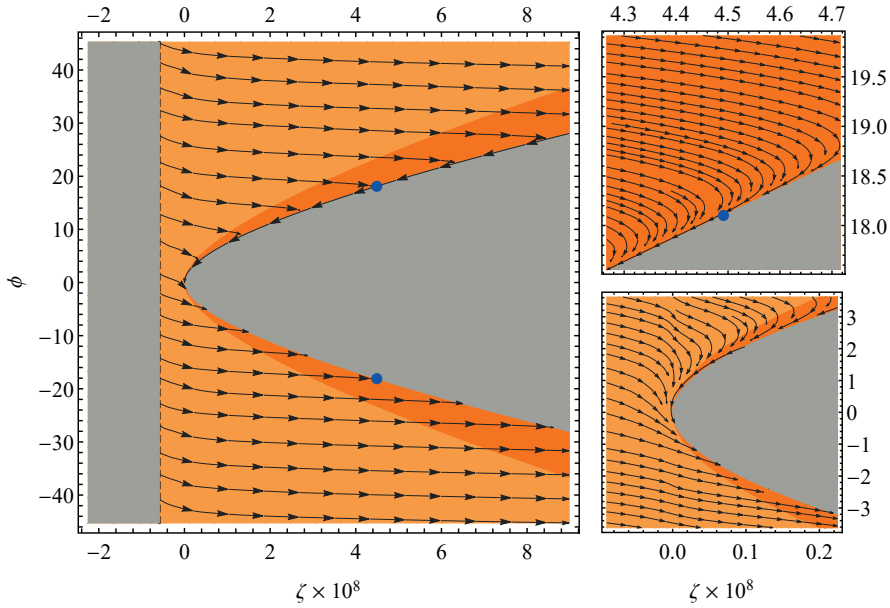

Figure 4. Time evolution of the model (3.1) for the benchmark point in (4.9) in the (ζ, ϕ) plane as given by (4.3), (4.6) (the $\dot{\phi} < 0$, $H > 0$ branch). The grey areas are excluded because either $F'(\zeta) < 0$ or (4.3) can't be satisfied. The darker orange region corresponds to inflation. The blue dots denote the CMB scale with $N_e = 50$, and have $A_s = 2.1 \cdot 10^{-9}$, $n_s = 0.967$, $r = 0.096$.

$\phi > 0$ approach the upper edge, but slow down due to Hubble friction and enter slow-roll right next to the edge on the same branch. This can be seen as sharp turns in the (ζ, ϕ) trajectories in the top right panel of figure 4. Note that two more branches, with $H < 0$, can be obtained by simply switching the direction of the flow; these can't be reached smoothly from the inflating branches in a spatially flat universe filled only with a scalar field.

Near the end of a slow-roll trajectory, the field approaches the origin with $\phi = \zeta = 0$, oscillating around it. This can be seen in the bottom right panel of figure 4. Here $\dot{\phi}$ changes sign repeatedly, and the evolution jumps from one branch to another as the oscillation amplitude dies down due to Hubble friction. Note that $\zeta < 0$ repeatedly during the oscillations.

Due to a rescaling symmetry of the action, the stream lines of a figure like 4 exactly describe the dynamics of a family of models where n and $\alpha \cdot m^{2(n-1)}$ are kept constant [57], up to a linear rescaling of ζ. This rescaling preserves the values of N_e, n_s, and r, but changes A_s. Beyond that, a chart that is qualitatively similar to figure 4 can be drawn for any model of the form (3.1) with $1 < n < 2$. Remarkably, in these models all trajectories with large enough initial field values eventually end up in the inflationary region and on a slow-roll trajectory.

JHEP06(2022)106

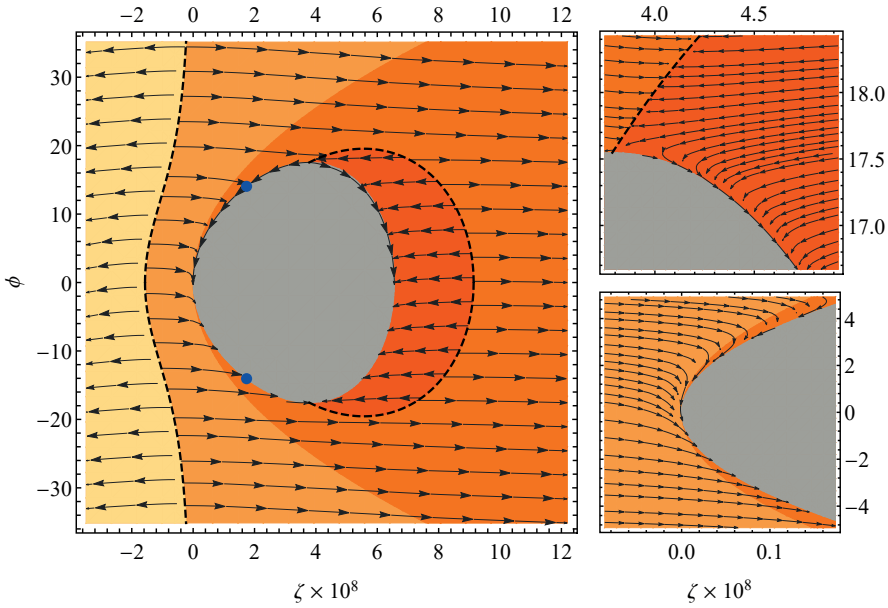

Figure 5. Time evolution of the model (3.1) for the benchmark point in (4.10) in the (ζ, ϕ) plane as given by (4.3), (4.6) (the $\dot{\phi} < 0$, $H > 0$ branch). Same as figure 4 with differences discussed in the text. The CMB numbers at the blue dot are $N_e = 50$, $A_s = 2.1 \cdot 10^{-9}$, $n_s = 0.952$, $r = 0.116$.

4.2 $n > 2$

In this subsection we study the time evolution beyond the slow-roll approximation for the test scenario in (3.1) with $n > 2$. In particular, we consider the following benchmark point:

$$n = 3\,, \quad \alpha = 2.32 \cdot 10^{14}\,, \quad m = 6.40 \cdot 10^{-6}\,. \tag{4.10}$$

The corresponding time evolution given by (4.3), (4.6) (the $\dot{\phi} < 0$, $H > 0$ branch) in the (ζ, ϕ) plane is depicted in figure 5. This is analogous to figure 4, but with the crucial difference that now $G(\zeta)$ has a maximum (here at $\zeta = 3.79 \cdot 10^{-8}$, corresponding to $|\phi| = 17.5$ on the slow-roll line) and begins to decrease for larger ζ, making the grey region where constraint (4.3) can't be satisfied terminate at $\zeta = 6.62 \cdot 10^{-8}$. Note also that for $|\phi| > 17.5$, not all $\dot{\phi}$-values are allowed, but there's a minimum value of $|\dot{\phi}|$ needed to solve (4.3). This limits the possible initial conditions of the system in terms of the Jordan frame variables.

A new feature emerges for $\zeta > 3.79 \cdot 10^{-8}$, marked by the dashed black line: a divergence of $\dot{\zeta}$ from (4.6), possible here since $G'(\zeta) < 0$. The darkest orange region inside this curve is separated from the rest of phase space — as figure 5 shows, it either attracts or repels all trajectories around it and can't be dynamically crossed — and while the system inflates there, and is even attracted to a slow-roll trajectory near the grey boundary as shown by the top right panel of figure 5, it is driven towards the point $(6.62 \cdot 10^{-8}, 0)$ where condition (2.22) is broken and we don't have the usual Einstein-Hilbert low-energy limit for gravity.

JHEP06(2022)106

We also have $G(\zeta) < 0$ for $\zeta < 0$. The low ζ limit is not given by the condition $F'(\zeta) = 0$ as above (here $F'(\zeta) > 0$ everywhere), but instead another divergence of $\dot{\zeta}$ (this time caused by $F''(\zeta) < 0$), denoted by the left-most dashed line. We cut off figure 5 near this line since, once again, it can't be crossed dynamically, so the left hand side is cut off from the observationally allowed trajectories in the vicinity of $\phi = \zeta = 0$.

These features are generic for models with $n > 2$ and signify their unhealthiness. Slow-roll can still happen at the edge of the grey area and terminate succesfully near $\phi = \zeta = 0$, as depicted by the bottom right panel of figure 5, though the maximum number of slow-roll e-folds is limited, as discussed above. However, most trajectories pass the slow-roll region and continue to $\zeta \to \infty$, never turning back. In this sense, the slow-roll region is not an attractor of the dynamics on a global scale.

5 Conclusions

We studied the dynamics of a (minimally coupled) single field inflaton in the presence of Palatini $F(R)$ gravity. Since such a scenario is not always explicitly solvable, we developed a method that allows the computation of the inflationary parameters if certain conditions are satisfied. Apart from the usual requirements of a generic $F(R)$ theory, as reproducing GR in the low energy limit or having attractive gravity, we found one additional constraint to be important: for curvatures going to infinity, either $F(R)$ should not diverge or it should not diverge faster than R^2. In case this last requirement is not satisfied, the theory exhibits problematic UV behaviour with additional divergences in phase space, though it can treated as an effective theory during slow-roll inflation. Moreover, to successfully apply our procedure, the Jordan frame inflaton potential $V(\phi)$ has to be an invertible function of ϕ.

We applied our method to a test scenario of an inflaton with a canonical kinetic term and a quadratic potential embedded in $F(R) = R + \alpha R^n$ gravity. We computed the inflationary predictions for both the $n < 2$ case, which satisfies all the requirements, and the $n > 2$ case with problematic behaviour. Both cases share the same effect on the tensor-to-scalar ratio r: for α increasing, r decreases, with the effect getting enhanced with n approaching 2. For the other phenomenological parameters, the two cases have opposite behaviours: for α increasing when $n < 2$ ($n > 2$), n_s and m are increasing (decreasing). Moreover, for $n > 2$ and given n and N_e, α shows an upper limit. We also checked the evolution of the system beyond the slow-roll approximation for both models. We discovered that $n < 2$ behaves well: all trajectories with large enough initial field values eventually end up in the inflationary region and on a slow-roll trajectory. On the other hand, in the $n > 2$ case, the slow-roll region is not an attractor of the dynamics on a global scale, another sign of the intrinsic illness of this setup.

We conclude with a remark about the $n = 2$ scenario. Such a configuration has been quite a powerful tool to adjust inflationary models, reducing r while leaving n_s practically unchanged. However, our study proves that in the strong coupling limit $\alpha \gg 1$, a slight variation from $n = 2$ can induce a large change in the n_s predictions. This might have a dramatic impact in ruling in/out inflationary models, especially in light of the increased

JHEP06(2022)106

Our notation	Notation of S. Bekov et al. [55]
ϕ	χ
$V(\phi) = \frac{1}{2}m^2\phi^2$	$U(\chi) = \frac{1}{2}m_\chi^2\chi^2$
$R = \zeta$	$\mathcal{R}$
$F(\zeta)$	$f(\mathcal{R})$
$F'(\zeta)$	ϕ
$\zeta F'(\zeta) - F(\zeta)$	$V(\phi) = \mathcal{R}\phi - f(\mathcal{R})$
ζ	$V'(\phi)$
$G(\zeta) = \frac{1}{4}[2F(\zeta) - \zeta F'(\zeta)]$	$-\frac{1}{4}[2V(\phi) - \phi V'(\phi)]$
$\sqrt{F'(\zeta)}\dot{\phi}$	$\dot{\chi}$

Table 1. A dictionary between the notation of this article and that of [55]. Note, in particular, the relation of the time derivatives: we use the Einstein frame time, whereas [55] works in the Jordan frame, leading to a difference related to the conformal factor $F'(\zeta)$. We have set $k(\phi) = 1$, and worked in Planck units, $M_P \equiv \kappa^{-1} = 1$.

precision of future experiments (e.g. Simons Observatory [58], PICO [59], CMB-S4 [60] and LITEBIRD [61]).

Acknowledgments

This work was supported by the Estonian Research Council grants MOBTT5, MOBTT86, PRG1055 and by the ERDF Centre of Excellence project TK133.

A Comparison to S. Bekov et al.

The authors of S. Bekov et al. [55] also studied slow-roll inflation in Palatini $F(R)$ models, with the same potential $V(\phi) = \frac{1}{2}m^2\phi^2$ as our (3.1), but choosing $F(R) = \alpha R^n$ without the linear part. As noted in section 2.1, this may be problematic for not producing the right low-R limit. Nevertheless, our results from section 3 should coincide with theirs in the limit $\alpha \to \infty$, but this is not the case. In particular, their prediction of $r = 0.34$ for $n = 3$ is significantly larger than ours, see figure 3.

One culprit for the difference is a sign error in equation (49) of [55]:

$$\phi(\chi) \approx \left(-\frac{k(n-2)}{2m_\chi^2(n-1)} \frac{1}{\kappa^2\chi^2} \right)^{\frac{1-n}{n}} . \tag{A.1}$$

Solving for $\phi(\chi)$ from their equations (37) and (48) produces the extra minus sign, here in red, that they omitted. Note that we use a different notation, and a somewhat different formalism, from that of [55]. Table 1 presents a dictionary between the two computations.

The minus sign in (A.1) makes $\phi(\chi)$ complex for $n > 2$, providing no slow-roll solutions. Indeed, for $n > 2$ their constraint equation for the auxiliary field in (35),

$$2V(\phi) - \phi V'(\phi) = \kappa^2\left(\dot{\chi}^2 - 4U(\chi)\right), \tag{A.2}$$

JHEP06(2022)106

can't be solved in the slow-roll limit of small field velocities. Using the dictionary of table 1 we see that (A.2) corresponds to our constraint equation (2.7), or equivalently (4.3), and for $n > 2$, we have $G(\zeta) = \frac{\alpha}{4}(2-n)\zeta^n < 0$ for all $\zeta > 0$, explaining the inability to find a solution. We see similar behaviour in our $F(R) = R + \alpha R^n$ case, where G becomes negative when the αR^n term starts to dominate at large field values, see the discussion in sections 2.1, 3.3, and 4.2. Indeed, in our slow-roll results in section 3.3, slow-roll always happens in the small-field regime where the linear R term is still significant.

In addition to the sign error, the authors of [55] used slow-roll parameters computed in the Jordan frame in the standard CMB formulae (2.17), (2.18). However, these formulae assume metric Einstein-Hilbert gravity with a canonical scalar field, and thus only work with slow-roll parameters computed in the Einstein frame as we did in our sutdy. These problems render the results of [55] invalid and explain the differences between our results and theirs.

References

[1] A.A. Starobinsky, *A New Type of Isotropic Cosmological Models Without Singularity*, *Phys. Lett. B* **91** (1980) 99 [INSPIRE].

[2] A.H. Guth, *The Inflationary Universe: A Possible Solution to the Horizon and Flatness Problems*, *Phys. Rev. D* **23** (1981) 347 [INSPIRE].

[3] A.D. Linde, *A New Inflationary Universe Scenario: A Possible Solution of the Horizon, Flatness, Homogeneity, Isotropy and Primordial Monopole Problems*, *Phys. Lett. B* **108** (1982) 389 [INSPIRE].

[4] A. Albrecht and P.J. Steinhardt, *Cosmology for Grand Unified Theories with Radiatively Induced Symmetry Breaking*, *Phys. Rev. Lett.* **48** (1982) 1220 [INSPIRE].

[5] BICEP and KECK collaborations, *Improved Constraints on Primordial Gravitational Waves using Planck, WMAP, and BICEP/Keck Observations through the 2018 Observing Season*, *Phys. Rev. Lett.* **127** (2021) 151301 [arXiv:2110.00483] [INSPIRE].

[6] L. Järv et al., *Frame-Independent Classification of Single-Field Inflationary Models*, *Phys. Rev. Lett.* **118** (2017) 151302 [arXiv:1612.06863] [INSPIRE].

[7] F. Bauer and D.A. Demir, *Inflation with Non-Minimal Coupling: Metric versus Palatini Formulations*, *Phys. Lett. B* **665** (2008) 222 [arXiv:0803.2664] [INSPIRE].

[8] T. Koivisto and H. Kurki-Suonio, *Cosmological perturbations in the palatini formulation of modified gravity*, *Class. Quant. Grav.* **23** (2006) 2355 [astro-ph/0509422] [INSPIRE].

[9] N. Tamanini and C.R. Contaldi, *Inflationary Perturbations in Palatini Generalised Gravity*, *Phys. Rev. D* **83** (2011) 044018 [arXiv:1010.0689] [INSPIRE].

[10] F. Bauer and D.A. Demir, *Higgs-Palatini Inflation and Unitarity*, *Phys. Lett. B* **698** (2011) 425 [arXiv:1012.2900] [INSPIRE].

JHEP06(2022)106

[11] S. Räsänen and P. Wahlman, *Higgs inflation with loop corrections in the Palatini formulation*, *JCAP* **11** (2017) 047 [arXiv:1709.07853] [INSPIRE].

[12] T. Tenkanen, *Resurrecting Quadratic Inflation with a non-minimal coupling to gravity*, *JCAP* **12** (2017) 001 [arXiv:1710.02758] [INSPIRE].

[13] A. Racioppi, *Coleman-Weinberg linear inflation: metric vs. Palatini formulation*, *JCAP* **12** (2017) 041 [arXiv:1710.04853] [INSPIRE].

[14] T. Markkanen, T. Tenkanen, V. Vaskonen and H. Veermäe, *Quantum corrections to quartic inflation with a non-minimal coupling: metric vs. Palatini*, *JCAP* **03** (2018) 029 [arXiv:1712.04874] [INSPIRE].

[15] L. Järv, A. Racioppi and T. Tenkanen, *Palatini side of inflationary attractors*, *Phys. Rev. D* **97** (2018) 083513 [arXiv:1712.08471] [INSPIRE].

[16] A. Racioppi, *New universal attractor in nonminimally coupled gravity: Linear inflation*, *Phys. Rev. D* **97** (2018) 123514 [arXiv:1801.08810] [INSPIRE].

[17] K. Kannike, A. Kubarski, L. Marzola and A. Racioppi, *A minimal model of inflation and dark radiation*, *Phys. Lett. B* **792** (2019) 74 [arXiv:1810.12689] [INSPIRE].

[18] V.-M. Enckell, K. Enqvist, S. Räsänen and E. Tomberg, *Higgs inflation at the hilltop*, *JCAP* **06** (2018) 005 [arXiv:1802.09299] [INSPIRE].

[19] V.-M. Enckell, K. Enqvist, S. Räsänen and L.-P. Wahlman, *Inflation with R^2 term in the Palatini formalism*, *JCAP* **02** (2019) 022 [arXiv:1810.05536] [INSPIRE].

[20] S. Räsänen, *Higgs inflation in the Palatini formulation with kinetic terms for the metric*, *Open J. Astrophys.* **2** (2019) 1 [arXiv:1811.09514] [INSPIRE].

[21] N. Bostan, *Non-minimally coupled quartic inflation with Coleman-Weinberg one-loop corrections in the Palatini formulation*, *Phys. Lett. B* **811** (2020) 135954 [arXiv:1907.13235] [INSPIRE].

[22] N. Bostan, *Quadratic, Higgs and hilltop potentials in the Palatini gravity*, *Commun. Theor. Phys.* **72** (2020) 085401 [arXiv:1908.09674] [INSPIRE].

[23] P. Carrilho, D. Mulryne, J. Ronayne and T. Tenkanen, *Attractor Behaviour in Multifield Inflation*, *JCAP* **06** (2018) 032 [arXiv:1804.10489] [INSPIRE].

[24] J.P.B. Almeida, N. Bernal, J. Rubio and T. Tenkanen, *Hidden inflation dark matter*, *JCAP* **03** (2019) 012 [arXiv:1811.09640] [INSPIRE].

[25] T. Takahashi and T. Tenkanen, *Towards distinguishing variants of non-minimal inflation*, *JCAP* **04** (2019) 035 [arXiv:1812.08492] [INSPIRE].

[26] T. Tenkanen, *Minimal Higgs inflation with an R^2 term in Palatini gravity*, *Phys. Rev. D* **99** (2019) 063528 [arXiv:1901.01794] [INSPIRE].

[27] T. Tenkanen and L. Visinelli, *Axion dark matter from Higgs inflation with an intermediate H_**, *JCAP* **08** (2019) 033 [arXiv:1906.11837] [INSPIRE].

[28] T. Tenkanen, *Trans-Planckian censorship, inflation, and dark matter*, *Phys. Rev. D* **101** (2020) 063517 [arXiv:1910.00521] [INSPIRE].

[29] A. Kozak and A. Borowiec, *Palatini frames in scalar-tensor theories of gravity*, *Eur. Phys. J. C* **79** (2019) 335 [arXiv:1808.05598] [INSPIRE].

JHEP06(2022)106

[30] I. Antoniadis, A. Karam, A. Lykkas, T. Pappas and K. Tamvakis, *Rescuing Quartic and Natural Inflation in the Palatini Formalism*, *JCAP* **03** (2019) 005 [arXiv:1812.00847] [INSPIRE].

[31] I. Antoniadis, A. Karam, A. Lykkas and K. Tamvakis, *Palatini inflation in models with an R^2 term*, *JCAP* **11** (2018) 028 [arXiv:1810.10418] [INSPIRE].

[32] I.D. Gialamas and A.B. Lahanas, *Reheating in R^2 Palatini inflationary models*, *Phys. Rev. D* **101** (2020) 084007 [arXiv:1911.11513] [INSPIRE].

[33] A. Racioppi, *Non-Minimal (Self-)Running Inflation: Metric vs. Palatini Formulation*, *JHEP* **21** (2020) 011 [arXiv:1912.10038] [INSPIRE].

[34] J. Rubio and E.S. Tomberg, *Preheating in Palatini Higgs inflation*, *JCAP* **04** (2019) 021 [arXiv:1902.10148] [INSPIRE].

[35] A. Lloyd-Stubbs and J. McDonald, *Sub-Planckian ϕ^2 inflation in the Palatini formulation of gravity with an R^2 term*, *Phys. Rev. D* **101** (2020) 123515 [arXiv:2002.08324] [INSPIRE].

[36] N. Das and S. Panda, *Inflation and Reheating in f(R,h) theory formulated in the Palatini formalism*, *JCAP* **05** (2021) 019 [arXiv:2005.14054] [INSPIRE].

[37] J. McDonald, *Does Palatini Higgs Inflation Conserve Unitarity?*, *JCAP* **04** (2021) 069 [arXiv:2007.04111] [INSPIRE].

[38] M. Shaposhnikov, A. Shkerin and S. Zell, *Quantum Effects in Palatini Higgs Inflation*, *JCAP* **07** (2020) 064 [arXiv:2002.07105] [INSPIRE].

[39] V.-M. Enckell, S. Nurmi, S. Räsänen and E. Tomberg, *Critical point Higgs inflation in the Palatini formulation*, *JHEP* **04** (2021) 059 [arXiv:2012.03660] [INSPIRE].

[40] L. Järv, A. Karam, A. Kozak, A. Lykkas, A. Racioppi and M. Saal, *Equivalence of inflationary models between the metric and Palatini formulation of scalar-tensor theories*, *Phys. Rev. D* **102** (2020) 044029 [arXiv:2005.14571] [INSPIRE].

[41] I.D. Gialamas, A. Karam and A. Racioppi, *Dynamically induced Planck scale and inflation in the Palatini formulation*, *JCAP* **11** (2020) 014 [arXiv:2006.09124] [INSPIRE].

[42] A. Karam, M. Raidal and E. Tomberg, *Gravitational dark matter production in Palatini preheating*, *JCAP* **03** (2021) 064 [arXiv:2007.03484] [INSPIRE].

[43] I.D. Gialamas, A. Karam, A. Lykkas and T.D. Pappas, *Palatini-Higgs inflation with nonminimal derivative coupling*, *Phys. Rev. D* **102** (2020) 063522 [arXiv:2008.06371] [INSPIRE].

[44] A. Karam, S. Karamitsos and M. Saal, *β-function reconstruction of Palatini inflationary attractors*, *JCAP* **10** (2021) 068 [arXiv:2103.01182] [INSPIRE].

[45] A. Karam, E. Tomberg and H. Veermäe, *Tachyonic preheating in Palatini R^2 inflation*, *JCAP* **06** (2021) 023 [arXiv:2102.02712] [INSPIRE].

[46] I.D. Gialamas, A. Karam, T.D. Pappas and V.C. Spanos, *Scale-invariant quadratic gravity and inflation in the Palatini formalism*, *Phys. Rev. D* **104** (2021) 023521 [arXiv:2104.04550] [INSPIRE].

[47] J. Annala and S. Räsänen, *Inflation with $R_{(\alpha\beta)}$ terms in the Palatini formulation*, *JCAP* **09** (2021) 032 [arXiv:2106.12422] [INSPIRE].

[48] A. Racioppi, J. Rajasalu and K. Selke, *Multiple point criticality principle and Coleman-Weinberg inflation*, arXiv:2109.03238 [INSPIRE].

JHEP06(2022)106

[49] D.Y. Cheong, S.M. Lee and S.C. Park, *Reheating in models with non-minimal coupling in metric and Palatini formalisms*, *JCAP* **02** (2022) 029 [arXiv:2111.00825] [INSPIRE].

[50] Y. Mikura and Y. Tada, *On UV-completion of Palatini-Higgs inflation*, *JCAP* **05** (2022) 035 [arXiv:2110.03925] [INSPIRE].

[51] A. Ito, W. Khater and S. Räsänen, *Tree-level unitarity in Higgs inflation in the metric and the Palatini formulation*, arXiv:2111.05621 [INSPIRE].

[52] A. Racioppi and M. Vasar, *On the number of e-folds in the Jordan and Einstein frames*, *Eur. Phys. J. Plus* **137** (2022) 637 [arXiv:2111.09677] [INSPIRE].

[53] K. Kannike et al., *Dynamically Induced Planck Scale and Inflation*, *JHEP* **05** (2015) 065 [arXiv:1502.01334] [INSPIRE].

[54] A. Karam, T. Pappas and K. Tamvakis, *Nonminimal Coleman-Weinberg Inflation with an R^2 term*, *JCAP* **02** (2019) 006 [arXiv:1810.12884] [INSPIRE].

[55] S. Bekov, K. Myrzakulov, R. Myrzakulov and D.S.-C. Gómez, *General slow-roll inflation in $f(R)$ gravity under the Palatini approach*, *Symmetry* **12** (2020) 1958 [arXiv:2010.12360] [INSPIRE].

[56] PLANCK collaboration, *Planck 2018 results. X. Constraints on inflation*, *Astron. Astrophys.* **641** (2020) A10 [arXiv:1807.06211] [INSPIRE].

[57] T. Tenkanen and E. Tomberg, *Initial conditions for plateau inflation: a case study*, *JCAP* **04** (2020) 050 [arXiv:2002.02420] [INSPIRE].

[58] SIMONS OBSERVATORY collaboration, *The Simons Observatory: Science goals and forecasts*, *JCAP* **02** (2019) 056 [arXiv:1808.07445] [INSPIRE].

[59] NASA PICO collaboration, *PICO: Probe of Inflation and Cosmic Origins*, arXiv:1902.10541 [INSPIRE].

[60] K. Abazajian et al., *CMB-S4 Science Case, Reference Design, and Project Plan*, arXiv:1907.04473 [INSPIRE].

[61] LITEBIRD collaboration, *LiteBIRD: JAXA's new strategic L-class mission for all-sky surveys of cosmic microwave background polarization*, *Proc. SPIE Int. Soc. Opt. Eng.* **11443** (2020) 114432F [arXiv:2101.12449] [INSPIRE].

JHEP06(2022)106

Publication II

Christian Dioguardi and Antonio Racioppi. Palatini F(R,X): A new framework for inflationary attractors. *Phys. Dark Univ.*, 45:101509, 2024

Physics of the Dark Universe 45 (2024) 101509

Contents lists available at ScienceDirect

Physics of the Dark Universe

journal homepage: www.elsevier.com/locate/dark

Full length article

Palatini $F(R, X)$: A new framework for inflationary attractors

Christian Dioguardi [a,b], Antonio Racioppi [b,*]

[a] Tallinn University of Technology, Akadeemia tee 23, Tallinn, 12618, Estonia
[b] National Institute of Chemical Physics and Biophysics, Rävala 10, Tallinn, 10143, Estonia

ARTICLE INFO

Keywords:
Inflation
Attractors
Palatini

ABSTRACT

Palatini $F(R)$ gravity proved to be a powerful tool in order to realize asymptotically flat inflaton potentials. Unfortunately, it also inevitably implies higher-order inflaton kinetic terms in the Einstein frame that might jeopardize the evolution of the system out of the slow-roll regime. We prove that a $F(R+X)$ gravity, where X is the inflaton kinetic term, solves the issue. Moreover, when F is a quadratic function such a choice easily leads to a new class of inflationary attractors, fractional attractors, that generalizes the already well-known polynomial α-attractors.

1. Introduction

The observation of the cosmic microwave background radiation (CMB) supports the cosmological principle. In order to explain the observed flatness and homogeneity a period of accelerated expansion (inflation) is required in the very early universe [1–4]. With the inflationary mechanism we also achieve to produce primordial inhomogeneities that seed the current large-scale structure of the universe. The most simple model requires a scalar field embedded in Einstein gravity which drives the initial expansion. However, more sophisticated models have shown to achieve interesting results in predicting the CMB observables (e.g. [5] and refs. therein). The Palatini formulation of gravity (e.g. [6–8] and refs. therein), in which the Levi-Civita connection is considered to be independent from the metric, shows many appealing features. In particular $F(R)$ models, for which the gravity sector is taken to be a general function of the Ricci scalar, generate asymptotically flat potentials that can be used to describe experimentally viable slow-roll inflation (e.g. [9–11] and refs. therein). However, models that diverge faster than R^2, are not well behaved beyond slow-roll [11], hence they could only be used as effective theories during the slow-roll phase. In this paper we extend the class of $F(R)$ theories to the class of $F(R, X)$ where X is the inflaton kinetic term. Models with non minimal couplings involving R and X have been already explored in the past (e.g. [12,13] and refs. therein) but in the metric formulation of gravity. According to our knowledge, this is the first time where such kind of study is performed in the Palatini approach.

In particular we focus on the quadratic models $F(R_X) = 2\Lambda + \omega R_X + \alpha R_X^2$ where $R_X = R + X$. We classify those models and derive their general predictions for inflation introducing two new inflationary attractors that we called *canonical* and *tailed* fractional attractors.

2. Palatini $F(R, X)$

Consider the action

$$S = \int d^4x\sqrt{-g^J}\left(\frac{1}{2}F(R_X) - V(\phi)\right), \tag{1}$$

where we assumed Planck units, $M_P = 1$, and a space-like metric signature. $V(\phi)$ is the inflaton scalar potential and $F(R_X)$ is an arbitrary function of its argument. We define[1] $R_X = R_J + X$ with $X = -g_J^{\mu\nu}\partial_\mu\phi\partial_\nu\phi$ denoting the inflaton kinetic term and $R_J = g_J^{\mu\nu}R_{\mu\nu}(\Gamma)$ where $R_{\mu\nu}(\Gamma)$ is the Ricci tensor built from the independent connection i.e. we are operating in the Palatini formulation. We can rewrite the action in the following way by introducing an auxiliary field ζ:

$$S = \int d^4x\sqrt{-g^J}\left(\frac{F(\zeta) + F'(\zeta)(R_X - \zeta)}{2} - V(\phi)\right), \tag{2}$$

where the symbol $'$ indicates differentiation with respect to the argument of the function. It is easy to check that action (1) is obtained from action (2) by taking the solution of the equation of motion for ζ i.e. $\zeta = R_X$. By means of a conformal transformation $g^E_{\mu\nu} = F'(\zeta)g^J_{\mu\nu}$ we can rewrite the action in the Einstein frame where the theory is

* Corresponding author.
E-mail addresses: christian.dioguardi@kbfi.ee (C. Dioguardi), antonio.racioppi@kbfi.ee (A. Racioppi).

[1] In a similar way, this setup can be easily generalized to $S = \frac{1}{2}\int d^4x\sqrt{-g^J}F(R_\mathcal{L})$, where $R_\mathcal{L} = R_J + \mathcal{L}(\phi^i, \psi^j, A^k_\mu)$ with $\mathcal{L}(\phi^i, \psi^j, A^k_\mu)$ representing the Lagrangian for all the scalars, fermions and vectors of the theory. After introducing the auxiliary field ζ, this would imply having all Lagrangian $\mathcal{L}(\phi^i, \psi^j, A^k_\mu)$ with a $F'(\zeta)$ prefactor (cf. Eq. (2)). The corresponding model building and phenomenology are beyond the scope of this paper and postponed to a future work.

https://doi.org/10.1016/j.dark.2024.101509
Received 28 September 2023; Received in revised form 6 March 2024; Accepted 21 April 2024
Available online 23 April 2024

linear in R and minimally coupled to the metric $g^E_{\mu\nu}$. The action in the Einstein frame reads:

$$S = \int d^4x\sqrt{-g^E}\left(\frac{R_E}{2} - \frac{1}{2}g_E^{\mu\nu}\partial_\mu\phi\partial_\nu\phi - U(\zeta,\phi)\right), \tag{3}$$

with

$$U(\zeta,\phi) = \frac{V(\phi)}{F'(\zeta)^2} - \frac{F(\zeta)}{2F'(\zeta)^2} + \frac{\zeta}{2F'(\zeta)}. \tag{4}$$

First of all we notice that the scalar field ϕ has a canonical kinetic term in the Einstein frame while ζ has no kinetic term at all, therefore it is still auxiliary also in the Einstein frame, as typical of the Palatini formulation.[2] As we will discuss shortly, this is a crucial difference with respect to [10,11]. By taking the variation with respect to ζ we get the equation of motion for the auxiliary field (and the consistency condition $F'' \neq 0$):

$$\frac{1}{4}\big(2F(\zeta) - \zeta F'(\zeta)\big) = V(\phi), \tag{5}$$

which in principle can be solved in ζ to get $\zeta(\phi)$. By using (5) into (4) we get the potential in terms of the auxiliary field only

$$U(\zeta) = \frac{\zeta}{4F'(\zeta)}. \tag{6}$$

Such a result has an immediate consequence on the allowed values of ζ. When written in the form of Eq. (2), it is easy to understand which consistency constraints are imposed on the theory and its parameters: $F'(\zeta) > 0$ is necessary to achieve a low-energy GR limit and a well defined conformal transformation. Hence, in order to have a stable positive potential suitable for inflation (see action (3) and (6)) $\zeta \geq 0$ must hold.

Before concluding we remark that Eq. (5) was already introduced in [10] where it holds as an approximation valid in the slow-roll regime.[3] However, in this case Eq. (5) is exact and valid even in presence of arbitrary large kinetic terms for the scalar field ϕ. In other words, the auxiliary field $\zeta = \zeta(\phi)$ is a function of the scalar field only and not of its derivatives. This happens because the inflaton kinetic term in the Einstein frame does not have anymore any F' contribution. This allows us to find an explicit form for $U(\zeta(\phi))$ in terms of the canonical scalar field whenever it is possible to solve (5) explicitly for $\zeta = \zeta(\phi)$.

3. Quadratic $F(R, X)$

Now we focus on a quadratic F, parametrized as

$$F(R_X) = 2\Lambda + \omega R_X + \alpha {R_X}^2, \tag{7}$$

with Λ, ω, α real constants. This is the most general form for a quadratic $F(R_X)$.

In such a case Eq. (5) takes the simple form

$$\Lambda + \frac{\omega}{4}\zeta = V(\phi), \tag{8}$$

with exact solution

$$\zeta = \frac{4}{\omega}\left(V(\phi) - \Lambda\right) = \frac{4\bar{V}(\phi)}{\omega}, \tag{9}$$

where $\bar{V}(\phi) = V(\phi) - \Lambda$. This leads to the Einstein frame potential

$$U(\phi) = \frac{V(\phi) - \Lambda}{8\alpha(V(\phi) - \Lambda) + \omega^2} = \frac{\bar{V}(\phi)}{8\alpha\bar{V}(\phi) + \omega^2}. \tag{10}$$

The corresponding vacuum (i.e. $V(\phi) = 0$) solutions are

$$\zeta_0 = -4\Lambda/\omega, \qquad U_\Lambda = \frac{\Lambda}{8\alpha\Lambda - \omega^2}. \tag{11}$$

[2] See Appendices A and B for further details.

[3] See Appendix A for further details.

Moreover, the large potential configuration ($V(\phi) \to \pm\infty$) presents a plateau at (see Figs. 1, 3)

$$U \approx U_\alpha = \frac{1}{8\alpha}. \tag{12}$$

Requiring the positivity of ζ and $U(\phi)$ at any ϕ values, vacuum configuration included (i.e. $\zeta_0, U_\Lambda \geq 0$) leads to two possible scenarios:

$$(1) \quad \omega > 0, \quad \Lambda \leq 0, \quad \bar{V} \geq 0, \tag{13}$$

$$(2) \quad \omega < 0, \quad \Lambda > 0, \quad \bar{V} < 0, \tag{14}$$

with the common constraint

$$\alpha > \frac{\omega^2}{8\Lambda}, \tag{15}$$

only in case $\Lambda \neq 0$. Notice that an exactly null Λ (or alternatively $\zeta_0 = 0$) is allowed only for $\omega > 0$. The sign of ω affects the behavior of the Einstein frame potential (10) in a way that will be clarified later on. In the following we will study the two different sign choices separately.

3.1. The standard case: $\omega > 0$

First of all we notice that, if $V(\phi)$ has an absolute minimum (or alternatively a horizontal asymptote), we can set it to be null via a redefinition of Λ as long as (13) is satisfied. Without loss of generality, in this subsection we work in this configuration. Moreover, Eq. (13) would in principle allow for negative values for α. However, unless some *ad hoc* choice of $V(\phi)$, negative values for α would also imply the insurgence of a pole in $U(\phi)$. In order to avoid such a case, we restrict ourselves to $\alpha > 0$. In such a case, given the constraints (13), we can easily check that $U_\alpha > U_\Lambda$ and U_Λ becomes the cosmological constant U_{CC}. Consistency with data [14] then requires $U_\Lambda = U_{CC} \sim 10^{-47}\text{GeV}^4$. Treating α and ω as free parameters, such a constraint can be solved in function of Λ, giving

$$\Lambda = \frac{\omega^2 U_{CC}}{8\alpha U_{CC} - 1}. \tag{16}$$

Unless we choose ad hoc gigantic values for α and/or ω, it is easy to check that $|\Lambda|$ must be approximately of the same order of magnitude as U_{CC}. Therefore this setup cannot actually solve the cosmological constant problem, but only reproduce its value by tuning the free parameters of the model. Comparing our result (10) with the one in [9], we notice that we retain the same form of the potential (i.e. a plateau for big enough $\bar{V}(\phi)$, see Fig. 1). In particular, at large potential configuration $V(\phi) \to \infty$, this plateau takes the form:

$$U(\phi) \approx U_\alpha\left(1 - \frac{\omega^2 U_\alpha}{V(\phi)}\right). \tag{17}$$

Hence, we can provide an asymptotically flat potential independently of the original choice of $V(\phi)$ as in the standard $F(R)$ case [9] but with the advantage of having a canonically normalized scalar field ϕ and no higher order kinetic term.

In order to describe the inflationary predictions, we need first of all the slow roll-parameters, defined as:

$$\epsilon(\phi) = \frac{1}{2}\left(\frac{U'(\phi)}{U(\phi)}\right)^2, \tag{18}$$

$$\eta(\phi) = \frac{U''(\phi)}{U(\phi)}. \tag{19}$$

The first slow-roll parameter ϵ allows us to compute the number of e-folds of expansion of the Universe as

$$N_e = \int_{\phi_{\text{end}}}^{\phi_N} d\phi\, \frac{U(\phi)}{U'(\phi)}, \tag{20}$$

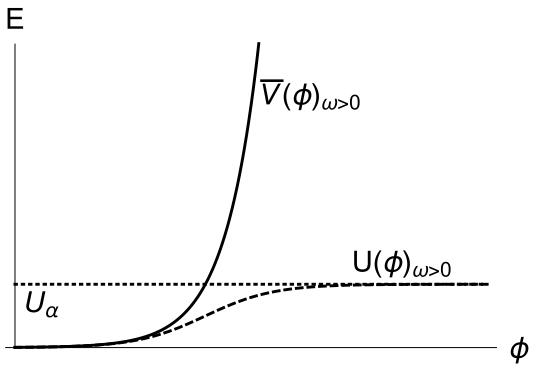

Fig. 1. Reference plots for $\bar{V}(\phi)$ (continuous) and $U(\phi)$ (dashed) vs. ϕ when $\omega > 0$.

where the field value at the end of inflation[4] is given by $\epsilon(\phi_{\rm end}) = 1$, while the field value ϕ_N at the time a given scale left the horizon is given by the corresponding N_e. The spectral index $n_{\rm s}$ and the tensor-to-scalar ratio r are:

$$n_{\rm s} = 1 + 2\eta(\phi_N) - 6\epsilon(\phi_N)\,, \tag{21}$$

$$r = 16\epsilon(\phi_N)\,, \tag{22}$$

and the amplitude of the scalar power spectrum [15] is

$$A_{\rm s} = \frac{1}{24\pi^2}\frac{U(\phi_N)}{\epsilon(\phi_N)} \simeq 2.1\times 10^{-9}\,. \tag{23}$$

In the standard quadratic $F(R)$ case [9], at the leading order, only r is affected by the Palatini R^2 term, while all the other observables stay unchanged. In contrast to that, here we cannot find a compact straightforward expression for the phenomenological parameters in Eqs. (21), (22) and (23) in terms of the corresponding ones computed for $V(\phi)$, because now the inflaton field ϕ is already canonically normalized in the Einstein frame action (3). However we can still find a compact expression for r in the strong coupling limit $\alpha \to \infty$. In such a case, the Einstein frame potential asymptotically approaches the plateau (12). Therefore, inserting this value in (23) we can easily prove that at the leading order

$$r \approx \frac{1}{12\pi^2 A_s \alpha}\,. \tag{24}$$

This means that we can arbitrarily lower r by increasing α, exactly as found in [9]. On the contrary, we cannot make a model independent prediction for n_s.

For illustrative purposes, we consider a monomial potential of the form

$$V(\phi) = \lambda_k \phi^k, \qquad \lambda_k = \frac{\lambda^k}{k!} \tag{25}$$

where the unusual prefactor, λ_k, is chosen for numerical convenience. In such a case, we have:

$$N_e = \int_{\phi_{end}}^{\phi_N} d\phi \frac{1}{\sqrt{2}\sqrt{\epsilon_+(\phi)}} \tag{26}$$

$$r = 16\epsilon_+(\phi_N) \tag{27}$$

$$n_s = 1 - 6\epsilon_+(\phi_N) + 2\eta_+(\phi_N) \tag{28}$$

$$A_s = \frac{\omega^2 \bar{V}(\phi_N)}{24\pi^2 \epsilon_+(\phi_N)\left(8\alpha\bar{V}(\phi_N) + \omega^2\right)} \tag{29}$$

where

$$\epsilon_+(\phi) = \frac{\lambda_k^2 k^2 \omega^4 \phi^{2k-2}}{2\bar{V}(\phi)^2(8\alpha\bar{V}(\phi) + \omega^2)^2} \tag{30}$$

$$\eta_+(\phi) = \frac{2\lambda_k \omega^2 \phi^{k-2}}{\bar{V}(\phi)(8\alpha\bar{V}(\phi) + \omega^2)^2}\left(8\alpha(k+1)\lambda_k\phi^k + (k-1)(8\alpha\Lambda - \omega^2)\right) \tag{31}$$

In the strong coupling limit $\alpha \to \infty$, we recover the well-known polynomial α-attractors [17], whose predictions are:

$$r \sim 0 \tag{32}$$

$$n_s = 1 - \frac{k+1}{k+2}\frac{2}{N_e} \tag{33}$$

A numerical analysis for the reference value $\omega = 1$ with Λ and λ fixed using λ Eqs. (16) and (23) is showed in Fig. 2 , where we plot the observables r vs. n_s (a), r vs. α (b), α vs. n_s (c), λ vs. α (d) for $V(\phi) = \lambda_k\phi^k$ with $k = 1$ (purple), $k = 2$ (blue), $k = 3$ (green), $k = 4$ (red) and $k \to \infty$ (equivalent to $V(\phi) = e^{\lambda\phi}$) (black) for $N_e = 50$ (thin, dot-dashed line) and $N_e = 60$ (thick, dot-dashed line). In the same color code we show the limiting values[5] $\alpha = 0$ (continuous line, bullets) and $\alpha \to \infty$ (triangles). In (a) the dashed lines represent the prediction of the standard Palatini R^2 model [9] for the corresponding potential and the squares the limiting values for $\alpha \to \infty$. The gray areas represent the $1,2\sigma$ allowed regions coming from the latest combination of Planck, BICEP/Keck and BAO data [16]. Comparing the results of the quadratic R_X model with the standard one [9], we notice that, as expected, we still have a suppression in r. On the other hand, while in [9] n_s stays essentially unchanged, now it increases by increasing α. In this way, for any $k \geq 1$, it is possible to find a N_e value so that the predicted r and n_s lay in the experimentally allowed region [16]. Finally, in (d) we notice that the coupling λ has to increase along with α in order to satisfy the constraint (23). Notice in particular that the value of λ does not change substantially between $N_e = 50$ and $N_e = 60$ so the two lines appear almost superimposed in the plot.

To conclude we stress that the form of (17) is the same as in [17] but our construction is certainly more immediate as it does not require any field redefinition, and more general because it can be applied to any positive V, not just monomial choices. Since the potential in (10) with the setup (13) predicts asymptotically flat potentials whenever $\alpha \gg \omega$, we label such a choice as *canonical fractional attractors*, to be counterposed to a more *exotic* configuration which will be discussed in the next subsection.

3.2. The alternative case: $\omega < 0$

The first peculiar feature of this configuration is the *wrong* sign for the linear term in R in the Jordan frame action (2). At first glance it might seem that such a configuration is forbidden, coming with issues in the Jordan frame like repulsive gravity or a negative inflaton kinetic energy. However, as explained after Eq. (6), the condition $F' > 0$ ensures that gravity stays attractive. The same holds for the inflaton kinetic term, which receives not only contributions from the linear term in ω but also from the quadratic term αR_X^2 (see Eq. (7)). When all the contributions are taken into account, it is easy to prove that the positivity of F' ensures also the positivity of the inflaton kinetic energy (see also Eq. (B.4)). Therefore such a setup is allowed as long as the consistency constraint of $F' > 0$ is satisfied (provided that $F'' \neq 0$) (e.g. [10,11] and refs. therein). This happens when all the conditions in Eq. (14) are respected. Particularly relevant is the role of $\Lambda > 0$ and of the lower bound on α in Eq. (15) that ensure the positivity of F' wherever Eq. (9) admits a solution. The simplest way[6] to achieve it is

[4] One might argue that also $|\eta| = 1$ could trigger the end of slow-roll before reaching $\epsilon = 1$. However, this is never the case in our example scenarios, at least for the parameter space that we considered.

[5] The case $k \to \infty$ for $\alpha = 0$ is not visible in Fig. 2(a) because far away from the allowed region.

[6] Another possible, but more tuned, choice is to have $V(\phi)$ positive but bounded from above in such a way that $\bar{V}$ remains negative.

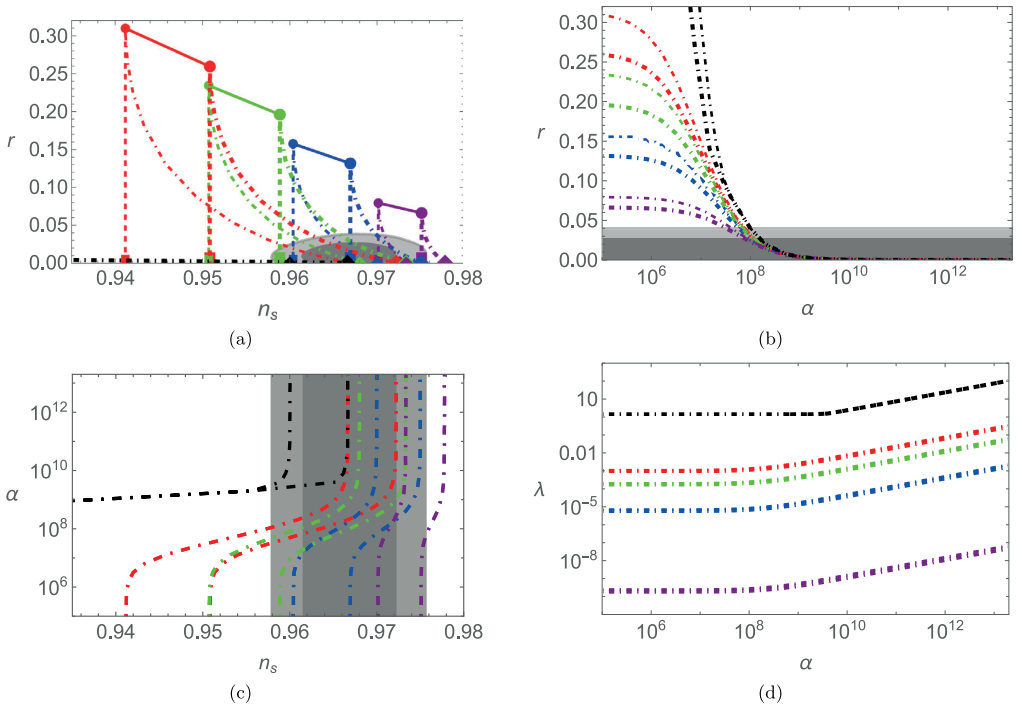

Fig. 2. r vs. n_s (a), r vs. α (b), α vs. n_s (c), λ vs. α (d) for $\omega = 1$ and $V(\phi) = \lambda_k \phi^k$ with $k = 1$ (purple), $k = 2$ (blue), $k = 3$ (green), $k = 4$ (red) and $k \to \infty$ (black) for $N_e = 50$ (thin, dot-dashed line) and $N_e = 60$ (thick, dot-dashed line). In the same color code we show the limiting values $\alpha = 0$ (continuous line, bullets) and $\alpha \to \infty$ (triangles). In (a) the dashed lines represent the prediction of the standard Palatini R^2 model [9] for the corresponding potential and the squares the limiting values for $\alpha \to \infty$. The gray areas represent the $1,2\sigma$ allowed regions coming from the latest combination of Planck, BICEP/Keck and BAO data [16]. (For interpretation of the references to color in this figure legend, the reader is referred to the web version of this article.)

to have the Jordan frame scalar potential $V(\phi)$ (semi)definite negative. Analogously to the previous case, also now α needs to be constrained to positive values. It is convenient to introduce

$$\underline{V}(\phi) = -\bar{V}(\phi) = -V(\phi) + \Lambda > \frac{\omega^2}{8\alpha}\,, \tag{34}$$

which is strictly positive and bounded from below because of (14). In this way we can rewrite the Einstein frame potential as

$$U(\phi) = \frac{\underline{V}(\phi)}{8\alpha \underline{V}(\phi) - \omega^2}\,. \tag{35}$$

Comparing with Eq. (10), now ω^2 contributes with a negative sign to the denominator. However it can be easily proven that the Einstein frame potential (35) is positive and bounded from above (without any appearance of a pole) thanks to (14) and (34). A reference plot for $U(\phi)$ is given in Fig. 3. We notice that now the potential exhibits two plateaus, the usual U_α in (12), when $\underline{V} \to \infty$, but also another one, $U \approx U_\Lambda$ in (11), when $\underline{V} \to \Lambda$ i.e. $V \to 0$. Notice that in opposition to the previous $\omega > 0$ case, given (14) and (34), now $U_\Lambda > U_\alpha$. The height of the plateaus is dictated only by the F's parameters Λ, ω, α regardless[7] of the initial choice of $V(\phi)$. We label such class of potentials as *tailed-fractional attractors*. Since we have two plateaus, it is in principle possible to use one single potential to explain both early universe inflation, which happens close to the U_Λ plateau, and late universe acceleration, where the value U_α sets the value of the cosmological constant observed today. We will discuss such a topic later on. Now we focus on the phenomenology around the first plateau. In its proximity (in the strong coupling regime), the scalar potential can be approximated as:

$$U(\phi) = U_\Lambda \left(1 - \frac{U_\Lambda}{\Lambda U_\alpha} |V(\phi)|\right), \tag{36}$$

which has the form of a generalized hilltop potential. Also in this case we can get a universal limit for the tensor-to-scalar ratio r only

$$r \approx \frac{2}{3\pi^2 A_s} \frac{\Lambda}{8\Lambda\alpha - \omega^2}\,, \tag{37}$$

which holds around the first plateau, that is for $V \sim 0$. When $\alpha \gg 1$, the most trivial configuration is the one where ω can be neglected and Eq. (37) reduces to Eq. (24).

Before moving to a more quantitative analysis, it is important to stress that an additional constraint needs to be imposed in order to achieve the end of slow-roll. A qualitative plot for the first slow-roll parameter ϵ is shown in Fig. 4. As expected, for $V(\phi) \to 0$ (or $-\infty$), $\epsilon \to 0$ since $U(\phi)$ approaches the corresponding plateaus. However, in between the two plateaus, ϵ does not diverge to $+\infty$, ensuring a certain end of slow-roll, but it reaches a local maximum. This is because the absolute minimum of $U(\phi)$ is not null. Therefore, in order to end slow-roll, we need to ensure that the local maximum in ϵ is bigger than one. We can intuitively understand (cf. Eq. (18)) that this is achieved by lowering the second plateau $U \approx \frac{1}{8\alpha}$ i.e. by increasing α. Therefore this sets a minimum value $\alpha > \alpha_{min}$. Its numerical value is model dependent and must be calculated for the specific choice of the scalar potential $V(\phi)$. However, the existence of the minimum value α_{min} is model independent.

[7] If we would consider the Einstein frame action (3) with $U(\phi)$ given by (35) as a starting point, then all the dependence on the original parameter Λ would be moved to the existence of a strictly positive minimum value for $\underline{V}$.

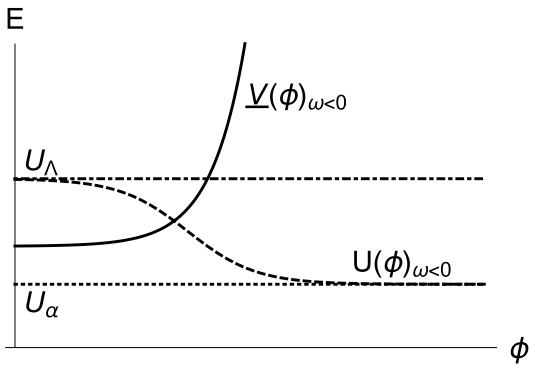

Fig. 3. Reference plots for $\underline{V}(\phi)$ (continuous) and $U(\phi)$ (dashed) vs. ϕ when $\omega < 0$.

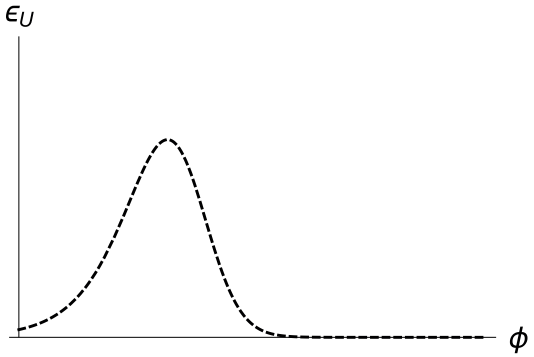

Fig. 4. Reference plot for $\epsilon(\phi)$ (dashed) vs. ϕ when $\omega < 0$.

In order to perform a more quantitative comparison with the canonical fractional attractors case, we consider now a negative monomial potential $V(\phi) = -\lambda_k \phi^k$ with $k \geq 3$ and λ_k defined in Eq. (25). In this case the inflationary observables are:

$$N_e = \int_{\phi_N}^{\phi_{end}} d\phi \frac{1}{\sqrt{2}\sqrt{\epsilon_-(\phi)}} \tag{38}$$

$$r = 16\epsilon_-(\phi_N) \tag{39}$$

$$n_s = 1 - 6\epsilon_-(\phi_N) + 2\eta_-(\phi_N) \tag{40}$$

$$A_s = \frac{\omega^2 \underline{V}(\phi_N)}{24\pi^2 \epsilon_-(\phi_N)\left(8\alpha \underline{V}(\phi_N) - \omega^2\right)} \tag{41}$$

where

$$\epsilon_-(\phi) = \frac{\lambda_k^2 k^2 \omega^4 \phi^{2k-2}}{2\underline{V}(\phi)^2 (8\alpha \underline{V}(\phi) - \omega^2)^2} \tag{42}$$

$$\eta_-(\phi) = \frac{2\lambda_k \omega^2 \phi^{k-2}}{\underline{V}(\phi)(8\alpha \underline{V}(\phi) - \omega^2)^2}\left(8\alpha(k+1)\lambda_k \phi^k + (k-1)(8\alpha\Lambda - \omega^2)\right) \tag{43}$$

The corresponding strong coupling results are:

$$r \sim 0 \tag{44}$$

$$n_s = 1 - \frac{k-1}{k-2}\frac{2}{N_e}, \tag{45}$$

which are the hilltop inflationary predictions for small r, as expected.

A numerical study for the reference value $\omega = -1$ with $\Lambda \simeq \frac{6}{5}\frac{1}{8\alpha}$, ensuring that Eq. (15) holds, and λ fixed using Eq. (23) is showed in Fig. 5, where we plot the observables r vs. n_s (a), r vs. α (b), α vs. n_s (c), λ vs. α (d) for $V(\phi) = -\lambda_k \phi^k$ with $k = 4$ (blue), $k = 6$ (red), $k = 8$ (green) and $k \to \infty$ (black) for $N_e = 50$ (dashed), and $N_e = 60$ (continuous). In the same color code the squares represent the value α_{min} for which we can have a graceful exit from inflation. The gray areas represent the $1,2\sigma$ allowed regions coming from the latest combination of Planck, BICEP/Keck and BAO data [16]. In this case we see that agreement with data requires $k \geq 6$. As in the previous case, from (d) we notice that the coupling λ has to increase along with α in order to satisfy the constraint (23). Notice in particular that the value of λ does not change substantially between $N_e = 50$ and $N_e = 60$ so the two lines appear almost superimposed in the plot. Moreover, we notice that for $k \to \infty$ (equivalent to replacing $\lambda_k \phi^k$ with $e^{\lambda\phi}$), (33) and (45) converge to the same limit. Before concluding, we stress that the model predicts $r \lesssim 10^{-4}$, implying that the predicted tensor-to-scalar ratio would not be measurable even by more futuristic high-resolution satellite mission, such as PICO [18]. This happens because the requirement $\alpha > \alpha_{min}$, needed to achieve the end of slow-roll, automatically forces α in the strong coupling regime.

Moreover, when $\alpha > \alpha_{min}$, not only slow-roll inflation ends but also restarts at a later time, allowing the possibility for a joined explanation of the earlier and later accelerated expansion of the Universe, as already mentioned before. In order to understand the corresponding phenomenology, it is convenient to introduce the parameter δ so that

$$\alpha\Lambda = \frac{\omega^2}{8}(1+\delta). \tag{46}$$

Using such a definition in (37), we obtain

$$r \approx \frac{1}{12\pi^2 A_s \alpha}\frac{1+\delta}{\delta}. \tag{47}$$

in the limit of $\alpha \gg 1$. Also, as long as $\delta \sim O(1)$ (in Fig. 5 we used $\delta \simeq 0.2$), the exact numerical value for r depends on the actual value of δ (unless $\delta \ll 1$), but it is still suppressed and of the same order of (24) in the big α limit. In this case, however, it is immediate to see that:

$$U_\Lambda = \frac{\Lambda}{8\alpha\Lambda - \omega^2} = \frac{1}{8\alpha}\frac{1+\delta}{\delta} \gtrsim \frac{1}{8\alpha}. \tag{48}$$

Therefore, adjusting $U_\alpha = \frac{1}{8\alpha}$ to the observed value of the vacuum energy density [14] also lowers the inflationary plateau making its value too low to be phenomenologically consistent with the evolution of the universe. An alternative option is to take $\delta \ll 1$, but $\alpha\delta A_s \gg 1$ so that we still get a small value

$$r \sim \frac{1}{12\pi^2 \alpha \delta A_s}. \tag{49}$$

For instance, if we consider $U_\alpha = \frac{1}{8\alpha} = U_{CC} \sim 10^{-47}\text{GeV}^4$ we have that $\alpha \sim 10^{122}$. In order to get a value of $r \sim 10^{-6}$ (which still corresponds to a high enough energy scale for inflation around 10^{15}GeV) we would need an extremely fine-tuned $\delta \sim 10^{-110}$. Unfortunately, even though mathematically possible, such a tuning of the parameters, looks more like a confirmation rather than a solution of the cosmological constant problem.

On the other hand, it has been proven that quadratic F's with negative ω, are the strong coupling limit configuration for F's of order higher than quadratic [11]. In such cases, independently of the chosen F, the energy potential tail automatically approaches zero by construction, resembling the feature of the quintessential inflation models (e.g. [19] and refs. therein), implying a possible more natural solution of the cosmological constant problem. However, the search for a successful quintessential $F(R_X)$ model is beyond the scope of the present article and will be postponed to a future work.

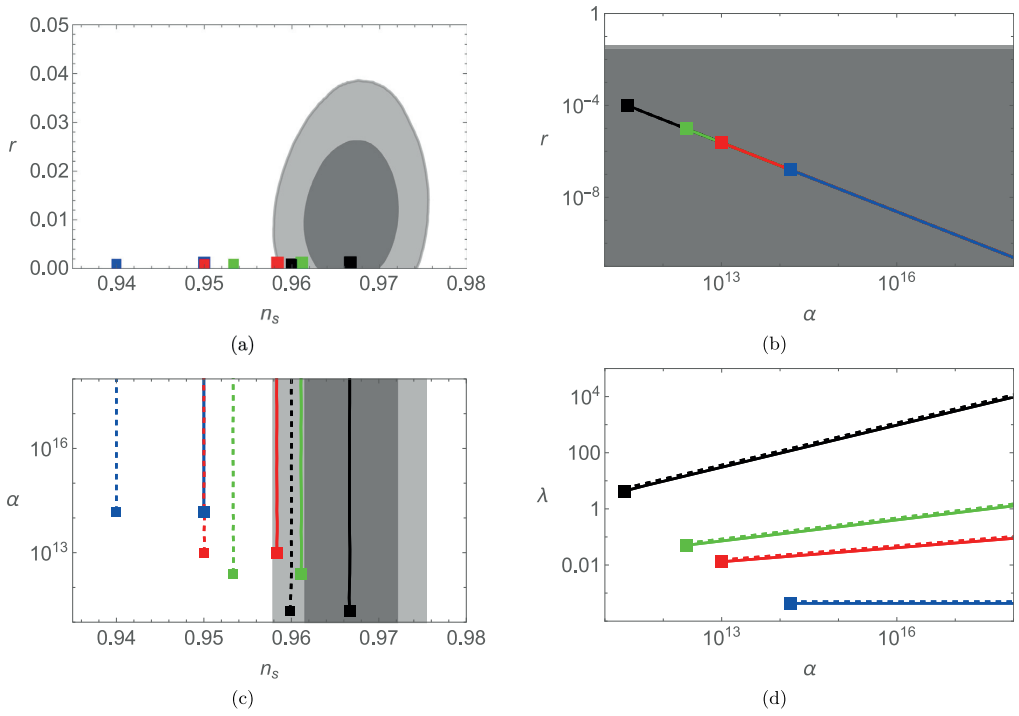

Fig. 5. r vs. n_s (a), r vs. α (b), α vs. n_s (c), λ vs. α (d) for $\omega = -1$ and $V(\phi) = -\lambda_k \phi^k$ with $k = 4$ (blue), $k = 6$ (red), $k = 8$ (green) and $k \to \infty$ (black) for $N_e = 50$ (dashed), and $N_e = 60$ (continuous). In the same color code the squares represent the value α_{min} for which we can have a graceful exit from inflation. The gray areas represent the $1{,}2\sigma$ allowed regions coming from the latest combination of Planck, BICEP/Keck and BAO data [16]. (For interpretation of the references to color in this figure legend, the reader is referred to the web version of this article.)

4. Conclusions

We studied single-field inflation embedded in $F(R_J)$ Palatini gravity. We showed that such a choice solves several of the issues arising from the usual Palatini $F(R)$ models while still providing flat inflaton potentials. In particular we focused on quadratic $F(R_J)$'s showing that only two possible configurations are possible. Those configurations both lead to flat inflaton potentials that can be classified as attractors given their general prediction on the inflationary observables. We named those two classes canonical fractional attractors, which generalize the well known polynomial α-attractors, and tailed fractional-attractors which generalize the predictions of hilltop potentials. Moreover, we showed that the class of quadratic theories with $\omega < 0$ can in principle explain both early and late universe accelerated expansion with one single potential. Even though fine tuned, this is a quite intriguing finding. In light of the results of [11], such an idea deserves further studies, going to appear in a future work.

CRediT authorship contribution statement

Christian Dioguardi: Investigation, Writing – original draft, Writing – review & editing. **Antonio Racioppi:** Investigation, Writing – original draft, Writing – review & editing.

Declaration of competing interest

The authors declare that they have no known competing financial interests or personal relationships that could have appeared to influence the work reported in this paper.

Data availability

No data was used for the research described in the article.

Acknowledgments

This work was supported by the Estonian Research Council grants PRG1055, RVTT3, RVTT7 and the CoE program TK202 "Fundamental Universe". All authors approved the version of the manuscript to be published.

Appendix A. Palatini $F(R)$ and its issues

In this appendix we give a brief summary of the results and issues found in the context of slow-roll inflation embedded in Palatini $F(R)$ gravity. More details can be found in [10,11]. We start by taking the action

$$S = \int d^4x\sqrt{-g^J}\left(\frac{1}{2}F(R_J) - \frac{1}{2}g_J^{\mu\nu}\partial_\mu\phi\partial_\nu\phi - V(\phi)\right) \tag{A.1}$$

where we assumed Planck units, $M_P = 1$, a space-like metric signature. $V(\phi)$ is the inflaton scalar potential and $F(R)$ is an arbitrary function of its argument with $R_J = g_J^{\mu\nu}R_{\mu\nu}(\Gamma)$ where $R_{\mu\nu}(\Gamma)$ is the Ricci tensor built from the independent connection i.e. we are operating in the Palatini formulation. We can rewrite the action by introducing an auxiliary field ζ:

$$S = \int d^4x\sqrt{-g^J}\left(\frac{F(\zeta) + F'(\zeta)(R_J - \zeta)}{2} - \frac{1}{2}g_J^{\mu\nu}\partial_\mu\phi\partial_\nu\phi - V(\phi)\right), \tag{A.2}$$

where the symbol $'$ indicates differentiation with respect to the argument of the function. It is easy to check that the action (A.1) is obtained from the action (A.2) by using the solution of the equation of motion for ζ i.e. $\zeta = R_J$. By means of a conformal transformation $g^E_{\mu\nu} = F'(\zeta) g^J_{\mu\nu}$ we can rewrite the action in the Einstein frame where the theory is linear in R and minimally coupled to the metric $g^E_{\mu\nu}$. The action in the Einstein frame reads:

$$S = \int d^4x\sqrt{-g^E}\left(\frac{R_E}{2} - \frac{g_E^{\mu\nu}\partial_\mu\phi\partial_\nu\phi}{2F'(\zeta)} - U(\zeta,\phi)\right), \tag{A.3}$$

with

$$U(\zeta,\phi) = \frac{V(\phi)}{F'(\zeta)^2} - \frac{F(\zeta)}{2F'(\zeta)^2} + \frac{\zeta}{2F'(\zeta)}\,. \tag{A.4}$$

Note that $U(\zeta,\phi)$ as the same functional form as for the $F(R_X)$ case shown in Eq. (4). Provided the consistency condition $F'' \neq 0$, the equations of motion of the system are (in the approximation of exactly homogeneous and isotropic Universe):

$$\ddot{\phi} + 3H\dot{\phi} + \frac{V'(\phi)}{F'(\zeta)} = \frac{\dot{\phi}\dot{\zeta}F''(\zeta)}{F'(\zeta)}\,, \tag{A.5}$$

$$3H^2 = \frac{1}{2}\frac{\dot{\phi}^2}{F'(\zeta)} + U(\phi,\zeta)\,, \tag{A.6}$$

$$-\frac{1}{2}\dot{\phi}^2F'(\zeta) + 2V(\phi) - G(\zeta) = 0\,, \tag{A.7}$$

with

$$G(\zeta) = \frac{1}{4}\left(2F(\zeta) - \zeta F'(\zeta)\right). \tag{A.8}$$

It can be easily checked that Eq. (A.7), when plugged back into action (A.3) induces non trivial higher order inflaton kinetic terms which complicate a lot the dynamics of the system. Moreover, solving exactly Eq. (A.7) proves to be hard for a generic $F(R)$, therefore we replace it with an equation for the time derivative of ζ [10],

$$\dot{\zeta} = \frac{3H\dot{\phi}^2F'(\zeta) + 3V'(\phi)\dot{\phi}}{2G'(\zeta) + \frac{3}{2}\dot{\phi}^2F''(\zeta)}\,. \tag{A.9}$$

As long as ζ solves (A.7) initially, Eq. (A.9) guarantees that (A.7) holds at all times. Eq. (A.9) also shows an issue that might arise in generic $F(R)$ models: if $G'(\zeta)$ and $F''(\zeta)$ have opposite signs, then $\dot{\zeta}$ presents a pole. Such a pole is a direct consequence of the $1/F'$ prefactor in front of the inflaton kinetic term in the Einstein frame (see Eq. (A.3)) and it might bring to catastrophic consequences for the dynamics of the system [11]. For instance, this happens when F is a function of higher order than quadratic. Such kind of $F's$ provide model independently an Einstein frame scalar potential featuring a plateau at early times and a tail at late times, allowing the possibility for a joined explanation of the earlier and later accelerated expansion of the Universe [11]. However the insurgence of $\dot{\zeta}$ pole before the end of inflation [11], makes such an idea unviable. As shown in Section 2, a possible solution is to upgrade to a $F(R_X)$ model.

Appendix B. Metric vs. Palatini

In this appendix we give more details about the differences that arise when using the metric or Palatini formulation of gravity in the context of $F(R)$ and $F(R_X)$ models. The starting point is the following action:

$$S = \int d^4x\sqrt{-g^J}\left(\frac{F(R_J + \sigma X) + (1-\sigma)X}{2} - V(\phi)\right), \tag{B.1}$$

where, again, we assumed Planck units, $M_P = 1$ and a space-like metric signature. $V(\phi)$ is the inflaton scalar potential, F is an arbitrary function of its argument, $X = -g_J^{\mu\nu}\partial_\mu\phi\partial_\nu\phi$ denotes the inflaton kinetic term and $R_J = g_J^{\mu\nu}R_{\mu\nu}(\Gamma)$ where $R_{\mu\nu}(\Gamma)$ is the Ricci tensor built from the connection $\Gamma^\rho_{J,\mu\nu}$. Setting $\sigma = 0, 1$ allows to describe respectively the $F(R)$ and the $F(R_X)$ scenario. It is easy to check that when $\sigma = 0$ action (B.1) becomes action (A.1), while when $\sigma = 1$ action (B.1) becomes action (1). Regardless of the gravity formulation, we can rewrite action (B.1) in terms of the auxiliary field ζ:

$$S_J = S_J(R_J) + S_J(\zeta,\phi)\,, \tag{B.2}$$

where

$$S_J(R_J) = \int \mathrm{d}^4x\sqrt{-g_J}\left[\frac{1}{2}F'(\zeta)R_J\right], \tag{B.3}$$

$$S_J(\zeta,\phi) = \int \mathrm{d}^4x\sqrt{-g_J}\,\mathcal{L}_J(\zeta,\phi) \tag{B.4}$$

with

$$\mathcal{L}_J(\zeta,\phi) = -\frac{1}{2}\left[\sigma F'(\zeta) + (1-\sigma)\right]\partial_\mu\phi\partial^\mu\phi - V(\zeta,\phi) \tag{B.5}$$

and

$$V(\zeta,\phi) = V(\phi) - \frac{F(\zeta) - \zeta F'(\zeta)}{2}\,. \tag{B.6}$$

Using the EoM $\zeta = R_J + \sigma X$ into (B.2), we restore Eq. (B.1). Performing the Weyl rescaling

$$g^E_{\mu\nu} = F'(\zeta)g^J_{\mu\nu}\,, \tag{B.7}$$

needed to move the theory to the Einstein frame, the term (B.4) becomes

$$S_E(\zeta,\phi) = \int d^4x\sqrt{-g^E}\,\mathcal{L}_E(\zeta,\phi)\,, \tag{B.8}$$

with

$$\mathcal{L}_E(\zeta,\phi) = -\frac{1}{2}\left[\sigma + \frac{(1-\sigma)}{F'(\zeta)}\right]g_E^{\mu\nu}\partial_\mu\phi\partial_\nu\phi - U(\zeta,\phi)\,, \tag{B.9}$$

and

$$U(\zeta,\phi) = \frac{V(\phi)}{F'(\zeta)^2} - \frac{F(\zeta)}{2F'(\zeta)^2} + \frac{\zeta}{2F'(\zeta)}\,, \tag{B.10}$$

both in the metric and Palatini formulation (cf. the second and third terms in actions (3) and (A.3)). The difference between the two types of gravity arises in the transformation of the term (B.3). Performing the rescaling (B.7) under Palatini gravity, action (B.3) becomes simply the Einstein–Hilbert action:

$$S^{EH}_{\text{Palatini}} = \int d^4x\sqrt{-g^E}\frac{R_E}{2}\,. \tag{B.11}$$

On the other hand, in case of metric gravity, an additional contribution is generated, giving

$$S^{EH}_{\text{metric}} = \int d^4x\sqrt{-g^E}\left(\frac{R_E}{2} - \frac{3}{2}\frac{\partial_\mu F'(\zeta)\partial^\mu F'(\zeta)}{(F'(\zeta))^2}\right). \tag{B.12}$$

The second term of Eq. (B.12) represents a kinetic term for ζ. This is the main difference between the two gravity formulations. Starting from a metric $F(R)$ or $F(R_X)$ theory, ζ becomes a dynamical degree of freedom after moving to the Einstein frame, implying an eventual double-field inflationary setup. On the other hand, starting from a Palatini $F(R)$ or $F(R_X)$ theory, ζ remains an auxiliary field after moving the theory to the Einstein frame, implying just a single-field inflationary setup.

References

[1] A.A. Starobinsky, Phys. Lett. B 91 (1980) 99–102, http://dx.doi.org/10.1016/0370-2693(80)90670-X.

[2] A.H. Guth, Phys. Rev. D 23 (1981) 347–356, http://dx.doi.org/10.1103/PhysRevD.23.347.

[3] A.D. Linde, Phys. Lett. B 108 (1982) 389–393, http://dx.doi.org/10.1016/0370-2693(82)91219-9.

[4] A. Albrecht, P.J. Steinhardt, Phys. Rev. Lett. 48 (1982) 1220–1223, http://dx.doi.org/10.1103/PhysRevLett.48.1220.

[5] J. Martin, C. Ringeval, V. Vennin, Phys. Dark Univ. 5-6 (2014) 75–235, http://dx.doi.org/10.1016/j.dark.2014.01.003, arXiv:1303.3787 [astro-ph.CO].

[6] T. Koivisto, H. Kurki-Suonio, Classical Quantum Gravity 23 (2006) 2355–2369, http://dx.doi.org/10.1088/0264-9381/23/7/009, arXiv:astro-ph/0509422 [astro-ph].

[7] F. Bauer, D.A. Demir, Phys. Lett. B 665 (2008) 222–226, http://dx.doi.org/10.1016/j.physletb.2008.06.014, arXiv:0803.2664 [hep-ph].

[8] I.D. Gialamas, A. Karam, T.D. Pappas, E. Tomberg, https://doi.org/10.1142/S0219887823300076, arXiv:2303.14148 [gr-qc].
[9] V.M. Enckell, K. Enqvist, S. Rasanen, L.P. Wahlman, J. Cosmol. Astropart. Phys. 02 (2019) 022, http://dx.doi.org/10.1088/1475-7516/2019/02/022, arXiv:1810.05536 [gr-qc].
[10] C. Dioguardi, A. Racioppi, E. Tomberg, J. High Energy Phys. 06 (2022) 106, http://dx.doi.org/10.1007/JHEP06(2022)106, arXiv:2112.12149 [gr-qc].
[11] C. Dioguardi, A. Racioppi, E. Tomberg, arXiv:2212.11869 [gr-qc].
[12] L. Amendola, Phys. Lett. B 301 (1993) 175–182, http://dx.doi.org/10.1016/0370-2693(93)90685-B, arXiv:gr-qc/9302010 [gr-qc].
[13] S. Capozziello, G. Lambiase, H.J. Schmidt, Ann. Phys. 9 (2000) 39–48, http://dx.doi.org/10.1002/(SICI)1521-3889(200001)9:1<39::AID-ANDP39>3.0.CO, arXiv:gr-qc/9906051 [gr-qc].
[14] N. Aghanim, et al., Planck, Astron. Astrophys. 641 (2020) A6, http://dx.doi.org/10.1051/0004-6361/201833910, arXiv:1807.06209 [astro-ph.CO]; Astron. Astrophys. 652 (2021) C4, erratum.
[15] Y. Akrami, et al., [Planck], Astron. Astrophys. 641 (2020) A10, http://dx.doi.org/10.1051/0004-6361/201833887, arXiv:1807.06211 [astro-ph.CO].
[16] P.A.R. Ade, et al., [BICEP and Keck], Phys. Rev. Lett. 127 (15) (2021) 151301, http://dx.doi.org/10.1103/PhysRevLett.127.151301, arXiv:2110.00483 [astro-ph.CO].
[17] R. Kallosh, A. Linde, J. Cosmol. Astropart. Phys. 04 (04) (2022) 017, http://dx.doi.org/10.1088/1475-7516/2022/04/017, arXiv:2202.06492 [astro-ph.CO].
[18] S. Hanany, et al., [NASA PICO], arXiv:1902.10541 [astro-ph.IM].
[19] J. de Haro, L.A. Saló, Galaxies 9 (4) (2021) 73, http://dx.doi.org/10.3390/galaxies9040073, arXiv:2108.11144 [gr-qc].

Publication III

Konstantinos Dimopoulos, Christian Dioguardi, Gert Hütsi, Antonio Racioppi. Quintessential inflation in Palatini F(R, X)gravity. *The European Physical Journal Plus*, 140(11), November 2025

Eur. Phys. J. Plus (2025) 140:1109
https://doi.org/10.1140/epjp/s13360-025-07025-1

THE EUROPEAN PHYSICAL JOURNAL PLUS

Regular Article

Quintessential inflation in Palatini $F(R, X)$ gravity

Konstantinos Dimopoulos[1,a], **Christian Dioguardi**[2,3,b], **Gert Hütsi**[2,c], **Antonio Racioppi**[2,d]

[1] Consortium for Fundamental Physics, Physics Department, Lancaster University, Lancaster LA1 4YB, UK
[2] National Institute of Chemical Physics and Biophysics, Rävala 10, 10143 Tallinn, Estonia
[3] Tallinn University of Technology, Akadeemia tee 23, 12618 Tallinn, Estonia

Received: 29 July 2025 / Accepted: 2 November 2025

Abstract Palatini $F(R, X)$ gravity, with X the inflaton kinetic term, proved to be a powerful framework for generating asymptotically flat inflaton potentials. Here we show that a quadratic Palatini $F(R, X)$ restores compatibility with the observational data of the Peebles–Vilenkin quintessential inflation model. Moreover, the same can be achieved with an exponential version of the Peebles–Vilenkin potential if embedded in a Palatini $F(R, X)$ of order higher than two.

1 Introduction

The ΛCDM model represents today the Standard Cosmological Model. The main ingredients of the model are a relativistic matter component (radiation), some non-relativistic matter (cold dark matter, baryonic matter) and a cosmological constant, Λ, associated with dark energy. The latter drives the current accelerated expansion of the Universe.

ΛCDM, while being a simple model, requires extreme fine-tuning. The most popular way of improving ΛCDM is by introducing a scalar field, called quintessence in the literature (e.g., [1, 2] and refs. therein), that in contrast to Λ is a dynamical field. If the field varies slowly and has the appropriate energy density today, then it can lead to the aforementioned accelerated expansion at present.

At the same time, observations of the cosmic microwave background radiation (CMB) support the idea of a spatially flat and isotropic Universe at large scales, which can be explained by assuming cosmic inflation, i.e., another accelerated expansion of the Universe but during its very early stages [3–6]. In its simplest realization inflation is driven by another scalar field, the inflaton, with an almost flat potential energy.

Although similar in principle, inflation and dark energy late-time acceleration happen at very different energy scales, respectively, around 10^{16} GeV and 10^{-12} GeV. Hence, the two phenomena are usually considered to have different origins. At the same time, having an extra

quintessence field introduces the coincidence problem: one has to require specific initial conditions so that the current energy density of the scalar field matches the observed value of the cosmological constant.

Building a model of quintessential inflation overcomes this issue, by realizing the initial condition for quintessence through inflation [7]. However, a working model of the quintessential inflation must satisfy several conditions. First of all, it has to provide a graceful exit from inflation, providing good predictions for the CMB observables. Second, the scalar field has to survive until present days; this implies that a reheating mechanism that does not rely on its decay has to be provided such as instant preheating [8, 9], curvaton reheating [10, 11], gravitational reheating [12–14], Ricci reheating [15–17], reheating by primordial black hole evaporation [18, 19], and warm quintessential inflation [20, 21]. Finally, the scalar field potential needs to be very steep in order to bridge the energy gap between inflation and quintessence, allowing for a period of kination, which eventually ends due to reheating. This will eventually lead to the freezing of the scalar field at a value such that its energy density matches the value corresponding to the observed dark energy density.

Several models of quintessential inflation have been built by embedding a scalar field in General Relativity (e.g., [7, 22–25] and references therein). On the other hand, Palatini modifications of Einstein gravity proved to be very powerful tools in quintessential inflation model building (e.g., [26–30] and the references therein). In the standard metric formulation, the only dynamical degree of freedom is the metric tensor, while the affine connection is assumed a priori to be the Levi-Civita one. In the Palatini formulation instead, both the metric and the connection are considered independent dynamical degrees of freedom, and their relation is set by

[a] e-mail: k.dimopoulos1@lancaster.ac.uk
[b] e-mail: christian.dioguardi@kbfi.ee (corresponding author)
[c] e-mail: gert.hutsi@kbfi.ee
[d] e-mail: antonio.racioppi@kbfi.ee

Published online: 17 November 2025

their corresponding equations of motion (EoM). If the action is given by the simple Einstein–Hilbert term, the two formulations are equivalent, while in non-minimal theories of gravity they lead to substantially different phenomenological predictions, e.g., [31, 32].

In this article, we are interested in a particular class of non-minimal Palatini models: the $F(R, X)$ models, with X the inflaton kinetic term. Inflation in this class of theories has been extensively studied in [33–35] as a an extended generalization of the $F(R)$ models already explored in [34, 36]. The $F(R, X)$ models allow to simplify the structure of the scalar field kinetic term in the Einstein frame and consequently heal the dynamical issues of the $F(R)_{>2}$ (that is those containing terms diverging faster than R^2) theories out of the slow-roll regime. Remarkably, the $F(R,\ X)_{>2}$ theories, once the consistency criteria are satisfied, universally provide potential apparently suitable for quintessential inflation [33, 34].

Quintessential inflation was first introduced in Ref. [7] by Peebles and Vilenkin in order to model both early and late universe expansion utilizing a single scalar field with scalar potential which behaves as a quartic potential in the early universe, and as an inverse quartic potential at present times. The model successfully reproduces the quintessential inflation behavior; however, it predicts a tensor-to-scalar ratio r and spectral index n_s which are currently excluded by the current CMB observations [37, 38], while also featuring tracker quintessence with too large barotropic parameter. Since this pioneering work, a number of successful quintessential inflation models have been constructed (for recent reviews, see Refs. [23, 25]). More recently, quintessential inflation has been modeled in the context of modified gravity. For example, quintessential inflation models have also been studied in the context of Palatini $F(R)$ gravity for the quadratic choice $F(R) = R + \alpha R^2$. In Ref. [26] the Peebles–Vilenkin potential is discussed, while in Ref. [28] the case of the exponential tail is studied in presence of non-minimal coupling with the Ricci scalar. Both models provide the correct behavior for quintessence and predict r, n_s compatible with the current data. In this paper we embed the generalized version of the Peebles–Vilenkin potential and the exponential tail in the extended framework of $F(R, X)$ models and show that in the former case a viable model for quintessential inflation can be achieved, while the same cannot be achieved with an exponential tail.

In particular, the purpose of this work is to find, within the Palatini $F(R, X)$ framework, quintessential inflation setups that describe both inflation in the early Universe and the current accelerated expansion in agreement with the current observational data. While inflation has been extensively studied for this class of models, a description of both early and late universe acceleration is only achieved here for the first time. In particular we restore the compatibility with data of the Peebles–Vilenkin model with inflation and show how the same potential can lead to a dark-energy dominated phase in the late universe. We discuss the whole evolution of the scalar field, compute the predicted inflationary observables, and consider a kination period after the inflationary phase, typical of quintessential inflation models. We then consider reheating. Without specifying the reheating mechanism, we constrain the parameter space by taking into account the bounds coming from overproduction of gravitational waves during the kination phase. We finally consider a late-time dark-energy phase, modeled by the tail of the Peebles–Vilenkin potential, and show that it manages to satisfy the coincidence requirement. Moreover, we further constrain the parameter space of this class of models by imposing a barotropic parameter within the observational bounds. The full analysis is carried out for both a quadratic choice of $F(R, X)$ and higher-order models denoted by $F(R,\ X)_{>2}$.

The paper is organized as follows. In Sect. 2 we introduce the formalism of Palatini $F(R, X)$ theories. In Sect. 3 we consider the quadratic choice and compute the observables of the model for the Peebles–Vilenkin (PV) potential [7], for inflation, reheating and dark energy, showing the parameter space for which quintessential inflation is viable. At the end of the same section, we briefly consider an exponential tail and prove that, while giving very good predictions for the inflation CMB observables, it cannot predict a good quintessential tail for dark energy. In Sect. 4, for the sake of completeness, we repeat the same analysis of Sect. 3 for a specific higher-order $F(R,\ X)_{>2}$ model. We compute once again the observables for inflation, reheating and dark energy by using an exponential version of the Peebles–Vilenkin potential and constrain the parameter space for this model as well, proving that also higher-order $F(R, X)$ can account for quintessential inflation. Finally, in Sect. 5, we summarize the results of the paper and draw our conclusions.

We use geometric units where $c = \hbar = k_B = 1$ and $8\pi G = m_P^{-2} = 1$, while the signature of the metric is space-like.

2 Palatini $F(R, X)$ framework

The starting point for the Palatini $F(R, X)$ models is the following action:

$$S = \int \mathrm{d}^4x\sqrt{-g^J}\left(\frac{1}{2}F(R_X) - V(\phi)\right), \tag{1}$$

where F is an arbitrary function of its argument, $R_X \equiv R + X$ where $X = -g_J^{\mu\nu}\partial_\mu\phi\,\partial_\nu\phi$ is the scalar field kinetic term and $R = g_J^{\mu\nu}R_{\mu\nu}(\Gamma)$ is the Palatini Ricci scalar built from the metric-independent Ricci tensor, with Γ denoting the connection. We can rewrite the action (1) by introducing an auxiliary field ζ as follows:

$$S = \int \mathrm{d}^4x\sqrt{-g^J}\left(\frac{F(\zeta) + F'(\zeta)(R_X - \zeta)}{2} - V(\phi)\right). \tag{2}$$

One can easily check that by taking the variation of the action with respect to the auxiliary field ζ, the action in (1) is recovered (given that $F''(\zeta) \neq 0$.) By means of a conformal transformation $g^E_{\mu\nu} = F'(\zeta) g^J_{\mu\nu}$, we can rewrite the action in the Einstein frame, where the theory is linear in R and minimally coupled to the metric $g^E_{\mu\nu}$:

$$S = \int \mathrm{d}^4x \sqrt{-g^E} \left(\frac{R}{2} - \frac{1}{2} g_E^{\mu\nu} \partial_\mu \phi \, \partial_\nu \phi - U(\zeta, \phi) \right), \tag{3}$$

with

$$U(\zeta, \phi) = \frac{V(\phi)}{F'(\zeta)^2} - \frac{F(\zeta)}{2F'(\zeta)^2} + \frac{\zeta}{2F'(\zeta)}. \tag{4}$$

By taking the variation with respect to ζ, we get the corresponding equation of motion:

$$G(\zeta) \equiv \frac{1}{4}\big(2F(\zeta) - \zeta F'(\zeta)\big) = V(\phi), \tag{5}$$

which can be solved to get $\zeta(\phi)$. Equation (5) was already introduced in [36] where it holds as an approximation valid in the slow-roll regime. However, in this case, Eq. (5) is exact and valid even in the presence of large kinetic terms for the canonical scalar field. In other words, the auxiliary field $\zeta = \zeta(\phi)$ is a function of the canonically normalized field only and not of its derivatives. By using Eq. (5) one can rewrite $U(\zeta, \phi)$ in Eq. (4) in terms of ζ only, obtaining

$$U(\zeta) = \frac{\zeta}{4F'(\zeta)}. \tag{6}$$

This implies that even in the cases for which $G(\zeta)$ cannot be explicitly solved in terms of ζ, it can still be exploited for computing the inflationary observables [36]. In all the other (few) cases, $\zeta = \zeta(\phi)$ can be explicitly determined, allowing computations to proceed in the standard way.

In the following, we study two types of $F(\zeta)$ functions. First, we consider a quadratic $F(\zeta)$ which has the property to automatically flatten any diverging $V(\phi)$ when $\zeta \to +\infty$ (see Eqs. (5) and (6)). Then, we study a $F(\zeta)_{>2}$, i.e., a $F(\zeta)$ of order higher than two. This is a very special case because, first of all, in order to have a viable solution of Eq. (5), $V(\phi)$ must be negative [33, 34]. Secondly, even though $V(\phi) < 0$, the Einstein frame potential $U(\zeta)$ in Eq. (6) is positive as long as ζ, $F'(\zeta) > 0$. Finally, since $F(\zeta)$ is of order higher than two, $F'(\zeta)$ is of order higher than one, implying that at $\zeta \to +\infty$, $U(\zeta)$ automatically develops a tail approaching zero, which is exactly one of the requirements for quintessence.

3 Quintessential inflation for $F(R_X) = R_X + \alpha R_X^2$

This setup has been introduced in the context of fractional attractors in [33]. In such a scenario, from Eq. (5) we have $G(\zeta) = \frac{1}{4}\zeta = V(\phi)$. Hence, by using Eq. (6), we obtain an Einstein frame potential:

$$U(\zeta(\phi)) = \frac{\zeta(\phi)}{4(1 + 2\alpha\zeta(\phi))} = \frac{V(\phi)}{1 + 8\alpha V(\phi)}, \tag{7}$$

where we can immediately see that $U \to 0\,(\frac{1}{8\alpha})$ when $V \to 0\,(+\infty)$. Therefore, in order to have a quintessential tail for the potential we need to consider a form of $V(\phi)$ with a decreasing tail. The simplest example is the Peebles–Vilenkin (PV) potential, the first model made to describe quintessential inflation [7]. The Jordan frame potential has then following form:

$$V(\phi) = \begin{cases} \lambda^k(\phi^k + M^k) & \phi \leq 0 \\ \lambda^k \frac{M^{k+q}}{\phi^q + M^q} & \phi > 0, \end{cases} \tag{8}$$

with k an even number. We stress that such a configuration shares a similar form for the Einstein frame scalar potential as in Ref. [26]. However, in Ref. [26] the scalar field also needs to undergo a canonical normalization, while in our setup ϕ is already canonical normalized. This implies different phenomenological results with respect to Ref. [26].

3.1 Inflation

The original PV potential does not satisfy the experimental bounds from the CMB observations [37]. In our case instead, by starting from a Jordan frame potential with the form of the PV potential we obtain an Einstein frame potential with a plateau in the inflationary region, as shown in Fig. 1.

We plot the original PV potential (black) and the modified PV potential in Eq. (7) (blue) with $\alpha = 2 \cdot 10^8$, $q = k = 4$, predicting viable CMB observables $r = 0.017$, $n_s = 0.966$ (at $N_e = 60$) and a quintessential tail that solves the coincidence problem with the mass scale $M = 1.38 \cdot 10^{-13}$. We also show ϕ_N (star) and ϕ_{end} (dot) in the same color code. ϕ_N is not visible for the original PV potential as it lies at $V(\phi_N) \sim 10^{-8}$. The qualitative shape of the potential does not depend on the specific parameters. The value

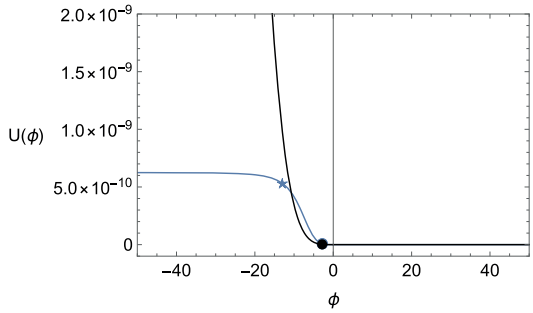

Fig. 1 The PV potential (black) and the modified PV potential (blue) with $\alpha = 2 \cdot 10^8, q = k = 4$, predicting viable CMB observables $r = 0.017, n_s = 0.966$ (at $N_e = 60$) and a quintessential tail that solves the coincidence problem at the mass scale $M = 1.38 \cdot 10^{-13}$. We also show ϕ_N (star) and ϕ_{end} (dot) in the same color code. ϕ_N is not visible for the original PV potential as it lays at $V(\phi_N) \sim 10^{-8}$. We notice that while the potential is modified at the inflation scale, it remains unchanged in the tail

$\phi_{\rm end}$ is such that $\epsilon(\phi_{\rm end}) = 1$ which corresponds to the end of slow-roll inflation, while ϕ_N is fixed by imposing $N_e \sim 60 - 70$, i.e., the number of e-folds between the time at which the CMB pivot scale $k = 0.05$ Mpc leaves the horizon, and the end of inflation.

We notice that, while the potential is modified at the inflation scale, it remains unchanged in the tail. This is indeed expected. By taking the limit $\phi \to -\infty$ of Eqs. (7) and (8), we see that $U(\phi) \to \frac{1}{8\alpha}$ which sets the height of the inflationary plateau. On the other hand, for $\phi \to \infty$ we get $U(\phi) \sim V(\phi)$, which reproduces the behavior of the original potential.

We now study the details of the inflationary phenomenology.

We compute the CMB observables in the slow-roll approximation by means of the slow-roll parameters:

$$\epsilon(\phi) \equiv \frac{1}{2}\left(\frac{U'(\phi)}{U(\phi)}\right)^2, \tag{9}$$

$$\eta \equiv \frac{U''(\phi)}{U(\phi)}. \tag{10}$$

In this approximation we can compute the tensor-to-scalar ratio r, the spectral index n_s, the amplitude of the scalar perturbations A_s and the number of e-folds N_e as:

$$r = 16\epsilon(\phi_N) \tag{11}$$

$$n_s = 1 - 2\eta(\phi_N) + 6\epsilon(\phi_N) \tag{12}$$

$$A_s = \frac{U(\phi_N)}{24\pi^2\epsilon(\phi_N)} \tag{13}$$

$$N_e = \int_{\phi_{\rm end}}^{\phi_N} d\phi \frac{U(\phi)}{U'(\phi)} \tag{14}$$

For our choice of the Einstein frame potential, we obtain:

$$\epsilon(\phi_N) = \frac{k^2\phi_N^{2k-2}}{2\left(M^k + \phi_N^k\right)^2\left(8\alpha\lambda^k\phi_N^k + 8\alpha\lambda^k M^k + 1\right)^2} \tag{15}$$

$$\begin{aligned}\eta(\phi_N) = {} & \frac{k\phi_N^{k-2}}{\left(M^k + \phi_N^k\right)\left(8\alpha\lambda^k\phi_N^k + 8\alpha\lambda^k M^k + 1\right)^2} \times \\ & \times \left(-8\alpha k\lambda^k\phi_N^k - 8\alpha\lambda^k\phi_N^k + 8\alpha k\lambda^k M^k \right. \\ & \left. -8\alpha\lambda^k M^k + k - 1\right)\end{aligned} \tag{16}$$

$$\begin{aligned}N_e = {} & \left[\frac{\phi^{2-k}}{2k}\left(\frac{\phi^k\left(16\alpha\lambda^k\phi^k + k + 2\right)}{k+2} - \frac{16\alpha\lambda^k M^{2k}}{k-2} + \right.\right. \\ & \left.\left. 2M^k\left(8\alpha\lambda^k\phi^k + \frac{1}{2-k}\right)\right)\right]_{\phi_{\rm end}}^{\phi_N}.\end{aligned} \tag{17}$$

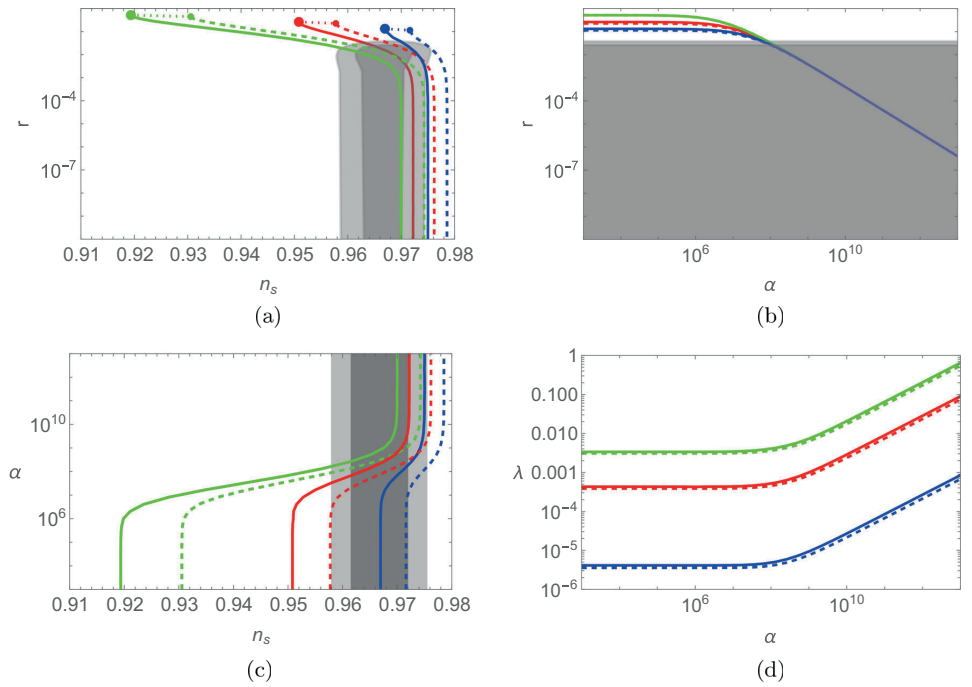

Fig. 2 r vs. n_s (a), r vs. alpha (b), α vs. n_s (c), λ vs. α (d) for the PV potential with $k = 2$ (blue), $k = 4$ (red), $k = 8$ (green) for $N_e = 60$ (thick) and $N_e = 70$ (dashed). The dots represents the predictions of the of the original PV potential in the same color code. For each value of k the plot is obtained fixing λ by imposing the condition on the observed amplitude of the scalar perturbations $A_s = 2.1 \cdot 10^{-9}$ and varying α in the range $0 < \alpha < 10^{13}$ (i.e., from small to large couplings of the higher-order term). The gray regions indicate the 95% (dark-gray) and 68% (light-gray) confidence levels (CL), respectively, based on the latest combination of Planck, BICEP/Keck, and BAO data [37]

In the strong coupling limit for $\alpha \to \infty$, $\phi_N \to -\infty$, and neglecting the contribution of $\phi_{\rm end}$, the inflationary observables can be approximated as:

$$N_e \simeq \frac{8\alpha\lambda^k {\phi_N}^{k+2}}{k(k+2)}, \tag{18}$$

$$r \simeq \frac{1}{12\pi^2\alpha A_s}, \tag{19}$$

$$n_s \simeq 1 - \frac{k+1}{k+2}\frac{2}{N_e}, \tag{20}$$

$$A_s \simeq \frac{k+2}{12\pi^2 k}\lambda^k N_e \left(\frac{k(k+2)N_e}{8\alpha\lambda^k}\right)^{\frac{k}{k+2}}. \tag{21}$$

We plot in Fig. 2 the numerical results for slow-roll inflation using this model. Notice that the number of e-folds is chosen in the range $N_e = 60 - 70$ instead of the usual $N_e = 50 - 60$, due to kination contribution during the Universe expansion, which is absent in models that consider an oscillatory reheating mechanism. The extra contribution to the number of e-folds can be computed as in Ref. [39]:

$$\Delta N = \frac{1-3w}{12(1+w)} \ln\left(\frac{\rho_{\rm reh}}{\rho_{\rm end}}\right) \simeq \frac{1}{3}\ln\left(\frac{U_{\rm end}^{1/4}}{T_{\rm reh}}\right), \tag{22}$$

where $\rho_{\rm reh}$ and $\rho_{\rm end}$ are, respectively, the energy density of the universe at the time of reheating and the end of inflation, $U_{\rm end}$ is the potential energy density at the end of inflation and $T_{\rm reh}$ is the reheating temperature. In the last expression, we used the fact that $w \equiv P/\rho = 1$ during kination. Notice, moreover, that ΔN is zero in standard Big Bang cosmology because $w = 1/3$ during radiation domination. For kination, the above gives $\Delta N \sim 10$ for $U_{\rm end}^{1/4} \sim 10^{16}$ GeV and $T_{\rm reh} \sim 10^3$ GeV, which justifies the choice $N_e \sim 60 - 70$. The relation between λ, α is imposed by fixing $A_s = 2.1 \cdot 10^{-9}$ [38]. From Fig. 2 we can see that agreement with data can easily be achieved with $\alpha \gtrsim 10^8$. To conclude, we note that the asymptotic results given in Eqs. (19) and (20) are exactly the same as the ones obtained in [33] because in the inflationary region the models are equivalent in the large α region.

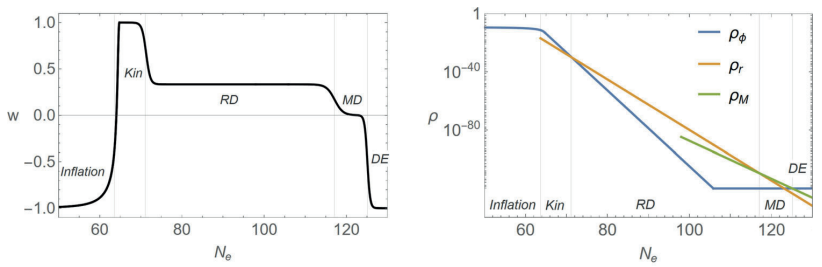

Fig. 3 **a** Evolution of the barotropic parameter of the universe in terms of the elapsing e-folds number N_e for the benchmark potential in Fig. 1 with $\alpha = 2 \cdot 10^8$, $q = k = 4$ and $M = 1.38 \cdot 10^{-13}$. The plot shows the natural appearance of a kination phase $w = 1$ right after the end of inflation (*Kin*). As radiation domination (RD) begins w drops to 1/3. After that we have matter domination (MD) with $w = 0$. Finally in the recent time the scalar field energy density becomes again the dominant source of energy density in the universe (DE). Today we have $w = -\Omega_\Lambda \simeq -0.7$. The vertical lines denote the corresponding e-folds number N_e for transitions between different epochs. **b** Evolution of the energy densities for the scalar field ρ_ϕ, the radiation fluid ρ_r and the matter fluid ρ_M in units of $m_P^4 = 1$. The vertical lines denote the corresponding e-folds number N_e for the transitions between different epochs. It is assumed that radiation is originally generated at the end of inflation (e.g., by Ricci reheating [15–17])

3.2 Kination

Right after the end of inflation, the equation of motion for the Einstein frame scalar field:

$$\ddot{\phi} + 3H\dot{\phi} + V'(\phi) = 0\,, \tag{23}$$

becomes dominated by kinetic energy and can be approximated as:

$$\ddot{\phi} + 3H\dot{\phi} \simeq 0\,. \tag{24}$$

It is evident that the evolution of the scalar field is now oblivious of the potential, and hence it is in essence model independent. The behavior of the rolling field is therefore generic.

The solution of the above for $\dot{\phi}$ is given by

$$\dot{\phi} = \sqrt{\frac{2}{3}}\frac{1}{t}\,. \tag{25}$$

Hence, by assuming that the scalar field behaves as a perfect fluid we have:

$$\rho_\phi = \frac{1}{2}\dot{\phi}^2 + V(\phi) \sim \frac{1}{2}\dot{\phi}^2 \propto a^{-6}\,, \tag{26}$$

with $a \propto t^{1/3}$, the scale factor of the universe during kination. Since from the Friedmann equations we have that $\rho \propto a^{-3(1+w)}$, the scalar field in this epoch behaves as a barotropic fluid with $w = 1$. By direct integration we have from Eq. (25):

$$\phi(t) = \phi_{\rm end} + \sqrt{\frac{2}{3}}\ln\left(\frac{t}{t_{\rm end}}\right). \tag{27}$$

We show in Fig. 3(a) the evolution of the of the barotropic parameter in terms of the e-folds number N_e for the benchmark potential in Fig. 1 with $\alpha = 2 \cdot 10^8$, $q = k = 4$ and $M = 1.38 \cdot 10^{-13}$. The plot shows the natural appearance of a kination phase $w = 1$ right after the end of inflation.

Kination finally needs to end in order to let the Hot Big Bang (HBB) take place. This has to happen before Big Bang Nucleosynthesis (BBN), so to reproduce the correct abundances of primordial nuclei. Since the radiation energy density scales as $\rho_r \propto a^{-4}$, as the Universe expands radiation will eventually become the dominant source of the energy-matter content of the Universe. This process is called reheating, and it can happen right after inflation ends or later on depending on the energy density of radiation at the end of inflation. The main constraint is that transition from kination to radiation domination has to happen before BBN takes place.

3.3 Reheating

We consider that radiation first appears at the end of inflation. We define:

$$\Omega_r^{\rm grav}|_{\rm end} \equiv \frac{\rho_r^{\rm grav}}{\rho}|_{\rm end} \tag{28}$$

the density parameter for radiation at the end of inflation. Its specific value will depend on the choice of the reheating mechanism, and in particular, the following general condition holds:

$$\Omega_r^{\rm grav}|_{\rm end} \leq \Omega_r|_{\rm end} \leq 1\,, \tag{29}$$

where the upper bound is found by choosing prompt reheating, while the lower bound is set by gravitational reheating which is the weakest reheating mechanism and hence produces the lowest possible value for the density parameter of radiation. The HBB starts with reheating and takes place at time given by:

$$t_{\rm reh} = \frac{t_{\rm end}}{(\Omega_r|_{\rm end})^{3/2}}\,, \tag{30}$$

which implies:

$$\phi_{\rm reh} = \phi_{\rm end} - \sqrt{\frac{3}{2}}\ln(\Omega_r|_{\rm end})\,. \tag{31}$$

Note that $\phi_{\rm reh}$ only depends on the potential $U(\phi)$ implicitly through the end of inflation, but its derivation is model independent. Now if we assume that radiation has the time to thermalize by the beginning of radiation domination, then we can compute the reheating temperature as:

$$T_{\rm reh} = \left(\frac{30}{\pi^2 g_*^{\rm reh}}(\Omega_r^{\rm end})^3\rho_\phi^{\rm end}\right)^{1/4}, \tag{32}$$

where $g_*^{\rm reh}$ are the effective relativistic degrees of freedom at the time of reheating. In the following we keep $\Omega_r^{\rm end}$ as a free parameter, i.e., we do not assume any specific reheating mechanism and proceed to find a lower bound for the reheating temperature from the constraints on overproduction of gravitational waves during the kination phase, as explained in "Appendix A". It is, in fact, well-known that a kination phase induces a peak in the amplitude of the gravitational wave background [40]. This peak has to be constrained in order to do not spoil the observations on Big Bang Nucleosynthesis. If detected in future, this would represent a confirmation of physics beyond ΛCDM and an hint for the viability of quintessential inflation models.

3.4 Quintessence

During radiation domination as the Universe keeps expanding; the field loses its kinetic energy while rolling down the field until it freezes. Since the potential is still negligible, the EoM for the scalar field is still given by Eq. (24), but H is now determined by the radiation content of the Universe so the equation yields:

$$\dot\phi = \sqrt{\frac{2}{3}\frac{t_{\rm reh}}{t^3}}\,. \tag{33}$$

Hence, by integrating it we get:

$$\phi(t) = \phi_{\rm reh} + 2\sqrt{\frac{2}{3}}\left(1 - \frac{t_{\rm reh}}{t}\right). \tag{34}$$

By using Eqs. (31) and (34), we get that the scalar field freezes at $t \gg t_{\rm reh}$ at the value:

$$\phi_F = \phi_{\rm end} + \sqrt{\frac{2}{3}}\left(2 - \frac{3}{2}\ln\Omega_r^{\rm end}\right). \tag{35}$$

In order to have a working quintessential inflation mechanism, we need to satisfy two more requirements. The first one is that the value of the scalar field potential energy density at freezing must match the value of the observed energy density of dark energy today (coincidence requirement), that is:

$$U(\phi_F) = \lambda^k\frac{M^{k+q}}{\phi_F^q + M^q} = \rho_0 \sim 7\cdot 10^{-121}. \tag{36}$$

Second, we need to check that the barotropic parameter at present w_0 for the quintessential tail is within the Planck observational bounds [41]. In order for this to happen, we need to make sure that the scalar field unfreezes only at the time of matter-dark energy equality. In other words, the field stays frozen until recent times and only unfreezes when it becomes dominating.

It is a well-known fact that in quintessence models, a competitor attractor behavior can appear. This attractor behavior is referred to in the literature as a tracker, if it leads to eventual quintessence domination. The condition for the tracker to appear is given by:

$$\Gamma \equiv \frac{UU''}{(U')^2} > 1. \tag{37}$$

Table 1 Results for reheating for the PV potential (8) with $q = k = 4$

α	$M_{\min}$[GeV]	$\phi_F^{\min}$	$T_{\rm reh}^{\max}$[GeV]	$T_{\rm reh}^{*}$[GeV]
10^8	$2.0 \cdot 10^5$	4.01	$4.6 \cdot 10^2$	$1.3 \cdot 10^7$
10^{12}	$2.7 \cdot 10^4$	4.01	$2.3 \cdot 10^3$	$1.9 \cdot 10^5$
10^{16}	$2.7 \cdot 10^3$	4.01	0.27	$5.9 \cdot 10^2$

The estimated maximum reheating temperature for the model $T_{\rm reh}^{\max}$ is below the lower bound $T_{\rm reh}^{*}$ for every choice of α, this implies that in general the model cannot account for the BBN constraints on overproduction of GWs (see "Appendix A"). However, compatibility with observations is restored if one assumes production of heavy particles in the early universe [14]

Note that, for an inverse-power-law potential like the one we have chosen, the tracker condition gives $\Gamma = \frac{q+1}{q}$ which implies that the tracker is always present. For the case $q = 4$ the energy density of the tracker solution scales as:

$$\rho_T \sim \left(\frac{M^8}{\alpha t^4}\right)^{1/3}, \tag{38}$$

which scales slower than a matter-dominated background.

While the field is frozen at ϕ_F, it has a constant contribution to the energy density. However, if it hits the tracker before becoming dominant, it unfreezes and starts following the tracker solution. Eventually, the scalar field becomes dominant with a barotropic parameter $w = -\frac{1}{3}$, which is not acceptable given the observational bound $w_{DE} < -0.95$ [41]. If, on the other hand, the value of $U(\phi_F)$ is small enough, i.e.,

$$U(\phi_F(t_{\rm eq})) < \rho_T(t_{\rm eq}), \tag{39}$$

then the scalar field unfreezes only at the matter-dark energy equality. After dominating, the field thaws and starts slow-rolling down its potential. The slow-rolling quintessence evolves as a fluid with a barotropic parameter given by:

$$w_\phi = \frac{\frac{1}{2}\dot{\phi}^2 - U(\phi)}{\frac{1}{2}\dot{\phi}^2 + U(\phi)} \simeq -1\,, \tag{40}$$

since the field changes very slowly with time. Note that, while close to -1, the barotropic parameter would be slightly larger, which, if confirmed by observations, would distinguish the model from ΛCDM.[1]

Imposing (39) is equivalent to impose a lower bound on the mass scale $M = M_{\min}$ in our potential (see Table 1). It can be checked that field does not evolve substantially from matter-dark energy equality to the present day. Therefore, it is safe to consider $\phi_0 \simeq \phi_F$ and $w_\phi \approx -1$.

We show in Table 1 the results for the case $k = q = 4$. We only report the values of α that allow good predictions for the CMB observables. The value $M_{\min}$ is the minimum value of the mass scale for the potential in Eq. (8) necessary to avoid the tracker solution and let the field unfreeze only at matter-dark energy equality. The corresponding $\phi_F^{\min}$ is obtained by imposing the solution of the coincidence problem in Eq. (36). The reheating temperature $T_{\rm reh}^{\max}$ is computed by means of Eq. (32) by setting $M = M_{\min}$ and $\phi = \phi_{\min}$.

Finally, we need to check if the model can satisfy the constraints on $T_{\rm reh}$ coming from gravitational wave (GW) overproduction. During kination, the $w = 1$ stiff period induces a spike in the density of the GWs, potentially spoiling BBN. This can be avoided if $T_{\rm reh}$ is large enough. The details on the calculation can be found in "Appendix A" (see Eqs. (74)–(78)) , while we show in Table 1 an estimate of the lower bound $T_{\rm reh}^{*}$ (depending on the value of α) that avoids GW overproduction.

Unfortunately, we always have $T_{\rm reh}^{\max} < T_{\rm reh}^{*}$ hence the model is not viable in general. However, compatibility with observation can be restored if we assume the gravitational production of very massive particles after the inflationary era [14]. How much the bound on reheating temperature relaxes, depends on the exact properties of such heavy particles, like mass and heating efficiency. However, regardless of the aforementioned details, an indicative validity range can be estimated to be [14]

$$1\ \text{MeV} \leq T_{\rm reh} \leq 5 \cdot 10^7 \text{GeV}\,, \tag{41}$$

which makes the results computed in Table 1 viable.

3.5 The case of the exponential tail

Most popular quintessence models assume an exponential tail in the form:

$$V(\phi) = M^4 e^{-\lambda\phi}. \tag{42}$$

By choosing a Jordan frame potential as in Eq. (42), we get the Einstein frame potential

[1] Indeed, recent DESI observations seem to suggest that quintessence is favored over ΛCDM [42].

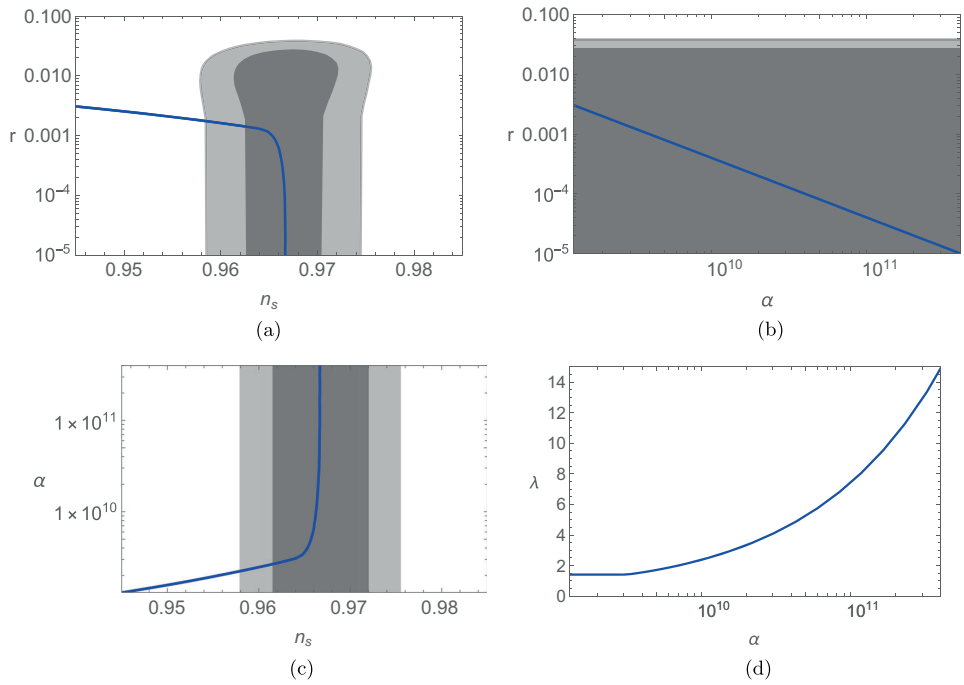

Fig. 4 r versus n_s (**a**), r versus α (**b**), α versus n_s (**c**), λ versus α (**d**) for the quadratic model with $V(\phi) = V_0 e^{-\lambda\phi}$ for $N_e = 60$. The relation between α and λ is imposed by fixing $A_s \sim 2.1 \cdot 10^{-9}$. The gray regions indicate the 95% (dark-gray) and 68% (light-gray) confidence levels (CL), respectively, based on the latest combination of Planck, BICEP/Keck, and BAO data [37]

$$U(\phi) = \frac{M^4 e^{-\lambda\phi}}{8\alpha M^4 e^{-\lambda\phi} + 1}, \tag{43}$$

and the corresponding the slow-roll parameters

$$\epsilon(\phi) = \frac{\lambda^2}{2}\left(\frac{1}{1 + 8\alpha M^4 e^{-\lambda\phi}}\right)^2, \tag{44}$$

$$\eta(\phi) = \frac{\lambda^2 e^{\lambda\phi}\left(1 - 8M^4\alpha e^{-\lambda\phi}\right)}{\left(8M^4\alpha e^{-\lambda\phi} + 1\right)^2}. \tag{45}$$

From Eq. (44) we see that:

$$\epsilon(\phi) \sim 0, \qquad \text{for } \phi \to -\infty \tag{46}$$

$$\epsilon(\phi) \sim \frac{\lambda^2}{2} \qquad \text{for } \phi \to \infty, \tag{47}$$

which implies that to end slow-roll during inflation and have a graceful exit we need $\lambda > \sqrt{2}$. While inflation works very well for this choice of parameters, as shown in Fig. 4, it does not provide a good tail for quintessence. The reason can be seen from Fig. 5.

The plot shows the change in the potential by varying the parameter M. The net result of changing M amounts to a translation along the $\phi-$axis, while $\phi_{end} - \phi_N$ remains constant (after fixing the other parameters α,λ,N_e), yielding the same results for the inflationary observables. The immediate consequence is that M cannot be used as a parameter to fix, in order to match the observed cosmological constant.

To see this explicitly, consider the tail of Eq. (43). For $\phi \to +\infty$, we have:

$$U(\phi) \sim M^4 e^{-\lambda\phi}. \tag{48}$$

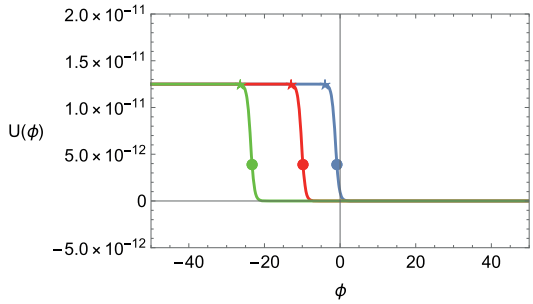

Fig. 5 Exponential potential for $M = 10^{-3}$ (blue), $M = 10^{-5}$ (red), $M = 10^{-8}$ (green) and $\alpha = 10^{10}$ and corresponding $\lambda = 2.05$ fixed by setting $A_s \sim 2.1 \cdot 10^{-9}$. We also show ϕ_N (star) and $\phi_{\rm end}$ (dot) in the same color code. Changing M amounts to a shift in the potential along ϕ-axis

Once again we want to understand if we can solve the coincidence problem:

$$U(\phi_F) = M^4 e^{-\lambda\phi_F} = \rho_0 \sim 7 \cdot 10^{-121}, \tag{49}$$

where ϕ_F is still given by Eq. (35). For the sake of simplicity, we now consider the case that maximizes Eq. (35), i.e., gravitational reheating. It can be computed that:

$$\phi_F \sim \phi_{\rm end} + 40, \tag{50}$$

where ϕ_{end} is obtained by solving $\epsilon(\phi) = 1$. Hence, we get:

$$U(\phi_F) = \frac{\sqrt{2}\lambda - 2}{16\alpha} e^{-\lambda 40}. \tag{51}$$

This implies that the only parameter in the model is λ and the two scales (inflation and dark-energy) cannot be decoupled. Even in the maximal case we cannot solve the coincidence problem unless $\lambda \sim 6.3$ which is too large and cannot reproduce dark-energy behavior. It is then impossible to use this model to achieve a viable quintessential inflation scenario.

4 Quintessential inflation for $F(R_X)_{>2}$

In this section, we discuss for completeness quintessential inflation for the higher-order case $F(R, X)_{>2}$. We carry the same analysis of Sect. 3 by computing the inflation and dark-energy observables and consider the bounds from overproduction of gravitational waves, in order to constrain the parameter space and prove the viability of quintessential inflation for this class as well.

For this class of functions, the behavior of $G(\zeta)$ changes drastically and one can see that the equation $G(\zeta) = 0$ always admits a solution for some $\zeta_0 > 0$ (see (5)). For any $\zeta > \zeta_0$, the $G(\zeta)$ function is negative. As shown in [33], this configuration works particularly well when considering negative and unbounded from below Jordan frame potentials $V(\phi)$. In fact, such a choice generates an Einstein frame potential U which is positive definite and has an asymptotically flat plateau that allows to perform inflation for $\zeta \to \zeta_0$ (i.e., $V(\phi) \to 0$). At the same time for $\zeta \to +\infty$, the potential U exhibits a tail that asymptotically approaches zero, giving the opportunity to mimic the quintessence behavior without the necessity of introducing a decaying tail behavior to begin with.

In order to give a concrete example, we now focus on the case:

$$F(\zeta) = \zeta + \alpha\zeta^2 \ln(\beta\zeta), \tag{52}$$

with $\beta > \alpha/e$, in order to ensure that $F' > 0$ for any $\zeta > \zeta_0$. This specific example allows for an exact solution for Eq. (5), which reads:

$$\zeta - \alpha\zeta^2 = V(\phi). \tag{53}$$

The above equation admits two solutions:

$$\zeta_\pm = \frac{1 \pm \sqrt{1 - 4\alpha V(\phi)}}{2\alpha} = \frac{1 \pm \sqrt{1 + 4\alpha|V(\phi)|}}{2\alpha}, \tag{54}$$

but the consistency constraints $\zeta \geq \zeta_0 = 1/\alpha$ and $V(\phi) < 0$, suggest

$$\zeta = \zeta_+ = \frac{1 + \sqrt{1 + 4\alpha|V(\phi)|}}{2\alpha}, \tag{55}$$

Table 2 Results for inflation for the *e*PV potential in Eq. (61) with $k = q = 4$ at $N_e = 60$

α	r	n_s	μ/M
10^8	0.03	0.963	0.06
10^{12}	$4 \cdot 10^{-6}$	0.972	$2.5 \cdot 10^{-5}$
10^{16}	$4 \cdot 10^{-10}$	0.972	$2.5 \cdot 10^{-9}$

Predictions for inflation lay inside the 2σ region for r, n_s. The ratio μ/M is fixed by requiring $A_s = 2.1 \cdot 10^{-9}$

is the only available solution. Using such a solution, we can provide the exact expression of the Einstein frame scalar potential:

$$U(\phi) = \frac{|V(\phi)|}{2}\left[4\alpha|V(\phi)|\ln\left(\frac{\beta\left(1+\sqrt{1+4\alpha|V(\phi)|}\right)}{2\alpha}\right) + 2\alpha|V(\phi)| + \sqrt{4\alpha|V(\phi)|+1} - 1\right]^{-1} \tag{56}$$

For $V(\phi) \to 0$, the above behaves as

$$U(\phi) \approx \frac{1}{8\alpha\left(\ln\left(\frac{\beta}{\alpha}\right)+1\right)}\left[1 + \frac{\alpha V(\phi)}{2\left(\ln\left(\frac{\beta}{\alpha}\right)+1\right)}\right], \tag{57}$$

while for $V(\phi) \to -\infty$, as

$$U(\phi) \approx \frac{1}{8\alpha\ln\left(\beta\sqrt{\frac{|V(\phi)|}{\alpha}}\right)} = \frac{1}{8\alpha\left(\frac{1}{2}\ln(|V(\phi)|) + \ln\left(\frac{\beta}{\sqrt{\alpha}}\right)\right)}, \tag{58}$$

where we emphasize once again that $V(\phi) < 0$. We conclude this preliminary discussion by noting that, if we plug-in an exponential potential with the an asymptotic behavior

$$V(\phi) \approx -e^{f(\phi)}, \tag{59}$$

into Eq. (58), then the tail of the potential behaves as

$$U(\phi) \approx \frac{1}{f(\phi)}. \tag{60}$$

We will use this last result as a guide to construct a working model of quintessential inflation, as we will see in the following subsection.

4.1 Exponential PV potential

Given the result of Eq. (60), we choose an exponential version[2] of the Peebles–Vilenkin (*e*PV) potential used in Sect. 3

$$V(\phi) = 1 - e^{V_{PV}(\phi)}, \tag{61}$$

with

$$V_{PV}(\phi) = \begin{cases} \frac{\mu^k}{M^q(\phi^k+M^k)} & \phi \le 0, \\ \frac{\phi^k+\mu^k}{M^{k+q}} & \phi > 0\,. \end{cases} \tag{62}$$

It is possible to show numerically that the parameter β appearing in Eq. (56) has a negligible effect on the computation of the CMB observables. Moreover, one can see from Eq. (58) that for realistic choices of α, β the dominant term in the denominator will be given by the $\ln(|V|)$ contribution. Thus, in what follows, we can safely set $\beta = \alpha$ without loss of generality. With this setup it is possible to produce viable predictions for the CMB observables by fixing the two mass scales M, μ without requiring extreme fine-tuning to solve the coincidence problem.

However, as we can see from Table 2, this setup is physical only for very large α. For this reason, we only compute the slow-roll parameters in the $\alpha \to \infty$ regime:

$$\epsilon(\phi_N) \sim \frac{1}{8}\alpha^2 k^2 \mu^{2k} \phi^{-2(k+1)} M^{-2q}, \tag{63}$$

[2] We added 1 to the definition of the potential in Eq. (59) in order to ensure that $V(\phi) \to 0$ for $\phi \to -\infty$.

Table 3 Results for reheating for the *e*PV potential in Eq. (61) with $k = q = 4$

α	$M_{\min}$[GeV]	$\phi_F^{\min}$	$T_{reh}^{\max}$[GeV]	$T_{\rm reh}^{*}$[GeV]
10^8	$5.5 \cdot 10^4$	4.01	$1.2 \cdot 10^6$	$2.9 \cdot 10^7$
10^{12}	$1.7 \cdot 10^5$	4.01	$1.5 \cdot 10^2$	$1.1 \cdot 10^5$
10^{16}	$5.5 \cdot 10^5$	4.01	0.015	305

The estimated maximum reheating temperature for the model $T_{\rm reh}^{\max}$ is below the lower bound $T_{\rm reh}^{*}$ for every choice of α, this implies that in general the model cannot account for the BBN constraints on overproduction of GWs (see appendix A). However, compatibility with observations are restored if one assumes production of heavy particles in the early universe

$$\eta(\phi_N) \sim -\frac{1}{2}\alpha k(k+1)\mu^k \phi^{-k-2} M^{-q}, \tag{64}$$

and the number of e-folds can be integrated explicitly giving:

$$N_e \sim \frac{2\mu^{-k}\phi^{k+2}M^q}{\alpha k(k+2)}. \tag{65}$$

Finally, the CMB observables read:

$$r \sim \frac{1}{12\pi^2 \alpha A_s}, \tag{66}$$

$$n_s \sim 1 - \frac{k+1}{k+2}\frac{2}{N_e}, \tag{67}$$

$$A_s \sim \frac{2^{-\frac{5k+8}{k+2}}\mu^{-2k}M^{2q}\left(\alpha k(k+2)N_e\mu^k M^{-q}\right)^{\frac{2(k+1)}{k+2}}}{3\pi^2\alpha^3 k^2}. \tag{68}$$

We note that the limits for r and n_s are the same as the ones shown in eqs. (19) and (20). Indeed, it can be easily proven that the current setup and the one in section 3.1 are actually equivalent in the inflationary region for $\alpha \to \infty$.

After inflation is over, kination and reheating follow (see Sects. 3.2–3.3). The reheating temperature must satisfy the bound $T_{\rm reh} > T_{\rm BBN} \sim 10^{-2}$ GeV. After reheating takes place, radiation eventually starts dominating. During the expansion, the scalar field ϕ_F freezes at the value given by Eq. (35).

In order to have a working quintessential inflation mechanism, we need to satisfy two more requirements. The first one is that the value of the scalar field potential energy density at freezing must match the value of the observed energy density of dark energy today (coincidence requirement). By using Eqs. (58) and (61), we find:

$$U(\phi_F) \approx \frac{M^k}{4\alpha(\phi_F^k + \mu^k)} = \rho_0 \sim 7 \cdot 10^{-121}. \tag{69}$$

Second, we need to check that the barotropic parameter at the present day w_0 for the quintessential tail is within the Planck observational bounds [41]. In order for this to happen, we need to make sure that the scalar field unfreezes only at the time of matter-dark energy equality. In other words, the field stays frozen until recent times and only unfreezes when it becomes dominating. The field then thaws and starts slow-rolling down its potential. This happens provided that the frozen scalar field does not hit the tracker before it starts dominating (see Sect. 3.4). The equation for the barotropic parameter in w_ϕ is given by Eq. (40). Once again the field will not substantially evolve till the present day, with $\phi_0 \simeq \phi_F$ and $w_\phi \approx -1$.

We show in Table 3 the results for the case $k = q = 4$. We only report the values of α for which we obtain viable CMB observables. The value $M_{\min}$ is the minimum value of the mass scale for the potential in Eq. (61) necessary to avoid the tracker solution and let the field unfreeze only at matter-dark energy equality. The corresponding $\phi_F^{\min}$ is obtained by imposing the solution of the coincidence problem in Eq. (69). The reheating temperature is computed by means of Eq. (32) by setting $M = M_{\min}$ and $\phi = \phi_{\min}$. Finally, we need to check if the model can satisfy the constraints on $T_{\rm reh}$ coming from GW overproduction. During kination, the $w = 1$ stiff period induces a spike in the density of the GWs, potentially spoiling BBN. This can be avoided if $T_{\rm reh}$ is large enough. The details on the calculation can be found in appendix A, while we show in Table 3 an estimate of the lower bound $T_{\rm reh}^{*}$ (depending on the value of α) that avoids GW overproduction.

Unfortunately, we always have $T_{\rm reh}^{\max} < T_{\rm reh}^{*}$; hence, the model is not in general viable. As before, compatibility with observation can be restored if we assume the gravitational production of very massive particles after the inflationary era [14] which naively relaxes the reheating temperature bound to the one showed in Eq. (41), making the results computed in Table 3 viable again.

4.2 A note on the exponential tail

Given Eq. (58), one can try to reproduce an exponential tail by choosing a Jordan frame potential in the form of a double exponential:

$$V(\phi) = 1 - e^{\sigma e^{\lambda\phi}}. \tag{70}$$

The Einstein frame tail would then behave as:

$$U(\phi) \approx \frac{e^{-\lambda\phi}}{4\alpha\lambda}. \tag{71}$$

However, this setup cannot be used to generate a quintessential tail.

Consider the slow-roll parameter $\epsilon(\phi) = \frac{U'(\phi)^2}{2U(\phi)^2}$ with $U(\phi)$ given by Eq. (56). It can be straightforwardly computed that this function is a monotonically increasing function with the following limits:

$$\epsilon(\phi) \sim 0, \qquad \text{for } \phi \to -\infty\,, \tag{72}$$

$$\epsilon(\phi) \sim \frac{\lambda^2}{2}, \qquad \text{for } \phi \to \infty\,, \tag{73}$$

which implies that to end slow-roll during inflation and have a graceful exit we need $\lambda > \sqrt{2}$. Once again the same parameter determines the behavior at inflation, and in the tail, this implies that the two scales cannot be decoupled. Since this setup is equivalent to the one presented in 3.5, we conclude that it is not viable.

5 Conclusions

We have studied modeling quintessential inflation in the context of $F(R, X)$ Palatini gravity. In particular, we considered a potential in the form of the generalized Peebles–Vilenkin (PV) potential for a quadratic $F(R, X)$. We proved that the model generates viable quintessential inflation in the case $k = q = 4$ with a mass scale $M \sim 10^3 - 10^5$ GeV, providing the right inflationary observables, a solution for the coincidence problem and a prediction for the barotropic parameter $w_\phi \approx -1$. The model predicts in general a value of $T_{\rm reh} < 10^5$ GeV, which contradicts the lower bound on $T_{\rm reh}$ necessary to avoid overproduction of GWs during kination. However, compatibility with observations can be restored if we assume production of heavy particles $\sim 10^{-6} m_P$, which later on decay in the SM sector. This relaxes the bound to $1\,\text{MeV} \leq T_{\rm reh} \leq 5 \cdot 10^7$ GeV, which is compatible with our predictions.

We also considered an example for a model $F(R,\ X)_{>2}$, in the form $F(R_X) = R_X + \alpha R_X^2 \ln(\alpha R_X)$ with a Jordan frame potential given by an exponential version of the PV potential, characterized by two mass scales $\mu,\ M$. The model predicts viable quintessential inflation for $k = q = 4$ with a mass scale of order $M \sim 10^5$ GeV which solves the coincidence problem and $1\,\text{MeV} < \mu < 10^3$ GeV fixed by the amplitude of scalar perturbations A_s. As in the previous case the model predicts in general a value of $T_{\rm reh} < 10^5$ GeV which cannot be accepted if one considers the lower bound on $T_{\rm reh}$ necessary to avoid overproduction of GWs during kination. The solution is again to assume production of heavy particles in the early Universe.

We also showed that a quintessential tail given by a simple exponential, although generating very good inflationary results, does not provide a solution for the coincidence problem (in both the $F(R, X)$ models).

All in all, this study demonstrated that $F(R, X)$ Palatini gravity is a promising framework for constructing viable quintessential inflation models, although it can be challenging to address successfully all the relevant constraints and, in particular, the overproduction of primordial gravitational waves during kination.

Acknowledgements KD is supported (in part) by the STFC consolidated Grant: ST/X000621/1. This work was supported by the Estonian Research Council grants PRG1055, RVTT3, RVTT7 and the CoE program TK202 "Foundations of the Universe." This article is based upon work from COST Actions COSMIC WISPers CA21106 and CosmoVerse CA21136, supported by COST (European Cooperation in Science and Technology).

Appendix

Constraints from the overproduction of GWs

In the following we briefly compute an estimate on the reheating temperature necessary to avoid overproduction of GWs during kination (see for example [43] for the details).

In order to respect the bounds from BBN, we need to constraint the intensity:

$$\Omega_{\rm peak} h^2 = \int_{\nu_{\rm BBN}}^{\nu_{\rm end}} \frac{\Omega_{GW} h^2}{\nu} d\nu \leq \frac{7}{8}\left(\frac{4}{11}\right)^{4/3} \Omega h^2 \Delta N_{\rm eff}\,, \tag{74}$$

where Ω_{GW} is the spectrum of the gravitational waves, $\Omega_r h^2 \sim 2.47 \cdot 10^{-5}$ is the relic density of radiation, $\nu_{\rm BBN} \sim 10^{-11}$Hz and $\Delta N_{\rm eff} \sim 0.17$ the extra relativistic degrees of freedom during BBN given by the current Planck bound [41].

The above can be related to the reheating temperature as follows. Consider the frequencies $\nu_{\rm end}$, $\nu_{\rm reh}$ corresponding to the GW modes that reenter the horizon, respectively, at the end of inflation and at reheating. We have:

$$\nu_{\rm end} = \frac{H_{\rm end}}{2\pi}\frac{a_{\rm end}}{a_0}, \tag{75}$$

$$\nu_{\rm reh} = \nu_{\rm end}\left(\frac{H_{\rm end}}{H_{\rm reh}}\right)^{2/3}, \tag{76}$$

with

$$H_{\rm reh} = \pi\sqrt{\frac{g^*_{\rm reh}}{90}}T^2_{\rm reh}. \tag{77}$$

Finally, between the end of the inflation and reheating we have that

$$\Omega_{\rm peak} = \Omega^{rd}_{GW}\frac{\nu_{\rm end}}{\nu_{\rm reh}}, \tag{78}$$

where $\Omega^{rd}_{GW} \propto H^2_{\rm end}$, is the GW density parameter of the modes that reenter the horizon during radiation domination. By comparing (74) with (78) and using (75)–(77), we get a lower bound on $T_{\rm reh}$. In this way, we can obtain the constraint on the reheating temperature appearing in Tables 1 and 3.

References

1. E.J. Copeland, M. Sami, S. Tsujikawa, Int. J. Mod. Phys. D **15**, 1753 (2006). https://doi.org/10.1142/S021827180600942X
2. S. Tsujikawa, Class. Quant. Grav. **30**, 214003 (2013). https://doi.org/10.1088/0264-9381/30/21/214003
3. A.A. Starobinsky, Phys. Lett. B **91**, 99 (1980). https://doi.org/10.1016/0370-2693(80)90670-X
4. A.H. Guth, Phys. Rev. D **23**, 347 (1981). https://doi.org/10.1103/PhysRevD.23.347
5. A.D. Linde, Phys. Lett. B **108**, 389 (1982). https://doi.org/10.1016/0370-2693(82)91219-9
6. A. Albrecht, P.J. Steinhardt, Phys. Rev. Lett. **48**, 1220 (1982). https://doi.org/10.1103/PhysRevLett.48.1220
7. P.J.E. Peebles, A. Vilenkin, Phys. Rev. D **59**, 063505 (1999). https://doi.org/10.1103/PhysRevD.59.063505
8. G. Felder, L. Kofman, A. Linde, Phys. Rev. D **59**(12) (1999). https://doi.org/10.1103/physrevd.59.123523
9. A. Campos, H. Reis, R. Rosenfeld, Phys. Lett. B **575**(3–4), 151–156 (2003). https://doi.org/10.1016/j.physletb.2003.09.064
10. B. Feng, M. Li, Phys. Lett. B **564**(3–4), 169–174 (2003). https://doi.org/10.1016/s0370-2693(03)00589-6
11. J.C. Bueno Sanchez, K. Dimopoulos, JCAP **11**, 007 (2007). https://doi.org/10.1088/1475-7516/2007/11/007
12. L.H. Ford, Phys. Rev. D **35**, 2955 (1987). https://doi.org/10.1103/PhysRevD.35.2955
13. E.J. Chun, S. Scopel, I. Zaballa, JCAP **07**, 022 (2009). https://doi.org/10.1088/1475-7516/2009/07/022
14. J. de Haro, Phys. Rev. D **109**(2), 023517 (2024). https://doi.org/10.1103/PhysRevD.109.023517
15. K. Dimopoulos, T. Markkanen, JCAP **06**, 021 (2018). https://doi.org/10.1088/1475-7516/2018/06/021
16. T. Opferkuch, P. Schwaller, B.A. Stefanek, JCAP **07**, 016 (2019). https://doi.org/10.1088/1475-7516/2019/07/016
17. D. Bettoni, A. Lopez-Eiguren, J. Rubio, JCAP **01**(01), 002 (2022). https://doi.org/10.1088/1475-7516/2022/01/002
18. I. Dalianis, G.P. Kodaxis, Galaxies **10**(1), 31 (2022). https://doi.org/10.3390/galaxies10010031
19. M. Riajul Haque, E. Kpatcha, D. Maity, Y. Mambrini, Phys. Rev. D **108**(6), 063523 (2023). https://doi.org/10.1103/PhysRevD.108.063523
20. K. Dimopoulos, L. Donaldson-Wood, Phys. Lett. B **796**, 26 (2019). https://doi.org/10.1016/j.physletb.2019.07.017
21. J.A.G. Rosa, L.B. Ventura, Phys. Lett. B **798**, 134984 (2019). https://doi.org/10.1016/j.physletb.2019.134984
22. K. Dimopoulos, C. Owen, JCAP **06**, 027 (2017). https://doi.org/10.1088/1475-7516/2017/06/027
23. J. de Haro, L.A. Saló, Galaxies **9**(4), 73 (2021). https://doi.org/10.3390/galaxies9040073
24. D. Bettoni, J. Rubio, Galaxies **10**(1), 22 (2022). https://doi.org/10.3390/galaxies10010022
25. N. Jaman, M. Sami, Galaxies **10**(2), 51 (2022). https://doi.org/10.3390/galaxies10020051
26. K. Dimopoulos, S. Sánchez López, Phys. Rev. D **103**(4), 043533 (2021). https://doi.org/10.1103/PhysRevD.103.043533
27. K. Dimopoulos, A. Karam, S. Sánchez López, E. Tomberg, Galaxies **10**(2), 57 (2022). https://doi.org/10.3390/galaxies10020057
28. K. Dimopoulos, A. Karam, S. Sánchez López, E. Tomberg, JCAP **10**, 076 (2022). https://doi.org/10.1088/1475-7516/2022/10/076
29. I.D. Gialamas, A. Karam, T.D. Pappas, E. Tomberg, Int. J. Geom. Methods Mod. Phys. **20**(13), 2330007 (2023). https://doi.org/10.1142/S0219887823300076
30. J.J. Terente Díaz, K. Dimopoulos, M. Karčiauskas, A. Racioppi, JCAP **02**, 040 (2024). https://doi.org/10.1088/1475-7516/2024/02/040
31. T. Koivisto, H. Kurki-Suonio, Class. Quant. Grav. **23**, 2355 (2006). https://doi.org/10.1088/0264-9381/23/7/009
32. F. Bauer, D.A. Demir, Phys. Lett. B **665**, 222 (2008). https://doi.org/10.1016/j.physletb.2008.06.014
33. C. Dioguardi, A. Racioppi, Phys. Dark Univ. **45**, 101509 (2024). https://doi.org/10.1016/j.dark.2024.101509
34. C. Dioguardi, A. Racioppi, E. Tomberg, J. Cosmol. Astropart. Phys. **2024**(03), 041 (2024). https://doi.org/10.1088/1475-7516/2024/03/041
35. N. Bostan, R.H. Dejrah, C. Dioguardi, A. Racioppi (2025). https://arxiv.org/abs/2503.16324
36. C. Dioguardi, A. Racioppi, E. Tomberg, JHEP **06**, 106 (2022). https://doi.org/10.1007/JHEP06(2022)106
37. P.A.R. Ade et al., Phys. Rev. Lett. **127**(15), 151301 (2021). https://doi.org/10.1103/PhysRevLett.127.151301
38. Y. Akrami et al., Astron. Astrophys. **641**, A10 (2020). https://doi.org/10.1051/0004-6361/201833887
39. M. Drewes, J.U. Kang, U.R. Mun, JHEP **11**, 072 (2017). https://doi.org/10.1007/JHEP11(2017)072

40. J. Haro Cases, L. Aresté Saló, Universe **6**(6), 87 (2020). https://doi.org/10.3390/universe6060087
41. A. Planck Collaboration et al., A &A **641**, A6 (2020). https://doi.org/10.1051/0004-6361/201833910
42. A.G. Adame et al., JCAP **02**, 021 (2025). https://doi.org/10.1088/1475-7516/2025/02/021
43. C. Chen, S. Jyoti Das, K. Dimopoulos, A. Ghoshal (2025)

Curriculum Vitae

1. Personal data

Name	Christian Dioguardi
Date and place of birth	13 April 1994, Palermo, Italy
Nationality	Italian

2. Contact information

E-mail christiandioguardi@gmail.com

3. Education

2021–...	Tallinn University of Technology, School of Cybernetics PhD studies
2017–2020	Università degli Studi di Trento, Faculty of Physics, MSc *cum laude*
2013–2017	Università degli Studi di Trento, Faculty of Physics, BSc

4. Language competence

Italian	native
English	fluent
Estonian	intermediate

5. Professional employment

2021-... National Institute of Physics and Biophysics, Junior Researcher

6. Computer skills

- Document preparation: Latex, Microsoft Office
- Programming languages: Mathematica, C++, Python
- Scientific packages: GRQUICK, xAct

7. Defended theses

- 2020, Linear Stability of Black Holes in Quadratic Gravity, MSc, supervisor Prof. Massimiliano Rinaldi, Università degli Studi di Trento, Department of Physics
- 2017, Kerr geometries and Rotational Energy of Kerr Black Holes, BSc, supervisor Prof. Bruno Giacomazzo, Università degli Studi di Trento, Department of Physics

8. Field of research

- Cosmology
- High-Energy Physics

9. Scientific work
Papers

1. Christian Dioguardi, Antonio Racioppi, and Eemeli Tomberg. Slow-roll inflation in Palatini F(R) gravity. *JHEP*, 06:106, 2022
2. Christian Dioguardi and Antonio Racioppi. Palatini F(R,X): A new framework for inflationary attractors. *Phys. Dark Univ.*, 45:101509, 2024
3. Konstantinos Dimopoulos, Christian Dioguardi, Gert Hütsi, and Antonio Racioppi. Quintessential inflation in palatini F(R,X) gravity. *The European Physical Journal Plus*, 140(11), November 2025
4. Christian Dioguardi and Massimiliano Rinaldi. A note on the linear stability of black holes in quadratic gravity. *Eur. Phys. J. Plus*, 135(11):920, 2020
5. Christian Dioguardi, Antonio Racioppi, and Eemeli Tomberg. Beyond (and back to) Palatini quadratic gravity and inflation. *JCAP*, 03:041, 2024
6. N. Bostan, R. H. Dejrah, C. Dioguardi, and A. Racioppi. Natural inflation in Palatini F(R,X). *JCAP*, 07:082, 2025
7. Christian Dioguardi, Antonio J. Iovino, and Antonio Racioppi. Fractional attractors in light of the latest ACT observations. *Phys. Lett. B*, 868:139664, 2025
8. Christian Dioguardi and Alexandros Karam. Palatini linear attractors are back in action. *Phys. Rev. D*, 111(12):123521, 2025

Conference presentations

1. C.Dioguardi, *Slow-Roll Inflation in Palatini F(R) gravity*, Metric affine frameworks of gravity 2022: June 2022, Tartu, Estonia
2. C.Dioguardi, *Slow-Roll Inflation in Palatini F(R) gravity*, XX Frascati summer School "Bruno Touschek": July 2022, Frascati, Italy
3. C.Dioguardi, *Inflation in Palatini gravity*, CISF 2023: April 2023, Palermo, Italy
4. C.Dioguardi, *Inflationary attractors from quadratic Palatini F(R,X) formulation*, 25th International Conference: From the Planck Scale to the Electroweak Scale: May 2023, Warsaw, Poland
5. C.Dioguardi, *Beyond Palatini quadratic gravity and inflation*, 25th International Conference: Metric Affine frameworks of gravity 2024: June 2024, Tartu, Estonia
6. C.Dioguardi, *Electroweak metastability and Higgs inflation*, 4th CERN Baltic conference: October 2024, Tallinn, Estonia
7. C.Dioguardi, *Quintessential Inflation in Palatini F(R,X) gravity*, 2nd Nordic Cosmology Meeting: February 2025, Helsinki, Finland
8. C.Dioguardi, *Quintessential Inflation in Palatini F(R,X) gravity*, Geometric Foundations of Gravity 2025: June 2025, Tartu, Estonia

Elulookirjeldus

1. Isikuandmed

Nimi	Christian Dioguardi
Sünniaeg ja -koht	13 April 1994, Palermo, Itaalia
Kodakondsus	Itaalia

2. Kontaktandmed

e-post christiandioguardi@gmail.com

3. Haridus

2021–...	Tallinna Tehnikaülikool, Küberneetika instituut, doktoriõpe
2017–2020	Università degli Studi di Trento, Füüsikateaduskond, magistriõpe, *cum laude*
2013–2017	Università degli Studi di Trento, Füüsikateaduskond, bakalaureuseõpe

4. Keelteoskus

itaalia keel	emakeel
inglise keel	kõrgtase
eesti keel	kesktase

5. Teenistuskäik

2021– ...	KBFI, nooremteadur

6. Arvutioskus

- Kontoritarkvara: Latex, Microsoft Office
- Programmeerimiskeeled: Mathematica, C++, Python
- Teadustarkvara paketid: GRQUICK, xAct

7. Kaitstud lõputööd

- 2020, Linear Stability of Black Holes in Quadratic Gravity, MSc, juhendaja Prof. Massimiliano Rinaldi, Università degli Studi di Trento
- 2017, Kerr geometries and Rotational Energy of Kerr Black Holes, BSc, juhendaja Prof. Bruno Giacomazzo, Università degli Studi di Trento

8. Teadustöö põhisuunad

- Kosmoloogia
- Kõrge energia füüsika

9. Teadustegevus

Teadusartiklite, konverentsiteeside ja konverentsiettekannete loetelu on toodud ingliskeelse elulookirjelduse juures.

ISSN 2585-6901 (PDF)
ISBN 978-9916-80-494-0 (PDF)